PNAS RESEARCH ARTICLE | APPLIED PHYSICAL SCIENCES

Magnon-induced electric polarization and magnon Nernst effects

D. Quang To[a,1], Federico Garcia-Gaitan[b], Yafei Ren[b], Joshua M. O. Zide[a], M. Benjamin Jungfleisch[b], John Q. Xiao[b], Branislav K. Nikolić[b], Garnett W. Bryant[c,d], and Matthew F. Doty[a,1]

Affiliations are included on p. 11.

Edited by J. C. Davis, University of Oxford, Oxford, United Kingdom; received March 28, 2025; accepted September 19, 2025

Magnons offer a promising path toward energy-efficient information transmission and the development of next-generation classical and quantum computing technologies. However, efficiently exciting, manipulating, and detecting magnons remains a critical need. We show that magnons, despite their charge-neutrality, can induce electric polarization through their spin and orbital moments. This effect is governed by system symmetry, magnon band hybridization, and interactions with other quasiparticles. We calculate the electric polarization induced by magnons in two-dimensional collinear honeycomb and noncollinear antiferromagnets (AFMs), showing that the presence of the Dzyaloshinskii–Moriya interaction yields a finite net electric polarization. In $NiPSe_3$, a collinear honeycomb AFM with Zigzag order, the induced net electric polarization is about three orders of magnitude greater than in $MnPS_3$, a collinear honeycomb AFM with Néel phase. In the noncollinear AFM $KFe_3(OH)_6(SO_4)_2$, the net electric polarization can be tuned via magnon hybridization, which can be controlled by external magnetic fields. These findings reveal that electric fields could be used to both detect and manipulate magnons under certain conditions by leveraging their spin and orbital angular moment. They also suggest that the discovery or engineering of materials with substantial magnon orbital moments could enhance practical uses of magnons for future computing and information transmission applications.

magnon orbital moment | magnon Nernst effects | electric polarization | orbitronics | spintronics

Significance

The formalism we develop reveals that the transport of magnons can induce measurable electric polarization, enabling the control and detection of magnon spin and orbital transport through electrical or optical methods. This finding opens exciting opportunities across the fields of magnonics, spintronics, and orbitronics. We further show that magnon orbital transport can influence measurable properties even more significantly than magnon spin currents. Crucially, our framework not only reveals the existence of these phenomena but also provides strategies for designing and engineering materials to enhance conversions between magnons and electric polarization. Collectively, these advances reveal a path toward both a deeper understanding of magnetic materials and transformative advances in both classical and quantum technologies for information processing and storage.

The recent rapid advancement of information technology, exemplified by artificial intelligence systems, has driven the need for significant improvements in data storage and processing. In particular, these technologies demand high speed operations with reduced energy consumption and minimal energy loss. Identifying novel material systems with unique properties is critical to addressing these energy challenges and overcoming the limits of conventional devices based on electron charge and spin transport. In this context, magnons, collective spin excitations in magnetic materials, are of significant interest (1–3).

Magnons are bosonic quasi-particles arising from collective and charge-neutral excitations of localized spins. These quanta obey the Bose–Einstein distribution function at finite temperatures and have zero chemical potential in equilibrium. Because magnons can carry spin information without the need for moving electric charge, they enable low-power data transfer and energy-efficient classical computing technologies (1–6). Magnons can also hybridize with a variety of other quantum states, including photons (7, 8), electrons (9–11), phonons (12–14), plasmons (15, 16), excitons (17–19) and superconducting qubits (20, 21). Because of their remarkable properties, magnons are being explored as elements of quantum information processing systems (20–27).

Realizing the opportunities associated with magnons requires tools for their efficient excitation, manipulation, and detection. The field of spin caloritronics covers a wide range of relevant magnon effects including the magnon Seebeck effect (28), thermal Hall effect (29–37), and spin Nernst effect (38–44). These effects all involve the generation of longitudinal and transverse heat currents or spin currents, mediated by magnons, in response to a longitudinally applied temperature gradient. However, these effects are difficult to exploit for information processing because it is difficult to apply thermal gradients locally or to modulate them rapidly.

Electronic systems are easily manipulated by local electric fields and it has recently been recognized that the orbital angular moment (OAM) of electrons can generate a number

The authors declare no competing interest.

This article is a PNAS Direct Submission.

[1]To whom correspondence may be addressed. Email: quangto@udel.edu or doty@udel.edu.

This article contains supporting information online at https://www.pnas.org/lookup/suppl/doi:10.1073/pnas.2507255122/-/DCSupplemental.

Published October 23, 2025.

of previously overlooked transport effects (45–52). Magnon OAM is expected to play a similarly important role in the form of a magnon Orbital Nernst Effect (ONE). A few studies have recently explored magnon OAM within different crystalline lattices, (53–59) but these studies have focused on theoretical measures of magnon OAM such as magnon orbital magnetization (54) or the integral of magnon OAM over the orientation of the magnon wave vector (55, 57). Relating magnon Spin Nernst effect and Orbital Nernst Effect, which we collectively refer to as magnon Nernst effects, to experimentally measurable quantities (43) requires a more comprehensive theoretical framework.

In this work, we develop a quantum mechanical formalism that establishes the connection between magnon transport effects (e.g. magnon Nernst effects) and electric polarization. Specifically, we show that magnons, despite their charge-neutrality, can induce net electric polarization in systems with either the Dzyaloshinskii–Moriya interaction (DMI) or other interactions (e.g. magnon–phonon coupling) that break system symmetry in a similar manner. The formalism reveals that the magnon-induced electric polarization occurs as a result of both magnon spin and orbital moments. Furthermore, we show that the magnitude of this electric polarization can be significantly enhanced by the system's symmetry properties, the hybridization between magnon bands, and interactions between magnons and other quasiparticles such as phonons. This insight suggests that selecting materials with the appropriate symmetry and/or tuning magnon hybridization provide effective mechanisms for dramatically improving the conversion of magnon orbital moments into measurable voltages. Moreover, our findings suggest that the inverse process may also be possible, implying that control over hybridization also provides a mechanism for engineering materials in which electric fields, including those of light, can be used to control and detect magnon orbital moment transport.

To illustrate these effects, we compute and compare the electric polarizations induced by the magnon Nernst effects in a) 2D honeycomb materials with Néel and Zigzag magnetic ordering and b) noncollinear antiferromagnetic materials with a Kagomé lattice. Remarkably, our results show that in the presence of DMI the Zigzag-ordered phase of the honeycomb lattice, due to its underlying magnetic symmetry, induces a net electric polarization approximately three orders of magnitude greater than that of the Néel phase. Moreover, our study of noncollinear AFMs demonstrates that external parameters such as an applied magnetic field can effectively control magnon hybridization, leading to order-of-magnitude improvements in the voltage signals resulting from magnon Nernst effects. We emphasize that while this work explores magnon Nernst effects as a specific example of how our formalism predicts the electric polarization induced by magnons, the formalism is not limited to thermal effects. It can be applied to a broad range of magnon transport phenomena, including light-induced magnon transport and magnon generation via the spin Hall effect.

The paper is structured as follows. In Section 1, we describe the origin of magnon Nernst effects in magnetic systems and summarize what material properties are important for maximizing the Orbital Nernst effect. In Section 2, we introduce the quantum mechanical framework that reveals, and allows us to calculate, the electric polarization and transverse voltage induced by the motion of magnon wave-packets. In Sections 3 and 4, we demonstrate the value of this formalism by applying it to 2D collinear honeycomb antiferromagnets with Néel and Zigzag order. Through both our formalism and symmetry considerations, we show that spin–orbit coupling (SOC), specifically in the form of the Dzyaloshinskii–Moriya interaction or SOC-like interactions that couple spins to the lattice (e.g. magnon–phonon coupling), is essential for generating a finite net electric polarization across the sample from magnon Nernst effects. In Section 5, we demonstrate the tunability of net electric polarization induced by magnons in noncollinear antiferromagnets with a Kagomé lattice using an external magnetic field. Finally, we conclude the paper with a discussion and outlook in Section 6.

While the magnon Spin Nernst effect has been extensively studied in the literature (38–44), the magnon Orbital Nernst effect was introduced relatively recently using a semiclassical theory (60, 61). However, refs. 60 and 61 do not include a clear delineation of the conditions under which semiclassical theory is applicable. More importantly, in the previous semiclassical approach the authors describe magnons as carrying the orbital magnetic moment of electrons rather than the intrinsic orbital moment of the magnons themselves. Recently, the authors of ref. 59 discussed the magnon Orbital Nernst effect in a honeycomb lattice with Néel order in the absence of the Dzyaloshinskii–Moriya interaction, taking $MnPS_3$ as an example. The authors suggest that magnons in this system can induce electric polarization. However, ref. 59 does not establish a direct link between the magnon orbital moment and induced electric polarization. Instead, the authors attribute electric polarization to the spin-polarized current carried by magnons, which induces polarization through relativistic magnetoelectric coupling. Notably, their argument is purely phenomenological, leaving open the question of how a transverse spin-polarized current could be generated in $MnPS_3$ by a magnon OAM current in the absence of DMI. Their framework predicts a finite transverse voltage driven by the magnon orbital moment current in a honeycomb lattice with Néel order, even without DMI. However, as we will demonstrate, without DMI, the magnetic point group of $MnPS_3$ remains nonpolar, prohibiting net electric polarization and, consequently, any transverse voltage in the system.

The rigorous quantum mechanical framework presented here directly links both the spin current carried by magnons and the magnon orbital moment to magnon induced electric polarization. This formulation is crucial. Not only does this formulation provide a solid theoretical foundation for studying the magnon transport effects and their observable manifestations in the form of a net electric polarization, it also provides material design strategies to enhance the net electric polarization induced by magnons for practical applications involving magnon spin and orbital degrees of freedom. Taken together, the results reported here suggest a path toward exploiting the orbital degree of freedom of magnons in addition to their spin moment. Specifically, the results reveal that the measurement of induced electric polarization could be used both for the experimental study of magnon OAM and magnon Nernst effects and as a means of detecting the presence of magnon transport within devices. They also suggest that the discovery or engineering of materials with large magnon orbital moments could increase the interactions with electric dipoles, creating more opportunities for electrical read out or control of magnons in future computing and information transmission devices. Finally, the results suggest that it may also be possible to use electromagnetic waves to both manipulate and read out magnons through electric dipole interactions leveraging the spin and orbital angular moment degrees of freedom of magnons. This could potentially lead to phenomena, such as the conversion of the angular moment of light into that of magnons and vice versa.

1. Origin of Magnon Nernst Effects

Magnons are inherently charge-neutral entities and can be generated by the introduction of a temperature gradient that induces a transverse magnon thermal current via the thermal Hall effect and a magnon spin current via the Spin Nernst effect, as schematically depicted in Fig. 1*A*. In this section, we show that such thermal gradients can also generate a magnon orbital current as indicated in Fig. 1*B*. We call this effect the magnon Orbital Nernst Effect. We then discuss the importance of magnon OAM and Berry curvature to the magnon Orbital Nernst effect, which leads to predictions about what classes of materials are most likely to show a large magnon Orbital Nernst effect.

In the semiclassical picture, the motion of a magnon wavepacket in the n*th* band with position $\boldsymbol{r}_c^n$ and wavevector $\boldsymbol{k}$ subject to an applied temperature gradient is given by refs. 62 and 63

$$\dot{\boldsymbol{r}}_c^n = \frac{1}{\hbar}\frac{\partial E_{n,\boldsymbol{k}}}{\partial \boldsymbol{k}} - \dot{\boldsymbol{k}} \times \boldsymbol{\Omega}^n(\boldsymbol{k}) \qquad [1]$$

with $\hbar\dot{\boldsymbol{k}} = -\nabla U(\boldsymbol{r})$, where $U(\boldsymbol{r})$ is a slowly varying potential experienced by the magnons and $\boldsymbol{\Omega}^n(\boldsymbol{k}) = \sum_{m\neq n}\boldsymbol{\Omega}^{nm}(\boldsymbol{k})$ is the Berry curvature with

$$\boldsymbol{\Omega}^{nm}(\boldsymbol{k}) = i\hbar^2\sigma_3^{mm}\sigma_3^{nn}\frac{\langle n(\boldsymbol{k})|\hat{\boldsymbol{v}}_{\boldsymbol{k}}|m(\boldsymbol{k})\rangle \times \langle m(\boldsymbol{k})|\hat{\boldsymbol{v}}_{\boldsymbol{k}}|n(\boldsymbol{k})\rangle}{\left(\sigma_3^{nn}E_{n,\boldsymbol{k}} - \sigma_3^{mm}E_{m,\boldsymbol{k}}\right)^2} \qquad [2]$$

the projection of the Berry curvature of the n*th* band on the m*th* band. Here, $E_{n,\boldsymbol{k}}$ and $|n(\boldsymbol{k})\rangle$ are, respectively, the eigenvectors and eigenvalues of the bosonic Bogoliubov-de Gennes Hamiltonian $\hat{H}_{\boldsymbol{k}}$; $\hat{\boldsymbol{v}}_{\boldsymbol{k}} = \frac{1}{\hbar}\frac{\partial \hat{H}_{\boldsymbol{k}}}{\partial \boldsymbol{k}}$ denotes the velocity vector operator; and the $\boldsymbol{\sigma}_3$ matrix is given by $\boldsymbol{\sigma}_3 = \begin{pmatrix} \mathbf{1}_{N\times N} & 0 \\ 0 & -\mathbf{1}_{N\times N}\end{pmatrix}$, where $\mathbf{1}_{N\times N}$ is a $N \times N$ identity matrix and $\sigma_3^{nn} = \langle n(\boldsymbol{k})|\boldsymbol{\sigma}_3|n(\boldsymbol{k})\rangle$ is the n*th* diagonal element of $\boldsymbol{\sigma}_3$.

The key point of Eq. **1** at this stage of the discussion is the dependence on the Berry curvature $\boldsymbol{\Omega}^n(\boldsymbol{k})$. Berry curvature plays a pivotal role in generating both the magnon thermal Hall effect and the nontrivial topology of magnon bands (33, 62, 64–67). The nontrivial topology originates from the motion of magnon wavepackets along the edge of the system (62). Magnon wavepackets also exhibit self-rotation, referred to as magnon OAM, as elucidated by Matsumoto using linear response theory (62). As a result, in systems that have both a) nontrivial topological thermal transport of magnons and b) finite self-rotation of magnon wavepackets, the thermal Hall current induced by the magnon bands can also facilitate the transport of magnon OAM. This, in turn, gives rise to a magnon orbital current in response to an applied temperature gradient, i.e. the magnon Orbital Nernst effect. The consequence of a finite Orbital Nernst effect is the accumulation of the OAM of magnons at the boundaries of the system, as depicted in Fig. 1*B*. In this simple picture, the magnon orbital angular moment population accumulated at the edge of the system due to the Orbital Nernst effect is directly proportional to *SI Appendix*, section S4C:

$$\lambda_{\mu\nu}^{L^\alpha} = \frac{k_B}{2\hbar V}\sum_{\boldsymbol{k}}\sum_{n=1}^{N}\sum_{m\neq n}\left\{\left[\sigma_3^{nn}L_{nn}^{\alpha}(\boldsymbol{k}) + \sigma_3^{mm}L_{mm}^{\alpha}(\boldsymbol{k})\right] \times \Omega_{\mu\nu}^{nm}(\boldsymbol{k})\,F(\rho_{n,\boldsymbol{k}})\right\}. \qquad [3]$$

where $\lambda_{\mu\nu}^{L^\alpha}$ is the Orbital Nernst conductivity; V is the volume of the system; $\rho_{n,\boldsymbol{k}} = \left(e^{E_{n,\boldsymbol{k}}/k_BT} - 1\right)^{-1}$ is the Bose–Einstein distribution function; $F(\rho_{n,\boldsymbol{k}}) = (1+\rho_{n,\boldsymbol{k}})\,ln\,(1+\rho_{n,\boldsymbol{k}}) - \rho_{n,\boldsymbol{k}}ln\,(\rho_{n,\boldsymbol{k}})$; k_B is the Boltzmann constant; T represents the system's average temperature; $\Omega_{\mu\nu}^{nm}(\boldsymbol{k})$ is the $\mu\nu$-component of the projected Berry curvature Eq. **2** and L_{nn}^{α} is the α-component of the intraband magnon OAM in the Bloch wave of the n*th* band given by *SI Appendix*, section S2B:

$$\boldsymbol{L}_{nn}(\boldsymbol{k}) = -\frac{i\hbar}{2}\sum_{p\neq n}\sigma_3^{pp}\frac{\langle n(\boldsymbol{k})|\hat{\boldsymbol{v}}_{\boldsymbol{k}}|p(\boldsymbol{k})\rangle \times \langle p(\boldsymbol{k})|\hat{\boldsymbol{v}}_{\boldsymbol{k}}|n(\boldsymbol{k})\rangle}{\sigma_3^{nn}E_{n,\boldsymbol{k}} - \sigma_3^{pp}E_{p,\boldsymbol{k}}}. \qquad [4]$$

Several physical consequences related to the Orbital Nernst effect can be gleaned from Eqs. **3** and **4**. First, the representation of the magnon intraband OAM in Bloch states given by Eq. **4** has deep connections to the magnon Berry curvature given in Eq. **2**. Specifically, both are subject to the constraints of time reversal symmetry (TRS) and combined parity-time symmetry (CPTS). TRS requires that $\boldsymbol{L}_{nn}(\boldsymbol{k}) = -\boldsymbol{L}_{nn}(-\boldsymbol{k})$. CPTS requires the intraband OAM to be zero, as expressed by $\boldsymbol{L}_{nn}(\boldsymbol{k}) = 0$ (44). Thus, nonzero intraband OAM can only be achieved when CPTS is broken. Second, broken TRS is crucial for observing a finite magnon thermal Hall effect. However, Eq. **3** tells us that the magnon Orbital Nernst effect can exist even without breaking TRS. The term $\Omega_{\mu\nu}^{L^\alpha,nm}(\boldsymbol{k}) = \frac{1}{4}\left[\sigma_3^{nn}L_{nn}^{\alpha}(\boldsymbol{k}) + \sigma_3^{mm}L_{mm}^{\alpha}(\boldsymbol{k})\right]\Omega_{\mu\nu}^{nm}(\boldsymbol{k})$ has even parity with respect to the wavevector because both intraband OAM and

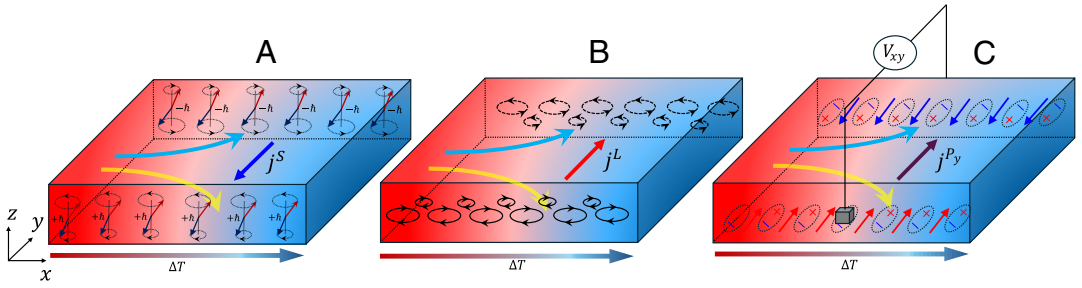

Fig. 1. Schematic illustration of (*A*) the magnon Spin Nernst Effect, (*B*) the magnon Orbital Nernst Effect, and (*C*) the magnon-induced electric polarization Nernst effect. Under an applied temperature gradient ΔT, magnons carrying opposite spin and orbital angular momenta are deflected toward opposite transverse edges, giving rise to transverse spin (*A*) and orbital (*B*) currents, accompanied by the accumulation of spin and orbital moments at the system's boundaries. This deflection simultaneously leads to the accumulation of electric polarization at the edges. (*C*) When the symmetry between oppositely oriented electric polarizations is broken, a finite transverse voltage V_{xy} emerges.

Berry curvature have the same parity with respect to the vector $\boldsymbol{k}$. As a result, $\lambda_{\mu\nu}^{L^\alpha}$ can be finite even in the presence of TRS. This observation, in combination with the first point above, suggests that the best strategy for experimentally observing the magnon Orbital Nernst effect is to identify material systems exhibiting finite Berry curvature (i.e. breaking CPTS) and thus having nonzero intraband OAM. In this context, collinear 2D honeycomb AFMs in both Néel and Zigzag phases, as well as noncollinear AFMs with Kagomé lattice structure, emerge as promising candidates. Third, magnon intraband OAM can have much larger magnitude than magnon spin moment, particularly in the vicinity of the anticrossing point between two distinct bands. This is similar to the behavior of Berry curvature. Consequently, the Orbital Nernst effect should be larger in magnonic crystals in which there are more band crossings for magnons and/or more coupling with other quasiparticles such as phonons (44, 68). This suggests that the Orbital Nernst effect will be more pronounced in systems characterized by strong band hybridization and a narrow energy gap between the bands because the magnitude of both intraband OAM and Berry curvature are significantly amplified under these conditions (44).

We note that our discussion above illustrates the Orbital Nernst effect using a simple picture in which the topological magnon thermal Hall current gives rise to the magnon Orbital Nernst effect through magnon intraband OAM. However, both magnon intraband and interband OAM can contribute. To treat intraband and interband OAM on an equal footing, we employ linear response theory to derive the linear thermal response mechanism (*SI Appendix*, section S4) governing the flow of magnon OAM $j_\mu^{L^\alpha} = -\lambda_{\mu\nu}^{L^\alpha}\partial_\nu T$, where

$$\lambda_{\mu\nu}^{L^\alpha} = \frac{2k_B}{\hbar V}\sum_{\boldsymbol{k}}\sum_{n=1}^{N}\Omega_{\mu\nu}^{L^\alpha,n}(\boldsymbol{k})\,F(\rho_{n,\boldsymbol{k}}) \qquad [5]$$

is the total Orbital Nernst conductivity.

For convenience, we define a generalized Berry curvature associated with an operator $\hat{\mathcal{A}}$ as

$$\Omega_{\mu\nu}^{\hat{\mathcal{A}},n}(\boldsymbol{k}) = -\sum_{m\neq n} 2\hbar^2\sigma_3^{nn}\sigma_3^{mm} \times Im\left\{\frac{\left\langle n(\boldsymbol{k})\left|\hat{j}_\mu^{\hat{\mathcal{A}}}\right|m(\boldsymbol{k})\right\rangle\left\langle m(\boldsymbol{k})\left|\hat{v}_\nu\right|n(\boldsymbol{k})\right\rangle}{\left[(\boldsymbol{\sigma}_3E_{\boldsymbol{k}})_{mm}-(\boldsymbol{\sigma}_3E_{\boldsymbol{k}})_{nn}\right]^2}\right\}, \qquad [6]$$

where $\hat{j}_\mu^{\hat{\mathcal{A}}} = \frac{1}{4}\left(\hat{\mathcal{A}}\boldsymbol{\sigma}_3\hat{v}_\mu + \hat{v}_\mu\boldsymbol{\sigma}_3\hat{\mathcal{A}}\right)$ is the current operator associated with $\hat{\mathcal{A}}$ along the μ-direction.

With this definition, the quantity $\Omega_{\mu\nu}^{L^\alpha,n}(\boldsymbol{k})$ appearing in Eq. **5** represents the orbital Berry curvature corresponding to the α-component of the total magnon orbital angular moment operator, i.e., $\hat{\mathcal{A}} \equiv \hat{L}^\alpha$.

2. Magnon-Induced Electric Polarization

2.1. Electric Polarization Induced by Magnons in Equilibrium: The Role of Spin and Orbital Degrees of Freedom. Experimental detection of the Orbital Nernst effect will be possible when the accumulation of magnon orbital angular moment can be transformed into a magnetization or electric polarization. This is analogous to the way the Orbital Hall effect for electrons can be measured via spin polarizations that are induced by the Orbital Hall effect via spin–orbit coupling (69, 70). Utilizing perturbation theory, Neumann et al. (54) revealed the dependence of the orbital magnetic moment of magnons on the external magnetic field:

$$\boldsymbol{\mu}_{n,\boldsymbol{k}}^{O} = -\sum_{m=1}^{N}\sum_{\alpha=x,y,z}\frac{\partial E_{n,\boldsymbol{k}}}{\partial\hat{\boldsymbol{\alpha}}_m}\cdot\frac{\partial\hat{\boldsymbol{\alpha}}_m}{\partial\boldsymbol{B}}, \qquad [7]$$

where $\boldsymbol{B}$ is the applied magnetic field, $\boldsymbol{\alpha}$ is the local spin coordinate system and $E_{n,\boldsymbol{k}}$ is the energy of the magnon in the nth state. This dependence is a result of spin–orbit coupling or SOC-like interactions that couple spins to the lattice (e.g. DMI or magnon–phonon coupling). Consequently, the accumulation of the orbital moment of magnons at the boundaries due to the Orbital Nernst effect can manifest as a measurable magnetization in systems featuring DMI, magnon–phonon coupling, or similar interactions (61, 71, 72). This edge magnetization can be detected using techniques such as the magneto-optical Kerr effect. In the following, we further show that the orbital and spin moments of magnons can give rise to a finite net electric polarization in the presence of DMI, magnon–phonon coupling, or similar interactions. This provides an alternative approach for detecting magnon Nernst effects and controlling magnon transport in magnetic systems.

Classically, magnons possess a magnetic moment $\boldsymbol{m}$ and the motion of a magnon wave packet can be viewed as a movement of magnetic moments. This leads to a current of magnetic dipoles which can indirectly generate an electric field, ultimately inducing a relativistic electric dipole moment $\boldsymbol{p} = \frac{\boldsymbol{m}\times\boldsymbol{v}}{c^2}$, where $\boldsymbol{v}$ is the magnon velocity and c is speed of light. This is called the vacuum magnetoelectric effect (VME) (73). Quantum mechanically, one can define the electric polarization density operator for magnons in a manner analogous to the classical relativistic electric dipole $\boldsymbol{p}$:

$$\hat{\boldsymbol{p}} = \frac{\hat{\boldsymbol{v}}\times\hat{\boldsymbol{m}} - \hat{\boldsymbol{m}}\times\hat{\boldsymbol{v}}}{2Vc^2}, \qquad [8]$$

where $\hat{\boldsymbol{m}} = g\mu_B\hat{\boldsymbol{S}}$ with $\hat{\boldsymbol{S}}$ the spin operator density of the magnon. Employing perturbation theory with the electric polarization density operator defined in Eq. **8**, we derive a formula to calculate the y-component of the net equilibrium electric polarization induced by magnon motion in magnetic materials (*SI Appendix*, section S3) $P_y = \sum_{n,\boldsymbol{k}}p_y(n,\boldsymbol{k}) = \sum_{n,\boldsymbol{k}}p_y^S(n,\boldsymbol{k}) + \sum_{n,\boldsymbol{k}}p_y^O(n,\boldsymbol{k}) = P_y^S + P_y^O$, where P_y represents the total net electric polarization, P_y^S represents the contribution from spin Berry curvature, and P_y^O represents contribution from the magnon OAM component. Similarly $p_y(n,\boldsymbol{k})$,

$$p_y^S(n,\boldsymbol{k}) = -\frac{g\mu_B}{\hbar W_y c^2 V}\left[\Omega_{xy}^{S^z,n}(\boldsymbol{k}) - \Omega_{zy}^{S^x,n}(\boldsymbol{k})\right] \times ln\left|e^{-\frac{E_{n,\boldsymbol{k}}}{k_BT}} - 1\right| k_BT \qquad [9]$$

and

$$p_y^O(n,\boldsymbol{k}) = -\frac{g\mu_B}{\hbar W_y c^2 V}\rho_{n,\boldsymbol{k}}\hbar\sigma_3^{nn}Im\left[\left\langle n(\boldsymbol{k})\left|\left(\partial_{k_y}\hat{v}_x\right)\boldsymbol{\sigma}_3\hat{S}^z\right|n(\boldsymbol{k})\right\rangle + 4\sum_{q\neq n}\sigma_3^{qq}\frac{\left\langle n(\boldsymbol{k})\left|\partial_{k_y}\hat{H}_{\boldsymbol{k}}\right|q(\boldsymbol{k})\right\rangle}{[\boldsymbol{\sigma}_3E_{\boldsymbol{k}}]_{nn} - [\boldsymbol{\sigma}_3E_{\boldsymbol{k}}]_{qq}} \times\left\langle q(\boldsymbol{k})\left|\hat{j}_x^{S^z}\right|n(\boldsymbol{k})\right\rangle - (x\leftrightarrow z)\right] \qquad [10]$$

are, respectively, the total electric polarization, the contribution from spin Berry curvature, and the contribution from magnon OAM induced by the magnon wave packet in the nth band with wave vector $\boldsymbol{k}$. Here, $\Omega_{\mu\nu}^{S^\alpha,n}(\boldsymbol{k})$ denotes the spin Berry curvature of the nth band, defined by Eq. **6** with $\hat{\mathcal{A}} \equiv \hat{S}^\alpha$, where $\hat{S}^\alpha$ is the α-component of the spin operator ($\alpha = x, z$); W_y is the width along the y-direction of the system; c is the speed of light in vacuum.

Eqs. **9** and **10** are important because they provide a microscopic framework for computing the electric polarization generated by magnon transport in an arbitrary magnetic system, even in a case where the spin moment of magnons is not conserved (e.g. due to magnon–phonon interactions). Analyzing Eqs. **9** and **10**, we find that the two parts of $p_y(n, \boldsymbol{k})$ describe two distinct contributions to the electric polarization induced by the motion of the magnon wave packets:

1. $p_y^S(n, \boldsymbol{k})$ Eq. **9** describes the electric polarization that arises from the magnon spin current. Specifically, the presence of the spin-Berry curvatures $\Omega_{xy}^{S^z,n}(\boldsymbol{k})$ and $\Omega_{zy}^{S^x,n}(\boldsymbol{k})$ result in a spin current in the y direction via the accumulation of spin angular momentum due to, for example, the magnon spin Nernst current carried by magnons under a temperature gradient along the x-direction (44).
2. $p_y^O(n, \boldsymbol{k})$ Eq. **10** originates in the orbital angular moment L^z of the magnons.

In other words, our quantum mechanical formulation reveals that the electric polarization induced by magnon motion in magnetic materials has distinct contributions from the magnon spin current [$p_y^S(n, \boldsymbol{k})$, Eq. **9**] and the magnon orbital angular moment [$p_y^O(n, \boldsymbol{k})$, Eq. **10**].

We note that the VME is predicted to be weak, generating a voltage of only a few nanovolts in topological chiral edge magnons within a ferromagnetic insulator (73). However, we will show that the VME in antiferromagnets can be enhanced by five or more orders of magnitude by harnessing the spin and orbital moments of magnons in these systems, leading to an observable transverse voltage induced by magnons. This enhancement is achieved through the selection of materials with appropriate symmetry and the tuning of either magnon band hybridization or magnon interactions with other quasiparticles to increase the spin current and orbital angular moment of propagating magnons. These findings underscore the importance of the formalism Eqs. **9** and **10** presented in this work.

2.2. Electric Polarization Induced by Magnons in Nonequilibrium. Magnon Nernst effects result in the accumulation of magnons with opposite orbital moments and spins at the system's edges. Consequently, an applied temperature gradient, ∇T, transports induced electric dipole moments with opposite orientation to opposite edges. This gives rise to a Nernst effect for electric polarization as indicated in Fig. 1*C*. The resulting transverse electric polarization current can be computed using Kubo's formula, given by $j_\mu^{P_\alpha} = -\lambda_{\mu\nu}^{P_\alpha}\partial_\nu T$ where

$$\lambda_{\mu\nu}^{P_\alpha} = \frac{2k_B}{\hbar V}\sum_{\boldsymbol{k}}\sum_{n=1}^{N}\Omega_{\mu\nu}^{P_\alpha,n}(\boldsymbol{k})\,F(\rho_n) \qquad [11]$$

is the electric polarization Nernst conductivity, $\Omega_{\mu\nu}^{P_\alpha,n}(\boldsymbol{k})$ represents the electric polarization Berry curvature of the nth band, defined in Eq. **6** with $\hat{\mathcal{A}} \equiv \hat{p}_\alpha$, where $\hat{p}_\alpha$ is the α-component of the electric dipole moment operator as given in Eq. **8**.

2.3. Transverse Voltage Generated by Finite Net Electric Polarization. Under a temperature gradient along the x-direction, a finite transverse magnon-induced electric polarization current results in the accumulation of electric polarization with opposite orientations at the system edges. Specifically -y oriented dipoles accumulate at the +y system boundary while +y oriented dipoles accumulate at the -y system boundary, as shown in Fig. 1*C*. However, what would be measured in practice is the transverse voltage along the y-direction (V_{xy}) induced by the total net electric polarization (P_y), as also shown in Fig. 1*C*. Thus, even if a finite electric polarization current leads to the accumulation of electric polarization with opposite orientations at the $\pm y$ system edges, the transverse voltage vanishes if the populations of electric polarization pointing in the positive and negative y-directions are equal. A finite V_{xy} can only be observed when this symmetry is broken. We will demonstrate that this occurs in the presence of DMI in the 2D AFMs considered in this work.

To derive a prediction of the measurable transverse voltage, we note that the electric field Ξ_y along the y-direction induced by P_y reads:

$$\Xi_y = \frac{P_y}{\varepsilon_0\chi}, \qquad [12]$$

where ε_0 is the electric permittivity of free space and χ is the electric susceptibility. Therefore, the transverse voltage is given by

$$\begin{aligned} V_{xy} = -\int_0^{W_y}\Xi_y dy = \frac{g\mu_B}{\hbar\varepsilon_0\chi c^2 V}\sum_{n,\boldsymbol{k}}\Big\{\Big[\Omega_{xy}^{S^z,n}(\boldsymbol{k}) - \Omega_{zy}^{S^x,n}(\boldsymbol{k})\Big] \\ \times ln\left|e^{-\frac{E_{n,\boldsymbol{k}}}{k_BT}} - 1\right| k_BT + \hbar\sigma_3^{nn} Im \\ \times \Bigg[4\sum_{q\neq n}\sigma_3^{qq}\frac{\left\langle n(\boldsymbol{k})\left|\partial_{k_y}\hat{H}_{\boldsymbol{k}}\right|q(\boldsymbol{k})\right\rangle}{[\boldsymbol{\sigma}_3 E_{\boldsymbol{k}}]_{nn} - [\boldsymbol{\sigma}_3 E_{\boldsymbol{k}}]_{qq}}\left\langle q(\boldsymbol{k})\left|\hat{j}_x^{S^z}\right|n(\boldsymbol{k})\right\rangle \\ + \left\langle n(\boldsymbol{k})\left|\left(\partial_{k_y}\hat{v}_x\right)\boldsymbol{\sigma}_3\hat{S}^z\right|n(\boldsymbol{k})\right\rangle - (x\leftrightarrow z)\Bigg]\rho_{n,\boldsymbol{k}}\Big\} \end{aligned} \qquad [13]$$

3. Magnon Nernst Effects and Electric Polarizations in 2D AFMs

We now apply our electric polarization formalism to predict the consequences of magnon Nernst effects in $MnPS_3$ and $NiPSe_3$, which are 2D honeycomb AFMs possessing Néel and Zigzag order as shown in Fig. 2 *C* and *D*, respectively. We emphasize that our formalism is not limited to these materials or to thermal effects, but the thermal effects in these materials provide valuable examples for two reasons. First, as we show in this section, they allow us to more clearly see and understand the spin and orbital contributions to the resulting electric polarization. Second, as we show in Section 4, they allow us to analyze the importance of symmetry breaking to the emergence of net electric polarization.

Both $MnPS_3$ and $NiPSe_3$ have spins that lie on A and B sublattices with $\boldsymbol{S}_A = -\boldsymbol{S}_B = S\hat{\boldsymbol{z}}$; the z-axis is out of the plane of the 2D material, as shown in Fig. 2*A*. The fundamental spin Hamiltonian for this type of system can be expressed as follows (39, 41, 44):

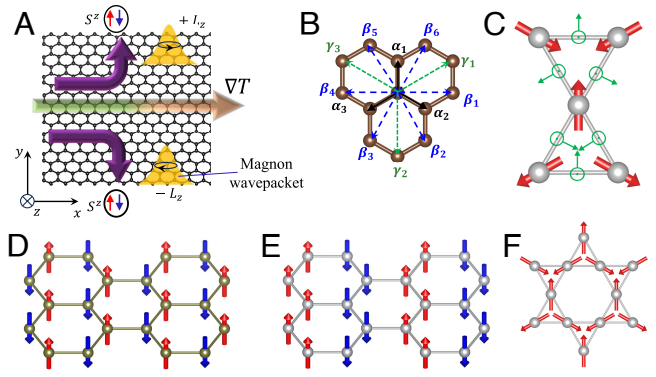

Fig. 2. (*A*) Schematic view of the magnon Orbital Nernst effect in a 2D AFM where transverse flow of magnons carrying opposite out-of-the plane orbital moment is induced by temperature gradient ∇T along the longitudinal direction. (*B*) The nearest, second-nearest, and third-nearest neighbor bonds in a honeycomb lattice are denoted by α_i, β_i and γ_i, respectively. (*C*) The Kagomé spin lattice of potassium iron jarosite with DMI vectors that have both in-plane (arrow) and out-of-plane ($\odot$) components shown in green. (*D*) Néel and (*E*) Zigzag ordering of honeycomb spin lattices. (*F*) The Kagomé spin lattice of potassium iron jarosite.

$$H = \sum_{i,j} J_{ij} \boldsymbol{S}_i \cdot \boldsymbol{S}_j + \Delta \sum_i \left(S_i^z\right)^2 + g\mu_B B_z \sum_i S_i^z + \sum_{\langle\langle i,j \rangle\rangle} \boldsymbol{D}_{ij} \left(\boldsymbol{S}_i \times \boldsymbol{S}_j\right), \quad [14]$$

where $\boldsymbol{S}_i = (S_i^x, S_i^y, S_i^z)$ is the operator of total spin localized at a site i of the lattice. The first term represents the exchange energy, with J_{ij} the exchange coupling between spins localized at sites i and j. The sum $\sum_{ij}$ runs over all atom pairs in the lattice up to the third-nearest neighbor, as shown in Fig. 2*B*. The second term involves Δ, the easy-axis anisotropy energy. The third term represents the Zeeman energy arising from coupling to the applied magnetic field B_z pointing along the z-axis, which is perpendicular to the plane. Here g is the Landé g-factor and μ_B is the Bohr magneton. The fourth term captures the Dzyaloshinskii–Moriya interaction with the DM vector $\boldsymbol{D}_{ij}$ oriented in the z-direction. The notation $\langle\langle , \rangle\rangle$ indicates a summation over second-nearest neighbors.

We employ the Holstein–Primakoff transformation (74) to recast the spin Hamiltonian as a bosonic Bogoliubov-de Gennes (BdG) Hamiltonian (35) $H = \sum_{\boldsymbol{k}} \Psi^\dagger H_{\boldsymbol{k}} \Psi$, where $\Psi^\dagger = [x^\dagger_{\boldsymbol{k},1}, x^\dagger_{\boldsymbol{k},2}, \ldots, x^\dagger_{\boldsymbol{k},n}, x_{-\boldsymbol{k},1}, x_{-\boldsymbol{k},2}, \ldots, x_{-\boldsymbol{k},n}]$ is the Nambu spinor. By using Colpa's method (75), we diagonalize this Hamiltonian to obtain the eigenenergies $E_{n,\boldsymbol{k}}$ and eigenvectors $|n(\boldsymbol{k})\rangle$ of the system, which is what we use in the following to compute the magnon Orbital Nernst effect from linear response theory. Please see *SI Appendix* for additional information on the construction of the BdG Hamiltonian and the magnetic parameters of the materials employed in this model Hamiltonian.

For the specific case of the 2D collinear AFMs we are now considering, and assuming the magnon's spin moment to be a well-defined quantum number, we derive:

$$p_y^S(n,\boldsymbol{k}) = -\frac{g\mu_B}{\hbar W_y c^2 V} \Omega_{xy}^{S^z,n}(\boldsymbol{k}) \, ln \left| e^{-\frac{E_{n,\boldsymbol{k}}}{k_B T}} - 1 \right| k_B T \quad [15]$$

$$p_y^O(n,\boldsymbol{k}) = -\frac{2g\mu_B}{W_y c^2 V} \sigma_3^{nn} S_{nn}^z L_{nn}^z(\boldsymbol{k}) \, \rho_{n,\boldsymbol{k}} \quad [16]$$

as the finite temperature electric polarization induced in the nth band with wave vector $\boldsymbol{k}$ by the magnon spin Berry curvature Eq. **15** and the magnon orbital angular moment Eq. **16**. Here S_{nn}^z and $L_{nn}^z(\boldsymbol{k})$ are, respectively, the spin and OAM of the magnon in the nth band. Eqs. **15** and **16** allow us to more clearly see that 1) the spin current term arises from the spin Berry curvature $[\Omega_{xy}^{S^z,n}(\boldsymbol{k})]$, which is intricately tied to the velocity of the magnon wavepacket's center and 2) the orbital term arises from the intraband OAM of the magnon $[L_{nn}^z(\boldsymbol{k})]$, which arises from the inherent self-rotation of the magnon wavepacket.

We can now apply our theory to explain the electric polarization induced by magnon Nernst effects in $MnPS_3$ and $NiPSe_3$. The presence of a temperature gradient along the x direction leads to the accumulation of magnons with opposite chirality along the $\pm$y boundaries of the system, as schematically depicted in Fig. 3*A*. A quantitative calculation of the resulting net electric polarization for $MnPS_3$ and $NiPSe_3$, as a function of the strength of the DMI, is shown in Fig. 4 *A* and *B*. Remarkably, in the absence of DMI the net electric polarization completely vanishes for both Néel and Zigzag magnetic orders, even in the presence of an externally applied magnetic field, as schematically depicted in Fig. 3*B*. In the presence of DMI, however, a net electric polarization emerges, leading to a measurable transverse voltage as schematically depicted in Fig. 3*C*. We will analyze the importance of DMI to the emergence of a nonzero net electric polarization in Section 4. In the remainder of this section we focus on three important observations about the emergent net electric polarization.

First, we emphasize that the contribution of magnon OAM to electric polarization should not be viewed as a consequence of magnetic dipole moment current circulation. Unlike electrons, which possess charge and whose motion is governed by electric forces, magnons are charge-neutral and their OAM originates solely from the geometric phase. Therefore, the contributions of magnon OAM to electric polarization should be understood as the changes in the magnon spin current due to the geometric phase of the magnon wave function, which adds a correction term (P_y^O) to the electric polarization induced by the magnon spin current (P_y^S) as described by Eqs. **15** and **16**, which are derived quantum mechanically.

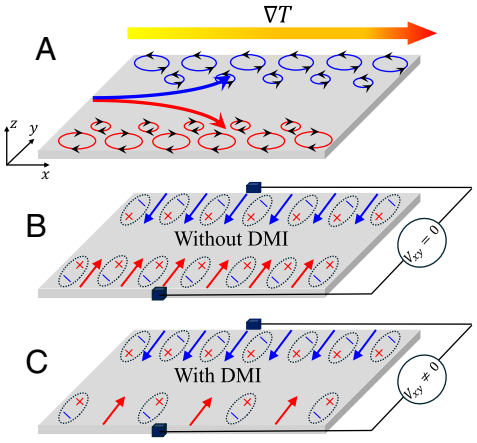

Fig. 3. (*A*) Schematic illustration of magnon orbital accumulation at the edges of a 2D honeycomb AFM with Néel order under an applied temperature gradient ∇T. (*B*) The local electric polarization (red and blue arrow) and local polarized charges induced by magnon spin and magnon orbital angular momentum accumulation due to the magnon Orbital Nernst effect in the absence of the DMI. The number of charges on each side is equal, resulting in zero net electric polarization in the absence of DMI. (*C*) The presence of DMI results in a nonzero net polarized charge due to the difference in the populations of magnons carrying opposite OAM.

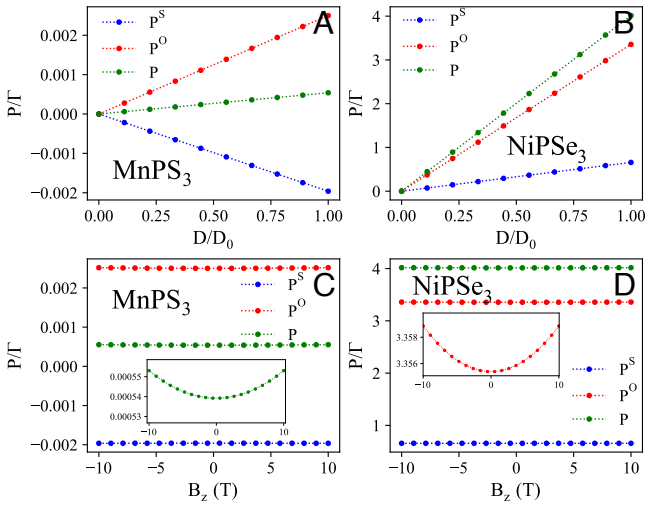

Fig. 4. The electric polarization (P) of $MnPS_3$ (*A*) and $NiPSe_3$ (*B*) normalized to the factor $\Gamma = -\frac{g\mu_B}{hW_y c^2}$. The polarization is plotted as a function of the Dzyaloshinskii–Moriya interaction strength, parameterized by the ratio D/D_0, where D_0 represents the baseline DMI strength for each material. These calculations were conducted under a constant applied magnetic field of $B_z = 1$ *T* and temperature of 100 K. The electric polarization of $MnPS_3$ (*C*) and $NiPSe_3$ (*D*) also varies as a function of the externally applied magnetic field B_z. The *Insets* in both (*C* and *D*) zoom in on the total electric polarization to reveal a weak dependence on B_z. These calculations were conducted for a temperature of 100 K.

Second, and perhaps most importantly, we see that the spin (P_y^S) and orbital (P_y^O) contributions to the overall net electric polarization (P_y) can differ in both sign and magnitude. For $MnPS_3$ (Fig. 4*A*) the magnitudes of the P_y^S and P_y^O terms have opposite sign and similar magnitude, leading to a small nonzero net electric polarization. In contrast, for $NiPSe_3$ (Fig. 4*B*) the spin and orbital contributions have the same sign, but the orbital contribution (P_y^O) is approximately one order of magnitude larger than the spin contribution (P_y^S), leading to a much larger net electric polarization. This striking contrast originates in the fact that the magnon spin angular moment in the systems we consider can only have one of two values: the z-component of spin is locked to the magnon chirality and is independent of the wave vector $\boldsymbol{k}$ (38). In contrast, there is no limit on the OAM of a magnon, as its properties are governed by system symmetry, magnon band hybridization, and interactions with other quasiparticles. As we will discuss in detail in the next section, the symmetry of the Néel order enforces an odd parity of the intraband magnon OAM $L^z_{nn}(\boldsymbol{k})$ with respect to the wave vector $\boldsymbol{k}$. This results in the small P_y^O and the small, though nonzero, net electric polarization. In contrast, the symmetry of Zigzag order permits an even parity of $L^z_{nn}(\boldsymbol{k})$ leading to the significantly larger P_y^O and net electric polarization. Moreover, strong band hybridization can amplify the magnitude of $L^z_{nn}(\boldsymbol{k})$, further enhancing the effect. These findings suggest that identifying materials with appropriate symmetry and the ability to host a large magnon orbital moment could be advantageous for future device applications.

In Fig. 5, assuming $\epsilon_0\chi$ is on the order of 10, we present the transverse voltage V_{xy} induced by the net total electric polarization as a function of the average temperature T for both $MnPS_3$ (Fig. 5*A*) and $NiPSe_3$ (Fig. 5*B*) (for a detailed discussion of the low-temperature regime, please refer to *SI Appendix*, section S3B). One observes that in $MnPS_3$, the transverse voltage is on the order of nanovolts (10^{-9} V), whereas in $NiPSe_3$ it reaches the microvolt range (10^{-6} V). This indicates that the amplitude of the transverse voltage can also be increased by several orders of magnitude by selecting materials with specific symmetries that amplify the orbital moment and spin current. In Section 5, we will show that engineering of magnon band hybridization in noncollinear AFMs with Kagomé structure through the application of an external magnetic field provides another tool that can be used to optimize this effect in noncollinear antiferromagnets, resulting in transverse voltages that are approximately five orders of magnitude larger than that of $MnPS_3$.

4. Symmetry Breaking and Magnon-Induced Electric Polarization

In this section, we investigate the symmetry breaking required for finite magnon-induced net electric polarization (P_y) and a resulting nonzero transverse voltage (V_{xy}) in 2D honeycomb antiferromagnets. We will demonstrate how the Dzyaloshinskii–Moriya interaction breaks mirror symmetry in the spin lattice, thereby enabling a finite net electric polarization.

Fig. 4 shows that total net electric polarization vanishes in the absence of DMI for both Néel and Zigzag magnetic orders. However, the reasons that total net electric polarization vanishes are different for the two orders. To understand this more clearly, in Fig. 6, we plot the Berry curvature, orbital angular moment, orbital Berry curvature, and the correlation $\langle L^z S^z \rangle^n = S^z_{nn} L^z_{nn}(\boldsymbol{k})$ as a function of in-plane wavevector (k_x, k_y) for both $MnPS_3$ (*A*–*D*) and $NiPS_3$ (*E*–*H*). As expected, these plots display, respectively, the C_3 and C_{2b} symmetries of the magnetic structure in the two materials. The orbital Berry curvature of both the Néel and Zigzag phases shows the even parity with respect to the wavevector, which may lead to a finite Orbital Nernst effect.

We first consider $MnPS_3$, which exhibits a Néel-ordered phase. In this material, a finite magnon orbital Nernst effect leads to the accumulation of magnons carrying opposite intraband orbital angular moment at the opposite edges of the system, even in the absence of DMI. This behavior is illustrated in Fig. 7*A*, where we plot the orbital Nernst conductivity of $MnPS_3$ as a function of temperature T with and without DMI. Notably, the spin Nernst current vanishes in this system in the absence of DMI. Even without DMI, the edge accumulation of intraband OAM due to magnon Orbital Nernst effect gives rise to a finite transverse transport of electric polarization, induced purely by magnon OAM without any contribution from the spin Nernst current. This results in the Nernst effect of electric polarization, with

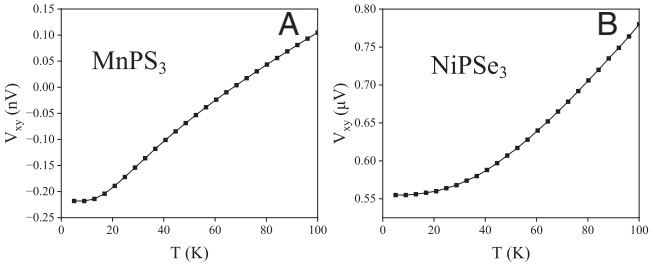

Fig. 5. The transverse voltage V_{xy} induced by the finite total net electric polarization in $MnPS_3$ (*A*) and $NiPSe_3$ (*B*) as a function of the average temperature *T*. The calculations are performed under an applied out-of-plane magnetic field of $Bz = 1$ T.

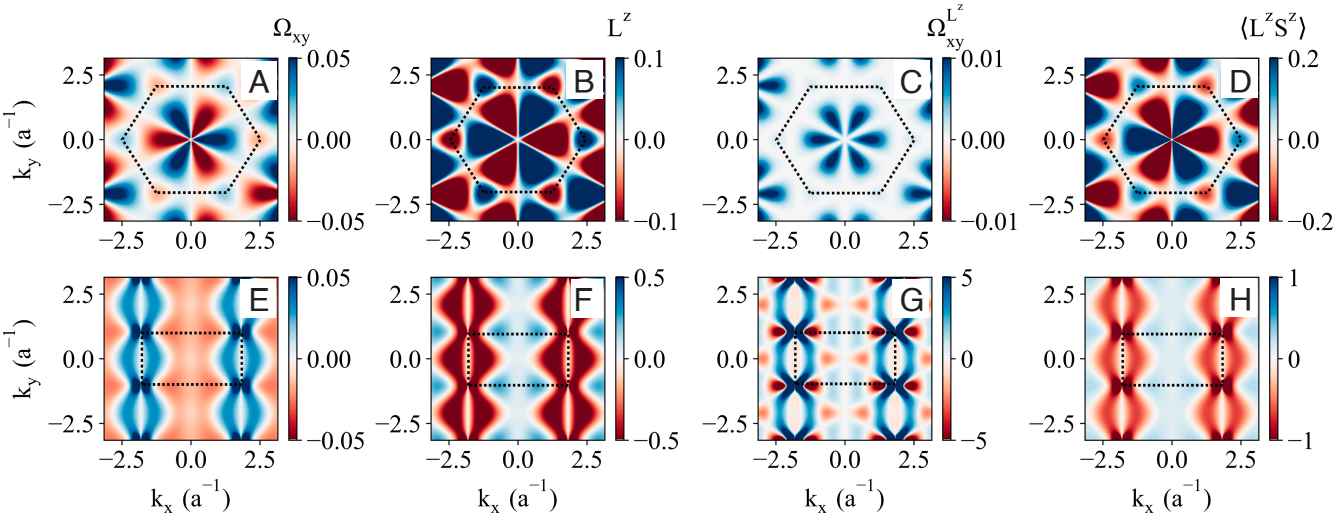

Fig. 6. (*A*) Berry curvature Ω_{xy}; (*B*) out-of-plane orbital angular momentum component L^z; (*C*) orbital Berry curvature $\Omega^{L^z}_{xy}$, and (*D*) correlation $\langle L^z S^z \rangle$ as a function of the in-plane wavevector (k_x, k_y). calculated under an applied magnetic field $B = 1$ *T* for the left-handed magnon mode of $MnPS_3$ with Néel magnetic order. (*E*–*H*) Corresponding results for $NiPSe_3$, which exhibits zigzag magnetic order.

opposite polarization directions accumulated at opposite edges. This phenomenon is depicted in Fig. 7*C*, where we present the electric polarization Nernst conductivity in $MnPS_3$ as a function of temperature T with and without DMI. However, as shown in Eq. **16**, the electric polarization induced by the magnon OAM is governed by the correlation term $S^z_{nn}L^z_{nn}(\boldsymbol{k})$. In the Néel phase, this correlation function is finite but exhibits odd parity with respect to the wavevector $\boldsymbol{k}$, as shown in Fig. 6*D*. This occurs because of the odd parity of the magnon intraband OAM $L^z_{nn}(\boldsymbol{k})$ even in the presence of DMI, as shown in Fig. 6*B*. Without DMI this correlation function maintains its odd parity and the system possesses effective TRS (44), i.e. $E_{n,\boldsymbol{k}} = E_{n,-\boldsymbol{k}}$. In other words, in the absence of DMI the magnon OAM induced electric polarizations accumulated at the edges of $MnPS_3$ are opposite in sign but equal in magnitude, resulting in zero total net electric polarization across the sample regardless of the externally applied magnetic field, as schematically illustrated in Fig. 3*B*. A finite total net electric polarization is only observed in the case of Néel order when DMI breaks the symmetry between magnons carrying opposite intraband OAM, as schematically illustrated in Fig. 3*C*, leading to $E_{n,\boldsymbol{k}} \neq E_{n,-\boldsymbol{k}}$. This disparity in energy levels results in an imbalance in the population at $\boldsymbol{k}$ and $-\boldsymbol{k}$, thereby inducing a finite net electric polarization as shown schematically in Fig. 3*C* and quantitatively in Fig. 4*A*.

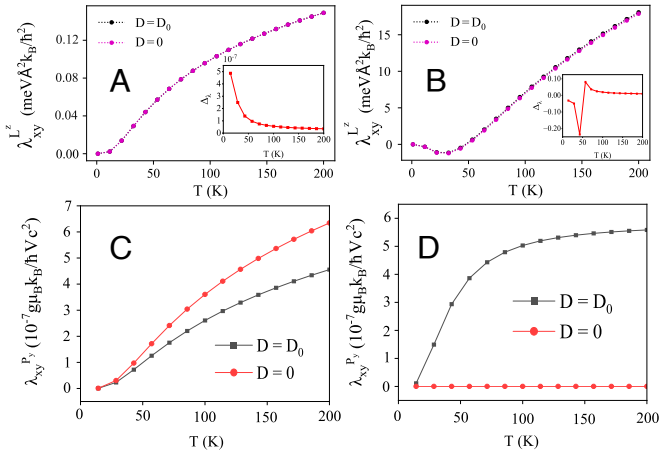

Fig. 7. The Orbital Nernst conductivity of $MnPS_3$ (*A*) and $NiPSe_3$ (*B*) as a function of temperature at fixed applied magnetic field $B_z = 1$ *T*. In (*A* and *B*) the black and pink colors indicate the results calculated with and without DMI, respectively, the *Insets* show the relative difference between the black and pink data points, defined as $\Delta_\lambda = \frac{\lambda^{L^z}_{xy}(D=D_0) - \lambda^{L^z}_{xy}(D=0)}{\lambda^{L^z}_{xy}(D=D_0)}$ plotted as a function of temperature. The electric polarization Nernst conductivity of $MnPS_3$ (*C*) and $NiPSe_3$ (*D*) as a function of temperature at fixed applied magnetic field $B_z = 1$ *T*. In (*C* and *D*) the black and red colors indicate the results calculated with and without DMI, respectively.

We now consider $NiPSe_3$, which has Zigzag order. In contrast to $MnPS_3$, the correlation function of $NiPSe_3$ has even parity with respect to the wavevector in the presence of DMI, as shown in Fig. 6*H*. The even parity leads to a substantial net electric polarization induced by magnons, as shown in Fig. 7*C*. However, in the absence of DMI, the correlation function of the Zigzag phase, given by $\langle L^z S^z \rangle^n = S^z_{nn}L^z_{nn}(\boldsymbol{k})$ vanishes because of vanishing magnon intraband OAM $L^z_{nn}(\boldsymbol{k})$, resulting in zero magnon OAM contribution to the electric polarization. Furthermore, because the spin Nernst current also vanishes when DMI is absent, $p_y(n,\boldsymbol{k}) = p^O_y(n,\boldsymbol{k}) = p^S_y(n,\boldsymbol{k}) = 0$. Consequently, no electric polarization resulting from the magnon Nernst effects occurs in $NiPSe_3$ when the DMI strength is zero, as shown in Fig. 7*D*. Nonzero total net electric polarization is only observed in $NiPSe_3$ when DMI induces a finite magnon intraband OAM along with the finite magnon spin Nernst effect in the system.

To further illustrate the importance of DMI in this picture, we return to Fig. 7, which plots the Orbital Nernst conductivity and electric polarization Nernst conductivity of $MnPS_3$ (*A* and *C*) and $NiPS_3$ (*B* and *D*) as a function of temperature T with and without DMI. We see that the Orbital Nernst conductivity exists even in the absence of DMI, which indicates that the Orbital Nernst effect does not require spin–orbit coupling akin to the Orbital Hall effect predicted for electronic systems (45, 76, 77). This stands in stark contrast to the spin Nernst effect, where DMI is required to observe nonzero spin Nernst effect (38). This disparity arises from the invariance of the systems under the combined $\mathcal{C}_S\mathcal{M}_x\mathcal{T}_a$ symmetry, where $\mathcal{C}_S$ is the spin rotation symmetry operation which flips all the spins (and magnetic fields)

in the system, $\mathcal{M}_x$ represents mirror symmetry with respect to the plane perpendicular to the x-axis, and $\mathcal{T}_a$ denotes the translation operator responsible for displacing the system by the vector $\boldsymbol{\beta}_1$ or $\boldsymbol{\beta}_4$ (Fig. 2*B*). The Orbital Nernst effect does not require the breaking of $\mathcal{C}_S\mathcal{M}_x\mathcal{T}_a$ symmetry, primarily because the OAM is not preserved under noncommutative rotation and translation operations. Consequently, the Orbital Nernst conductivity has nonzero values whether or not DMI is present to break $\mathcal{C}_S\mathcal{M}_x\mathcal{T}_a$ symmetry, as illustrated in Fig. 7 *A* and *B*. However, when the $\mathcal{C}_S\mathcal{M}_x\mathcal{T}_a$ symmetry is preserved, the spin polarized current along the y-direction $j_y^{s_z}$ must vanish (please see *SI Appendix* for further detail). In other words, regardless of the externally applied magnetic field, magnon Orbital Nernst effect does not induce a transverse spin-polarized current in the absence of DMI. Only when the presence of DMI breaks the $\mathcal{C}_S\mathcal{M}_x\mathcal{T}_a$ symmetry does a finite transverse spin-polarized current emerge within the system as a result of the Spin Nernst effect. The finite Spin Nernst effect in the presence of DMI coupled with finite Orbital Nernst effect results in the observable total net electric polarization as shown in Fig. 4 *A* and *B*. Meanwhile, as expected, the total net electric polarization vanishes when DMI is turned off.

The Nernst effect of electric polarization in $MnPS_3$ exhibits the same behavior as the magnon Orbital Nernst effect in this material, remaining finite even in the absence of DMI ($D = 0$, see Fig. 7*C*). Turning on the DMI leads to an observable reduction in the electric polarization Nernst conductivity, in contrast to the weak dependence of the Orbital Nernst conductivity on DMI in this material. This difference arises because the electric polarization Nernst conductivity in $MnPS_3$ is governed by both the spin Nernst current and the magnon intraband OAM, whose contributions are of the same order of magnitude, but opposite in sign, as shown in Fig. 4 *A* and *C*. In contrast, as shown in Fig. 7*D*, the electric polarization Nernst conductivity in $NiPSe_3$ vanishes in the absence of DMI due to the absence of intraband magnon OAM, as discussed earlier. The introduction of DMI induces a finite electric polarization Nernst conductivity in $NiPSe_3$. Notably, despite the fact that the Orbital Nernst conductivity in $NiPSe_3$ is two-order-of magnitude larger than in $MnPS_3$, the electric polarization Nernst conductivity in both materials remains of the same order. This discrepancy arises because the Orbital Nernst conductivity in $MnPS_3$ originates solely from intraband magnon OAM, whereas in $NiPSe_3$ the Orbital Nernst conductivity receives contributions from both interband and intraband OAM. In the absence of DMI, the intraband OAM in $NiPSe_3$ vanishes, leaving only the interband OAM to contribute. Consequently, the contribution of intraband OAM to the Orbital Nernst conductivity in $NiPSe_3$ can be estimated by subtracting the Orbital Nernst conductivity values with and without DMI, yielding a magnitude comparable to the Orbital Nernst conductivity in $MnPS_3$. This explains why the electric polarization Nernst conductivity in $MnPS_3$ and $NiPSe_3$ are of the same order, as shown in Fig. 7 *C* and *D*. In these materials, the electric polarization Nernst conductivity is determined solely by the magnon intraband OAM, given that the magnon's spin moment S^z is a well-defined quantum number.

The dependence of the total net electric polarization on the magnitude of the DMI strength, which is reported in Fig. 4 *A* and *B*, can also be understood from a symmetry perspective. In the absence of DMI, the magnetic point group of $MnPS_3$ and $NiPSe_3$ are 2'/m and 2/m' respectively. These magnetic point groups are nonpolar, which prohibits the existence of a finite total net electric polarization in these materials. However, the presence of DMI lowers the symmetry of the system, thereby allowing a finite total net electric polarization to emerge. Indeed, in the absence of DMI and externally applied magnetic field, the system maintains mirror symmetry ($\mathcal{M}_y$) for Néel order and glide mirror symmetry ($\mathcal{M}_y\tau$) for Zigzag order about the plane normal to the y-direction. Because the systems hold this symmetry, $P_y \equiv -P_y$, which means that P_y must vanish. The presence of an externally applied magnetic field breaks the mirror and glide mirror symmetry, but it does not induce any coupling between different magnon bands and therefore the wave functions are unchanged. The relation $E_{n,\boldsymbol{k}} = E_{n,-\boldsymbol{k}}$ is maintained, which means P_y remains zero despite the presence of the externally applied magnetic field when DMI is absent ($D/D_0 = 0$ as shown in Fig. 4 *A* and *B*). However, the presence of DMI breaks the $\mathcal{M}_y$ symmetry and yields $E_{n,\boldsymbol{k}} \neq E_{n,-\boldsymbol{k}}$ (78, 79), thereby allowing the nonzero P_y shown in Fig. 4 *A* and *B*.

In Fig. 4 *C* and *D* we present the dependence of the electric polarization on B_z, the magnetic field externally applied along the z-direction. The total net electric polarization P_y, along with its constituents from spin current P_y^S and orbital angular moment P_y^O, exhibit relatively small variations as a function of the magnetic field. The magnetic field has minimal impact because it splits the magnon bands corresponding to opposite spins without inducing any coupling between these distinct bands. Consequently, the weak response of the electric polarizations to the magnetic field B_z arises solely from changes in the magnon population $\rho_{n,\boldsymbol{k}}$ and the function $ln\left|e^{-\frac{E_{n,\boldsymbol{k}}}{k_BT}} - 1\right|$ in Eq. **15**, which are due to the shift in the magnon energy band caused by the Zeeman interaction between local spins and externally applied magnetic field. Crucially, all components remain finite even at zero magnetic field, suggesting the potential feasibility of detecting the magnon Orbital Nernst effect even in the absence of an external magnetic field.

We conclude this section with three notes about the possibility of observing the predicted effects in realistic materials. First, we note that the net electric polarization in $MnPS_3$ is approximately three orders of magnitude smaller than that in $NiPSe_3$. Additionally, the net electric polarization in $NiPSe_3$ is predominantly influenced by magnon orbital angular moment, whereas in $MnPS_3$ both the spin Berry curvature and magnon OAM contribute equally to the net electric polarization. This indicates that the measurement of net electric polarization in the Zigzag order of $NiPSe_3$ would provide direct evidence of magnon OAM and orbital Nernst effect in this material. Second, in the system considered here the DMI is oriented along the z-axis (out of plane), which means it cannot introduce scattering between magnons. In *SI Appendix*, section S7 we consider what would happen in materials for which this is not the case. Finally, we note that the interaction between magnons and phonons in collinear 2D antiferromagnets can break the mirror symmetry in the spin lattice in a manner similar to the Dzyaloshinskii–Moriya interaction. These effects may also lead to a finite contribution from magnon Orbital Nernst effect to the net electric polarization in these material systems.

5. Hybridization of Magnon Bands and Magnon-Induced Electric Polarization

We turn now to a study of the manipulation of magnon band hybridization to enhance the total net electric polarization magnitude. For that purpose we consider a noncollinear antiferromagnet with a Kagomé lattice structure; see Fig. 2*F* for

an illustration of one possible Néel state for such a structure. In the classical limit, all Kagomé lattice ground states have a structure in which the angle between each nearest neighbor spin pair is about 120°. Specifically, Fig. 2*F* shows a $\boldsymbol{q} = 0$ type ordering of a Kagomé jarosite with positive chirality (80–82). At low temperature, typically below the Néel temperature T_N ($T_N = 65\ K$ for potassium iron jarosite) the magnetic interactions in this lattice can be well described by the following Hamiltonian (40, 82–84)

$$H = J_1 \sum_{\langle i,j \rangle} \boldsymbol{S}_i \cdot \boldsymbol{S}_j + J_2 \sum_{\langle\langle i,j \rangle\rangle} \boldsymbol{S}_i \cdot \boldsymbol{S}_j + \sum_{\langle i,j \rangle} \boldsymbol{D}_{ij} \cdot \left(\boldsymbol{S}_i \times \boldsymbol{S}_j\right) - g\mu_B B_z \sum_i S_i^z, \qquad [17]$$

where the first and second terms represent the nearest-neighbor and next-nearest-neighbor antiferromagnetic interactions, respectively. The third term describes the Dzyaloshinskii–Moriya interaction, characterized by the DM vector $\boldsymbol{D}_{ij}$, which includes both in-plane (D_p) and out-of-plane (D_z) components for the bond (i,j). Here the out-of-plane component (D_z) stabilizes the 120° coplanar $\boldsymbol{q} = 0$ spin structure. When $D_z = 0$, the coplanar structure can still be stabilized by the next-nearest neighbor interaction J_2. In contrast, the in-plane component (D_p) breaks both the mirror symmetry with respect to the Kagomé plane and the global spin rotation symmetry. This in-plane component induces a canting of the spins out of the plane. The canting angle η is determined by minimizing the classical energy of the spin system in the Kagomé AFM, which is given by

$$\frac{E(\eta)}{NS^2} = \frac{1}{2}(J_1 + J_2)[3\cos(2\eta) - 1] - \sqrt{3}D_z \cos^2(\eta) - \sqrt{3}D_p \sin(2\eta) - \frac{\sin(\eta)\, g\mu_B}{S} B_z. \qquad [18]$$

Minimizing this energy would lead to a solution of

$$0 = \frac{1}{NS^2}\frac{\partial E(\eta)}{\partial \eta} = -3(J_1 + J_2)\sin(2\eta) + \sqrt{3}D_z \sin(2\eta) - 2\sqrt{3}D_p \cos(2\eta) - \frac{\cos(\eta)\, g\mu_B}{S} B_z. \qquad [19]$$

In the absence of an externally applied magnetic field, one obtains:

$$\eta = \frac{1}{2}\tan^{-1}\left[\frac{-2D_p}{\sqrt{3}(J_1 + J_2) - D_z}\right] \qquad [20]$$

When the applied magnetic field is present, this angle is given (to first order and for small η) by

$$\eta = \frac{-g\mu_B B/S - 2\sqrt{3}D_p}{6(J_1 + J_2) - 2\sqrt{3}D_z} \qquad [21]$$

The canted spin configuration induces weak out-of-plane ferromagnetism, resulting in a finite in-plane electric polarization P_y. Unlike 2D collinear honeycomb AFMs, where S^z remains a good quantum number, the presence of in-plane DMI leads to magnon band hybridization, making S^z no longer well-defined. Consequently, we employ Eqs. **9** and **10** to compute the magnon-induced electric polarization in these systems.

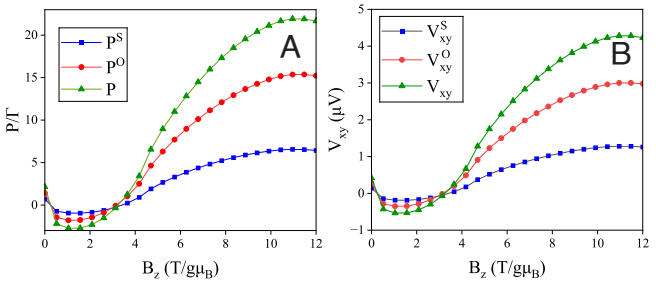

Fig. 8. The total electric polarization P (*A*) and the corresponding transverse voltage V_{xy} (*B*) are shown as functions of the externally applied magnetic field along the z-direction, expressed in units of $T/g\mu_B$. The individual contributions from the magnon orbital angular moment (P^O, V_{xy}^O) and spin current (P^S, V_{xy}^S) are also presented. The calculated electric polarizations are normalized by the factor $\Gamma = -\frac{g\mu_B}{\hbar W_y c^2}$.

Fig. 8 illustrates the dependence of the total net electric polarization and associated transverse voltage in $KFe_3(OH)_6(SO_4)_2$ on the externally applied magnetic field. The contributions from the magnon orbital moment and magnon spin current are shown separately. The net electric polarization and voltage induced by magnons in this system is proportional to the canting angle, which determines the out-of-plane magnetic moment. The external magnetic field not only shifts the magnon energy levels, but also acts as an effective DMI. From Eq. **21**, we observe that varying the field modifies the canting angle, thereby altering both the in-plane and out-of-plane DMI components and, in turn, affecting the strength of magnon band hybridization. As a result, the contributions from both the magnon orbital moment and the magnon spin Nernst current to the total electric polarization and voltage vary with the applied field, driven by the enhanced canting angle and changes in magnon band coupling. Notably, at $B_z = 11\ T/g\mu_B$ this effect leads to approximately an order of magnitude increase in polarization and voltage compared to the zero-field case.

Importantly, within the considered magnetic field range the magnon orbital moment emerges as the dominant contributor to electric polarization and voltage. This suggests that measuring the transverse voltage in this regime could provide direct evidence of the Orbital Nernst effect of magnons in the system. Even more strikingly, at $B_z = 9T/g\mu_B$ the transverse voltage in $KFe_3(OH)_6(SO_4)_2$ is about five orders of magnitude larger than in $MnPS_3$, highlighting the potential for significantly enhanced magnon-driven electric responses in this material by using external magnetic field to control magnon hybridization.

6. Conclusion and Outlook

In summary, we present a formalism that allows us to connect measurable quantities, namely electric polarization and transverse voltage, to magnon spin and orbital moment transport. This framework provides a robust theoretical foundation for studying magnon transport phenomena and their observable effects on electric polarization. Equally importantly, this framework reveals material design strategies that can be employed to enhance electric polarization for practical applications involving magnon spin and orbital degrees of freedom. We introduce the representation of magnon OAM within the Bloch wavefunction, establishing a profound connection between magnon intraband OAM and magnon Berry curvature. We also present a full quantum mechanical derivation of the electric polarization induced by magnon OAM and magnon spin current. We then apply

our formalism to phenomena, specifically the Magnon Orbital Nernst Effect and Magnon Spin Nernst Effect, in 2D AFMs exhibiting either Zigzag or Néel order on the honeycomb lattice. We demonstrate that materials with Néel order and/or Zigzag order in combination with DMI can generate a nonzero net electric polarization and thus a measurable transverse voltage. Using the noncollinear AFM $KFe_3(OH)_6(SO_4)_2$ as an example, we show that the net electric polarization can be enhanced by an order of magnitude through controlled magnon band hybridization via an external magnetic field. This serves as a means to detect the accumulation of magnon spin and magnon OAM at system edges as a result of magnon Nernst effects. These intriguing findings point the way toward experimental validation of the predicted magnon Spin Nernst effect and magnon Orbital Nernst effect phenomenon in magnetic systems. They may also catalyze further exploration of the emerging field of magnon orbitronics and magnon spinorbitronics. Finally, it is important to highlight that while our work primarily focuses on generating magnon Nernst effects through thermal mechanisms, its implications extend beyond this scope. Specifically, our results suggest that, despite being electrically neutral, magnons can interact with electromagnetic waves via the electric field component of light. Our theory shows that both the spin and orbital moments of magnons contribute to their electric activity. Consequently, we anticipate that light can transfer its angular moment into that of magnons. This insight suggests the possibility of future research on light-driven magnon dynamics in magnetic materials, leveraging the spin and orbital angular moment degrees of freedom of magnons.

Data, Materials, and Software Availability. All study data are included in the article and/or *SI Appendix*.

ACKNOWLEDGMENTS. This research was primarily supported by NSF through the University of Delaware Materials Research Science and Engineering Center, DMR-2011824.

Author affiliations: [a]Department of Materials Science and Engineering, University of Delaware, Newark, DE 19716; [b]Department of Physics and Astronomy, University of Delaware, Newark, DE 19716; [c]Nanoscale Device Characterization Division, Joint Quantum Institute, National Institute of Standards and Technology, Gaithersburg, MD 20899-8423; and [d]Joint Quantum Institute, University of Maryland, College Park, MD 20742

Author contributions: D.Q.T. and M.F.D. designed research; D.Q.T., F.G.-G., and M.F.D. performed research; D.Q.T., Y.R., J.M.O.Z., M.B.J., J.Q.X., B.K.N., G.W.B., and M.F.D. analyzed data; and D.Q.T., B.K.N., G.W.B., and M.F.D. wrote the paper.

1. A. V. Chumak, V. I. Vasyuchka, A. A. Serga, B. Hillebrands, Magnon spintronics. *Nat. Phys.* **11**, 453–461 (2015).
2. P. Pirro, V. I. Vasyuchka, A. A. Serga, B. Hillebrands, Advances in coherent magnonics. *Nat. Rev. Mater.* **6**, 1114–1135 (2021).
3. B. Flebus *et al*., The 2024 magnonics roadmap. *J. Phys. Condens. Matter* **36**, ead399c (2024).
4. Y. Kajiwara *et al*., Transmission of electrical signals by spin-wave interconversion in a magnetic insulator. *Nature* **464**, 262–266 (2010).
5. R. Lebrun *et al*., Tunable long-distance spin transport in a crystalline antiferromagnetic iron oxide. *Nature* **561**, 222–225 (2018).
6. W. Xing *et al*., Magnon transport in quasi-two-dimensional Van der Waals antiferromagnets. *Phys. Rev. X* **9**, 011026 (2019).
7. B. Bhoi, S. K. Kim, Photon-magnon coupling: Historical perspective, status, and future directions. *Solid State Phys.* **70**, 1–77 (2019).
8. I. A. Golovchanskiy *et al*., Ultrastrong photon-to-magnon coupling in multilayered heterostructures involving superconducting coherence via ferromagnetic layers. *Sci. Adv.* **7**, eabe8638 (2021).
9. E. Carpene *et al*., Dynamics of electron-magnon interaction and ultrafast demagnetization in thin iron films. *Phys. Rev. B* **78**, 174422 (2008).
10. N. Rohling, E. L. Fjærbu, A. Brataas, Superconductivity induced by interfacial coupling to magnons. *Phys. Rev. B* **97**, 115401 (2018).
11. K. Mæland, H. I. Røst, J. W. Wells, A. Sudbø, Electron-magnon coupling and quasiparticle lifetimes on the surface of a topological insulator. *Phys. Rev. B* **104**, 125125 (2021).
12. T. T. Mai *et al*., Magnon-phonon hybridization in 2D antiferromagnet $MnPSe_3$. *Sci. Adv.* **7**, eabj3106 (2021).
13. M. E. Manley *et al*., Hybrid magnon-phonon localization enhances function near ferroic glassy states. *Sci. Adv.* **10**, eadn2840 (2024).
14. D. Q. To *et al*., Hybridized magnonic materials for Thz frequency applications. *Appl. Phys. Lett.* **124**, e0189678 (2024).
15. A. T. Costa, M. I. Vasilevskiy, J. Fernández-Rossier, N. M. Peres, Strongly coupled magnon-plasmon polaritons in graphene-two-dimensional ferromagnet heterostructures. *Nano Lett.* **23**, 4510–4515 (2023).
16. A. Dyrdał, A. Qaiumzadeh, A. Brataas, J. Barnaś, Magnon-plasmon hybridization mediated by spin-orbit interaction in magnetic materials. *Phys. Rev. B* **108**, 045414 (2023).
17. Y. J. Bae *et al*., Exciton-coupled coherent magnons in a 2D semiconductor. *Nature* **609**, 282–286 (2022).
18. T. Wang *et al*., Magnetically-dressed CrSBr exciton-polaritons in ultrastrong coupling regime. *Nat. Commun.* **14**, 5966 (2023).
19. G. M. Diederich *et al*., Tunable interaction between excitons and hybridized magnons in a layered semiconductor. *Nat. Nanotechnol.* **18**, 23–28 (2023).
20. Y. Tabuchi *et al*., Coherent coupling between a ferromagnetic magnon and a superconducting qubit. *Science* **349**, 405–408 (2015).
21. D. Lachance-Quirion *et al*., Entanglement-based single-shot detection of a single magnon with a superconducting qubit. *Science* **367**, 425–428 (2020).
22. S. P. Wolski *et al*., Dissipation-based quantum sensing of magnons with a superconducting qubit. *Phys. Rev. Lett.* **125**, 117701 (2020).
23. H. Yuan, Y. Cao, A. Kamra, R. A. Duine, P. Yan, Quantum magnonics: When magnon spintronics meets quantum information science. *Phys. Rep.* **965**, 1–74 (2022).
24. D. Xu *et al*., Quantum control of a single magnon in a macroscopic spin system. *Phys. Rev. Lett.* **130**, 193603 (2023).
25. M. Fukami *et al*., Magnon-mediated qubit coupling determined via dissipation measurements. *Proc. Natl. Acad. Sci. U.S.A.* **121**, e2313754120 (2024).
26. M. Bejarano *et al*., Parametric magnon transduction to spin qubits. *Sci. Adv.* **10**, eadi2042 (2024).
27. M. Dols *et al*., Magnon-mediated quantum gates for superconducting qubits. *Phys. Rev. B* **110**, 104416 (2024).
28. J. Xiao, G. E. W. Bauer, K. C. Uchida, E. Saitoh, S. Maekawa, Theory of magnon-driven spin Seebeck effect. *Phys. Rev. B* **81**, 214418 (2010).
29. Y. Onose *et al*., Observation of the magnon Hall effect. *Science* **329**, 297–299 (2010).
30. H. Katsura, N. Nagaosa, P. A. Lee, Theory of the thermal Hall effect in quantum magnets. *Phys. Rev. Lett.* **104**, 066403 (2010).
31. R. Matsumoto, R. Shindou, S. Murakami, Thermal Hall effect of magnons in magnets with dipolar interaction. *Phys. Rev. B* **89**, 054420 (2014).
32. M. Hirschberger, R. Chisnell, Y. S. Lee, N. P. Ong, Thermal Hall effect of spin excitations in a Kagome magnet. *Phys. Rev. Lett.* **115**, 106603 (2015).
33. S. Murakami, A. Okamoto, Thermal Hall effect of magnons. *J. Phys. Soc. Jpn.* **86**, 011010 (2017).
34. X. Zhang, Y. Zhang, S. Okamoto, D. Xiao, Thermal Hall effect induced by magnon-phonon interactions. *Phys. Rev. Lett.* **123**, 167202 (2019).
35. S. Park, N. Nagaosa, B. J. Yang, Thermal Hall effect, spin nernst effect, and spin density induced by a thermal gradient in collinear ferrimagnets from magnon-phonon interaction. *Nano Lett.* **20**, 2741–2746 (2020).
36. R. R. Neumann, A. Mook, J. Henk, I. Mertig, Thermal Hall effect of magnons in collinear antiferromagnetic insulators: Signatures of magnetic and topological phase transitions. *Phys. Rev. Lett.* **128**, 117201 (2022).
37. J. N. Kløgetvedt, A. Qaiumzadeh, Tunable topological magnon-polaron states and intrinsic anomalous hall phenomena in two-dimensional ferromagnetic insulators. *Phys. Rev. B* **108**, 224424 (2023).
38. R. Cheng, S. Okamoto, D. Xiao, Spin Nernst effect of magnons in collinear antiferromagnets. *Phys. Rev. Lett.* **117**, 217202 (2016).
39. V. A. Zyuzin, A. A. Kovalev, Magnon spin Nernst effect in antiferromagnets. *Phys. Rev. Lett.* **117**, 217203 (2016).
40. B. Li, S. Sandhoefner, A. A. Kovalev, Intrinsic spin Nernst effect of magnons in a noncollinear antiferromagnet. *Phys. Rev. Res.* **2**, 013079 (2020).
41. N. Bazazzadeh *et al*., Magnetoelastic coupling enabled tunability of magnon spin current generation in two-dimensional antiferromagnets. *Phys. Rev. B* **104**, L180402 (2021).
42. N. Bazazzadeh *et al*., Symmetry enhanced spin-nernst effect in honeycomb antiferromagnetic transition metal trichalcogenide monolayers. *Phys. Rev. B* **103**, 014425 (2021).
43. H. Zhang, R. Cheng, A perspective on magnon spin Nernst effect in antiferromagnets. *Appl. Phys. Lett.* **120**, e2833021 (2022).
44. D. Q. To *et al*., Giant spin nernst effect in a two-dimensional antiferromagnet due to magnetoelastic coupling induced gaps and interband transitions between magnonlike bands. *Phys. Rev. B* **108**, 085435 (2023).
45. D. Go, D. Jo, C. Kim, H. W. Lee, Intrinsic spin and Orbital Hall effects from orbital texture. *Phys. Rev. Lett.* **121**, 086602 (2018).
46. D. Go, H. W. Lee, Orbital torque: Torque generation by orbital current injection. *Phys. Rev. Res.* **2**, 013177 (2020).
47. D. Go *et al*., Theory of current-induced angular momentum transfer dynamics in spin-orbit coupled systems. *Phys. Rev. Res.* **2**, 033401 (2020).
48. D. Go *et al*., Long-range orbital torque by momentum-space hotspots. *Phys. Rev. Lett.* **130**, 246701 (2023).
49. Y. G. Choi *et al*., Observation of the orbital Hall effect in a light metal Ti. *Nature* **619**, 52–56 (2023).
50. I. Lyalin, S. Alikhah, M. Berritta, P. M. Oppeneer, R. K. Kawakami, Magneto-optical detection of the Orbital Hall Effect in Chromium. *Phys. Rev. Lett.* **131**, 156702 (2023).
51. T. S. Seifert *et al*., Time-domain observation of ballistic orbital-angular-momentum currents with giant relaxation length in tungsten. *Nat. Nanotechnol.* **18**, 1132–1138 (2023).
52. M. B. Jungfleisch, Observation of ultrafast ballistic orbital transport. *Nat. Nanotechnol.* **18**, 1124–1125 (2023).
53. C. Jia, D. Ma, A. F. Schäffer, J. Berakdar, Twisted magnon beams carrying orbital angular momentum. *Nat. Commun.* **10**, 2077 (2019).

54. R. R. Neumann, A. Mook, J. Henk, I. Mertig, Orbital magnetic moment of magnons. *Phys. Rev. Lett.* **125**, 117209 (2020).
55. R. S. Fishman, J. S. Gardner, S. Okamoto, Orbital angular momentum of magnons in collinear magnets. *Phys. Rev. Lett.* **129**, 167202 (2022).
56. R. S. Fishman, L. Lindsay, S. Okamoto, Exact results for the orbital angular momentum of magnons on honeycomb lattices. *J. Phys. Condens. Matter* **51**, 015801 (2022).
57. R. S. Fishman, Gauge-invariant measure of the magnon orbital angular momentum. *Phys. Rev. B* **107**, 214434 (2023).
58. R. S. Fishman, T. Berlijn, J. Villanova, L. Lindsay, Magnon orbital angular momentum of ferromagnetic honeycomb and zigzag lattice models. *Phys. Rev. B* **108**, 214402. (2023).
59. G. Go, D. An, H. W. Lee, S. K. Kim, Magnon orbital nernst effect in honeycomb antiferromagnets without spin-orbit coupling. *Nano Lett.* **24**, 5968–5974 (2024).
60. L. C. Zhang *et al*., Orbital Nernst effect of magnons. arXiv [Preprint] (2019). http://arxiv.org/abs/1910.03317 (Accessed 15 October 2019).
61. Lc. Zhang *et al*., Imprinting and driving electronic orbital magnetism using magnons. *Commun. Phys.* **3**, 227 (2020).
62. R. Matsumoto, S. Murakami, Theoretical prediction of a rotating magnon wave packet in ferromagnets. *Phys. Rev. Lett.* **106**, 197202 (2011).
63. D. Xiao, M. C. Chang, Q. Niu, Berry phase effects on electronic properties. *Rev. Mod. Phys.* **82**, 1959–2007 (2010).
64. G. Go, S. K. Kim, K. J. Lee, Topological magnon-phonon hybrid excitations in two-dimensional ferromagnets with tunable Chern numbers. *Phys. Rev. Lett.* **123**, 237207 (2019).
65. S. Zhang, G. Go, K. J. Lee, S. K. Kim, Su(3) topology of magnon-phonon hybridization in 2D antiferromagnets. *Phys. Rev. Lett.* **124**, 147204 (2020).
66. S. A. Díaz, J. Klinovaja, D. Loss, Topological magnons and edge states in antiferromagnetic Skyrmion crystals. *Phys. Rev. Lett.* **122**, 187203 (2019).
67. E. Viñas Boström *et al*., Direct optical probe of magnon topology in two-dimensional quantum magnets. *Phys. Rev. Lett.* **130**, 026701 (2023).
68. S. Liu *et al*., Direct observation of magnon-phonon strong coupling in two-dimensional antiferromagnet at high magnetic fields. *Phys. Rev. Lett.* **127**, 097401 (2021).
69. S. Ding *et al*., Harnessing orbital-to-spin conversion of interfacial orbital currents for efficient spin-orbit torques. *Phys. Rev. Lett.* **125**, 177201 (2020).
70. T. Li *et al*., Giant orbital-to-spin conversion for efficient current-induced magnetization switching of ferrimagnetic insulator. *Nano Lett.* **23**, 7174–7179 (2023).
71. L. Alahmed *et al*., Evidence of magnon-mediated orbital magnetism in a quasi-2D topological magnon insulator. *Nano Lett.* **22**, 5114–5119 (2022).
72. L. Huang *et al*., Orbital current pumping from ultrafast light-driven antiferromagnetic insulator. *Adv. Mater.* **37**, 2402063 (2025).
73. R. R. Neumann, J. Henk, I. Mertig, A. Mook, Electrical activity of topological chiral edge magnons. *Phys. Rev. B* **109**, L180412 (2024).
74. T. Holstein, H. Primakoff, Field dependence of the intrinsic domain magnetization of a ferromagnet. *Phys. Rev.* **58**, 1098–1113 (1940).
75. J. Colpa, Diagonalization of the quadratic boson hamiltonian. *Phys. Stat. Mech. Appl.* **93**, 327–353 (1978).
76. B. A. Bernevig, T. L. Hughes, S. C. Zhang, Orbitronics: The intrinsic orbital current in *p*-doped silicon. *Phys. Rev. Lett.* **95**, 066601 (2005).
77. D. Go, D. Jo, H. W. Lee, M. Kläui, Y. Mokrousov, Orbitronics: Orbital currents in solids. *Europhys. Lett.* **135**, 37001 (2021).
78. K. H. Lee, S. B. Chung, K. Park, J. G. Park, Magnonic quantum spin hall state in the zigzag and stripe phases of the antiferromagnetic honeycomb lattice. *Phys. Rev. B* **97**, 180401 (2018).
79. D. Ghader, A. Khater, A new class of nonreciprocal spin waves on the edges of 2D antiferromagnetic honeycomb nanoribbons. *Sci. Rep.* **9**, 15220 (2019).
80. D. Grohol *et al*., Spin chirality on a two-dimensional frustrated lattice. *Nat. Mater.* **4**, 323–328 (2005).
81. T. Yildirim, A. B. Harris, Magnetic structure and spin waves in the kagomé jarosite compound $Kfe_3(SO_4)_2(OH)_6$. *Phys. Rev. B* **73**, 214446 (2006).
82. K. Matan *et al*., Spin waves in the frustrated kagomé lattice antiferromagnet $Kfe_3(OH)_6(SO_4)_2$. *Phys. Rev. Lett.* **96**, 247201 (2006).
83. P. Laurell, G. A. Fiete, Magnon thermal hall effect in kagome antiferromagnets with dzyaloshinskii-moriya interactions. *Phys. Rev. B* **98**, 094419 (2018).
84. Y. Lu, X. Guo, V. Koval, C. Jia, Topological thermal hall effect driven by spin-chirality fluctuations in frustrated antiferromagnets. *Phys. Rev. B* **99**, 054409 (2019).

Supporting Information for

Magnon-Induced Electric Polarization and Magnon Nernst Effects

Q. To, F. Garcia-Gaitan, Y. Ren, J. Zide, B. Jungfleisch, J. Xiao, B. Nikolić, G. Bryant, M. Doty

D. Quang To; Matthew F. Doty
E-mail: quangto@udel.edu; doty@udel.edu

This PDF file includes:

Contents

Supporting Information Text

S1. Magnon Hamiltonian via Holstein-Primakoff transformation and bosonic Bogoliubov–de Gennes Berry curvature

A. Model Hamiltonian for 2D collinear honeycomb spin systems. In this work we direct our attention to two distinct types of 2D honeycomb antiferromagnets: those with Néel and Zigzag orders whose magnetic structures are illustrated in Fig. S1 (b) and (c) respectively. The primitive cell of the Néel order comprises two magnetic atoms with opposing spins and lacks an inversion center and, thus, inversion symmetry. Conversely, the Zigzag order's primitive cell accommodates four magnetic atoms, denoted by numbers 1-4 in Fig. S1 (c), with the inversion center I_c positioned between two adjacent magnetic atoms exhibiting identical spins. We recall that the fundamental spin Hamiltonian for this type of system can be expressed as follows

$$H = \sum_{i,j} J_{ij} \boldsymbol{S}_i \cdot \boldsymbol{S}_j + \Delta \sum_i (S_i^z)^2 + g\mu_B B_z \sum_i S_i^z + \sum_{\langle\langle i,j \rangle\rangle} \boldsymbol{D}_{ij} (\boldsymbol{S}_i \times \boldsymbol{S}_j) \qquad [S1]$$

To derive a second-quantization version of Eq. (S1) in terms of bosonic operators creating and annihilating magnons, we employ the standard Holstein-Primakoff transformation (1) that maps spin operators residing on sublattice A or B of a two-dimensional antiferromagnet (2D AFM) to bosonic operators whose square root is expanded in a Taylor series and then truncated (2) to linear order

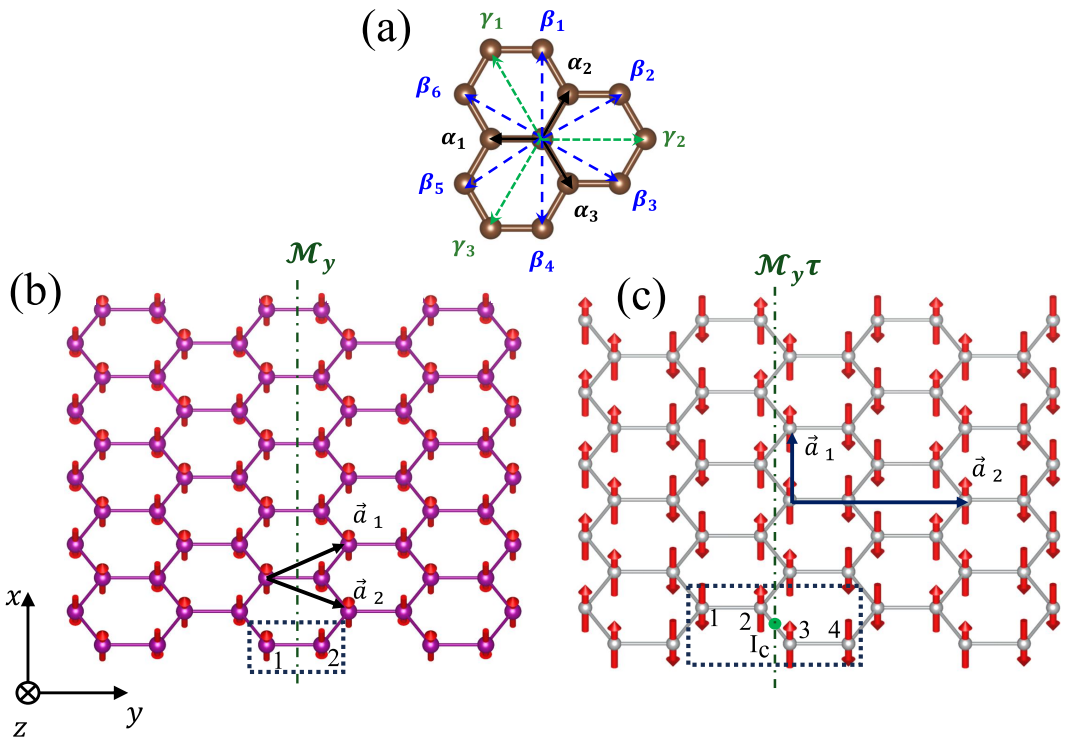

Fig. S1. (a) The nearest, second nearest and third nearest neighbor bonds in honeycomb lattice are denoted by α_i, β_i and γ_i, respectively. The quasi 2D honeycomb AFM lattice with Néel (b) and Zigzag (c) order formed by magnetic atoms. The arrows indicate the primitive vectors and the dashed rectangular shape shows the unit cell of corresponding lattice. The $\mathcal{M}_y$ and $\mathcal{M}_y\tau$ represent the mirror and glide mirror symmetry of the Néel and Zigzag order, respectively.

$$S_A^+ = \sqrt{2S} a_i \qquad S_A^- = \sqrt{2S} a_i^\dagger \qquad S_A^z = S - a_i^\dagger a_i, \qquad [S2]$$

$$S_B^+ = \sqrt{2S} b_j^\dagger \qquad S_B^- = \sqrt{2S} b_j \qquad S_B^z = -S + b_j^\dagger b_j. \qquad [S3]$$

Such truncation is valid as long as the temperature is low, $k_B T \ll J_{ij}$, where J_{ij} is the exchange coupling in Eq. (2) in the main text, and the number of magnons excited is sufficiently small (2). Here a_i and b_j ($a_i^\dagger$ and $b_j^\dagger$) are operators annihilating (creating) magnons at site $i \in A$ or site $j \in B$, respectively. Using the Fourier transform of these operators

$$a_i = \frac{1}{\sqrt{N}} \sum_{\boldsymbol{k}} e^{i\boldsymbol{k}\cdot\boldsymbol{r}_{a_i}} a_{\boldsymbol{k},i}, \qquad a_i^\dagger = \frac{1}{\sqrt{N}} \sum_{\boldsymbol{k}} e^{-i\boldsymbol{k}\cdot\boldsymbol{r}_{a_i}} a_{\boldsymbol{k},i}^\dagger, \qquad [S4]$$

$$b_i = \frac{1}{\sqrt{N}} \sum_{\boldsymbol{k}} e^{i\boldsymbol{k}\cdot\boldsymbol{r}_{b_i}} b_{\boldsymbol{k},i}, \qquad b_i^\dagger = \frac{1}{\sqrt{N}} \sum_{\boldsymbol{k}} e^{-i\boldsymbol{k}\cdot\boldsymbol{r}_{b_i}} b_{\boldsymbol{k},i}^\dagger, \tag{S5}$$

the Heisenberg Hamiltonian in Eq. (2) of the main text can be re-written in second-quantization form as

$$\hat{H} = E^0 + \hat{H}(\boldsymbol{k}). \tag{S6}$$

Here E^0 is a k-independent energy which simply shifts the energy-momentum dispersion of magnons by a constant value and, hence, can be neglected. The k-dependent terms, containing operators which create and annihilate magnons in momentum $\hbar\boldsymbol{k}$, are collected into $\hat{H}(\boldsymbol{k}) = \Psi^\dagger \hat{H}_{\boldsymbol{k}} \Psi$ where

$$\Psi^\dagger = \left(x_{\boldsymbol{k},1}^\dagger, x_{\boldsymbol{k},2}^\dagger, ..., x_{\boldsymbol{k},n}^\dagger, x_{-\boldsymbol{k},1}, x_{-\boldsymbol{k},2}, ..., x_{-\boldsymbol{k},n}\right) \tag{S7}$$

is the Nambu spinor.

For Néel order, $\Psi^\dagger = \left(a_{\boldsymbol{k}}^\dagger, b_{\boldsymbol{k}}^\dagger, a_{-\boldsymbol{k}}, b_{-\boldsymbol{k}}\right)$ the bosonic Bogoliubov-de Gennes (BdG) Hamiltonian is (3, 4)

$$\hat{H}_{\boldsymbol{k}} = R_m \begin{bmatrix} A(\boldsymbol{k}) & 0 \\ 0 & A^T(-\boldsymbol{k}) \end{bmatrix} R_m^\dagger \tag{S8}$$

where

$$A(\boldsymbol{k}) = S \begin{bmatrix} J + J_2\zeta_{\boldsymbol{\beta}} - D\zeta_D & J_1\zeta_{\boldsymbol{\alpha}} + J_3\zeta_{\boldsymbol{\gamma}} \\ J_1\zeta_{\boldsymbol{\alpha}}^* & J + J_2\zeta_{\boldsymbol{\beta}} + D\zeta_D \end{bmatrix} \tag{S9}$$

Here $J = 3J_1 - 6J_2 + 3J_3 - \Delta$; $\zeta_{\boldsymbol{\Sigma}} = \sum_m \zeta_{\boldsymbol{\Sigma}_m}$; $\zeta_{\boldsymbol{\Sigma}_m} = e^{i\boldsymbol{k}.\boldsymbol{\Sigma}_m}$ $(\boldsymbol{\Sigma} \equiv \boldsymbol{\alpha}, \boldsymbol{\beta}, \boldsymbol{\gamma})$ and $\zeta_D = \sum_{m \in odd} 2sin(\boldsymbol{k}.\boldsymbol{\beta}_m)$; R_m is the rotational matrix given by:

$$R_m = \begin{bmatrix} 1 & 0 & 0 & 0 \\ 0 & 0 & 0 & 1 \\ 0 & 0 & 1 & 0 \\ 0 & 1 & 0 & 0 \end{bmatrix} \tag{S10}$$

Table S1. The exchange coupling between localized spins, for 2D AFM used in the main text.

Materials	a (Å)	S(μ_B)	J_1 (meV)	J_2 (meV)	J_3 (meV)	Δ (meV)	D (μeV)
$MnPS_3$ (3, 4)	5.88	4.56	0.527	0.024	0.150	-0.002	0.39
$NiPSe_3$ (3, 4)	6.14	1.56	-1.131	-0.069	3.975	-0.19	43.90

In the same manner, the BdG Hamiltonian for Zigzag order reads (3, 4):

$$\hat{H}_{\boldsymbol{k}} = R_m \begin{bmatrix} B(\boldsymbol{k}) & 0 \\ 0 & B^T(-\boldsymbol{k}) \end{bmatrix} R_m^\dagger \tag{S11}$$

with $\Psi^\dagger = \left(a_{1,\boldsymbol{k}}^\dagger, b_{1,\boldsymbol{k}}^\dagger, b_{2,\boldsymbol{k}}^\dagger, a_{2,\boldsymbol{k}}^\dagger, a_{1,-\boldsymbol{k}}, b_{1,-\boldsymbol{k}}, b_{2,-\boldsymbol{k}}, a_{2,-\boldsymbol{k}}\right)$. Here

$$B(\boldsymbol{k}) = S \begin{bmatrix} C(\boldsymbol{k}) & D(\boldsymbol{k}) \\ D^\dagger(\boldsymbol{k}) & C(-\boldsymbol{k}) \end{bmatrix} \tag{S12}$$

$$\begin{aligned} C(\boldsymbol{k}) =& \sigma_0(-J_1 + 2J_2 + 3J_3 - \Delta) + J_2[\sigma_0(\zeta_{\boldsymbol{\beta}_1} + \zeta_{\boldsymbol{\beta}_4}) + \sigma_1(\zeta_{\boldsymbol{\beta}_2} + \zeta_{\boldsymbol{\beta}_3} + \zeta_{\boldsymbol{\beta}_5} + \zeta_{\boldsymbol{\beta}_6})] \\ &+ iD[\sigma_0(\zeta_{\boldsymbol{\beta}_1} - \zeta_{\boldsymbol{\beta}_4}) + \sigma_1(-\zeta_{\boldsymbol{\beta}_2} + \zeta_{\boldsymbol{\beta}_3} + \zeta_{\boldsymbol{\beta}_5} - \zeta_{\boldsymbol{\beta}_6})] \end{aligned} \tag{S13}$$

$$D(\boldsymbol{k}) = J_1[\sigma_0(\zeta_{\boldsymbol{\alpha}_2}^* + \zeta_{\boldsymbol{\alpha}_3}^*) + \sigma_1\zeta_{\boldsymbol{\alpha}_1}^*] + J_3\sigma_1\left(\zeta_{\boldsymbol{\gamma}_1}^* + \zeta_{\boldsymbol{\gamma}_2}^* + \zeta_{\boldsymbol{\gamma}_3}^*\right) \tag{S14}$$

Here

$$\sigma_0 = \begin{pmatrix} \mathbf{1}_{N\times N} & 0 \\ 0 & \mathbf{1}_{N\times N} \end{pmatrix}, \quad \sigma_1 = \begin{pmatrix} 0 & \mathbf{1}_{N\times N} \\ \mathbf{1}_{N\times N} & 0 \end{pmatrix}, \quad \sigma_2 = \begin{pmatrix} 0 & -i\mathbf{1}_{N\times N} \\ i\mathbf{1}_{N\times N} & 0 \end{pmatrix}, \quad \sigma_3 = \begin{pmatrix} \mathbf{1}_{N\times N} & 0 \\ 0 & -\mathbf{1}_{N\times N} \end{pmatrix}. \tag{S15}$$

are the Pauli matrices in Bogoliubov space, and the rotation matrix R_m is given by

$$R_m = \begin{bmatrix} 1 & 0 & 0 & 0 & 0 & 0 & 0 & 0 \\ 0 & 0 & 0 & 0 & 0 & 0 & 0 & 1 \\ 0 & 0 & 0 & 0 & 0 & 1 & 0 & 0 \\ 0 & 0 & 1 & 0 & 0 & 0 & 0 & 0 \\ 0 & 0 & 0 & 0 & 1 & 0 & 0 & 0 \\ 0 & 0 & 0 & 1 & 0 & 0 & 0 & 0 \\ 0 & 1 & 0 & 0 & 0 & 0 & 0 & 0 \\ 0 & 0 & 0 & 0 & 0 & 0 & 1 & 0 \end{bmatrix} \tag{S16}$$

The material parameters used in our numerical calculations based on these Hamiltonians are listed in Table S1. By using Colpa's method (5), we diagonalize this Hamiltonian to obtain the eigenenergies of the system $E_{\boldsymbol{k}}$ satisfying the following eigenvalue equation

$$\boldsymbol{\sigma}_3 \hat{H}_{\boldsymbol{k}} T(\boldsymbol{k}) = T(\boldsymbol{k}) \boldsymbol{\sigma}_3 E_{\boldsymbol{k}}, \tag{S17}$$

as the generalized eigenvalue problem in which $\boldsymbol{\sigma}_3 \hat{H}_{\boldsymbol{k}}$ is a non-Hermitian matrix even though $\hat{H}_{\boldsymbol{k}}$ is Hermitian. In other words, the diagonalization of the BdG Hamiltonian deals with non-Hermitian quantum mechanics (6), but the eigenvalues $E_{\boldsymbol{k}}$ remain real. In Eq. (S17), matrix $T(\boldsymbol{k})$ is "paraunitiary" satisfying

$$T^{\dagger}(\boldsymbol{k}) \boldsymbol{\sigma}_3 T(\boldsymbol{k}) = T(\boldsymbol{k}) \boldsymbol{\sigma}_3 T^{\dagger}(\boldsymbol{k}) = \boldsymbol{\sigma}_3, \tag{S18}$$

The eigenvector $|n(\boldsymbol{k})\rangle$ with mth element given by $|n(\boldsymbol{k})\rangle_m = [T(\boldsymbol{k})]_{mn}$, with associated eigen-energies $E_{\boldsymbol{k}}$, forms the basis for conducting calculations related to magnon Orbital Angular Moment (OAM), Berry curvature, Orbital Berry curvature, and other relevant quantities discussed in the main text.

One can observe that in 2D collinear antiferromagnets with out-of-plane (z-direction) magnetic order, both the exchange interaction and the Dzyaloshinskii-Moriya interaction maintain the rotational symmetry about the z-axis. Consequently, the z-component of the total spin, defined as $S^z = \sum_i (S^z_{iA} + S^z_{iB})$, remains a conserved quantum number (7). By applying the Holstein-Primakoff transformation, one derives the following:

$$S^z = \sum_{\boldsymbol{k}} \left(b^{\dagger}_{\boldsymbol{k}} b_{\boldsymbol{k}} - a^{\dagger}_{\boldsymbol{k}} a_{\boldsymbol{k}} \right) = \sum_{\boldsymbol{k}} S^z_{\boldsymbol{k}} \tag{S19}$$

Note that the $S^z_{\boldsymbol{k}}$ commutes with the Hamiltonian, i.e. $[H, S^z_{\boldsymbol{k}}] = 0$. Consequently, it is diagonal in the Nambu basis. Employing the Bogoliubov transformation to obtain the normal modes of the magnonic field yields:

$$S^z = \sum_{\alpha,\beta,\boldsymbol{k}} \left(\beta^{\dagger}_{\boldsymbol{k}} \beta_{\boldsymbol{k}} - \alpha^{\dagger}_{\boldsymbol{k}} \alpha_{\boldsymbol{k}} \right) \tag{S20}$$

where $\alpha_{\boldsymbol{k}} = u_{\boldsymbol{k}} a_{\boldsymbol{k}} - v_{\boldsymbol{k}} b^{\dagger}_{\boldsymbol{k}}$ and $\beta_{\boldsymbol{k}} = u_{\boldsymbol{k}} b_{\boldsymbol{k}} - v_{\boldsymbol{k}} a^{\dagger}_{\boldsymbol{k}}$ with the Bogoliubov coefficients $u_{\boldsymbol{k}}$ and $v_{\boldsymbol{k}}$ being thoughtfully selected to diagonalize the Hamiltonians Eq. (S8) and Eq. (S11). This demonstrates that $\langle 0 | \eta_{\boldsymbol{k}} S^z \eta^{\dagger}_{\boldsymbol{k}} | 0 \rangle = \pm 1$, where η represents either β or α. Specifically, the α and β magnon carry -1 and +1 spin angular momentum along the z-direction, respectively. Consequently, the z-component of spin is closely associated with the magnon chirality, allowing us to interpret ± 1 as the helicity of the magnon bands. Therefore, each magnon band is constrained to one of these two helicity values, which may result in a smaller spin Nernst effect compared to the orbital Nernst effect, as discussed in the main text.

In addition, it is important to note that the approach we have presented here relies on linear spin wave theory, which is applicable only when the temperature is significantly lower than the Néel temperature of the antiferromagnetic material.

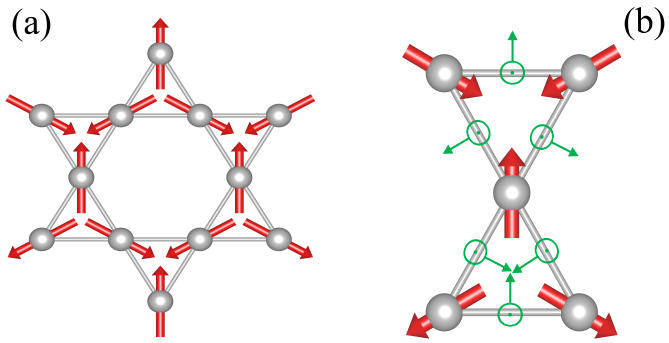

Fig. S2. (a) The Kagomé spin lattice of potassium iron jarosite along with (b) DM vectors comprising the in-plane direction shown by green arrows and out-of-plane components depicted by out or into the plane.

B. Model Hamiltonian for noncollinear spin systems. In addition to the 2D collinear honeycomb AFMs, we also investigate the jarosite compound. We take $KFe_3(OH)_6(SO_4)_2$, a material that crystallizes in a layered structure, as an example. The Fe ions in this compound form a two-dimensional Kagomé lattice, characterized by a network of corner-sharing triangles. Figure S2(a) illustrates a possible Néel state for an antiferromagnetic Kagomé lattice. The magnetic interactions in this lattice can be well described by the following Hamiltonian (8–11):

$$H = J_1 \sum_{\langle i,j \rangle} \boldsymbol{S}_i \cdot \boldsymbol{S}_j + J_2 \sum_{\langle\langle i,j \rangle\rangle} \boldsymbol{S}_i \cdot \boldsymbol{S}_j + \sum_{\langle i,j \rangle} \boldsymbol{D}_{ij} \cdot (\boldsymbol{S}_i \times \boldsymbol{S}_j) - g \mu_B B_z \sum_i S^z_i \tag{S21}$$

where first and second terms represent the nearest-neighbor and next-nearest-neighbor antiferromagnetic interactions, respectively. The third term describes the Dzyaloshinskii-Moriya interaction, characterized by the DM vector $\boldsymbol{D}_{ij}$ which includes both in-plane D_p and out-of-plane D_z components for the bond (i,j). Again, by applying the Holstein-Primakoff transformation (1) to the spin operators, truncated to linear order, and performing a Fourier transformation, we obtain the Hamiltonian in Eq. (S21) expressed in its second-quantized form which incorporates the canting angle η, as defined in the main text, and is formulated in the basis $\Psi_{\boldsymbol{k}} = \left(b_{1,\boldsymbol{k}}, b_{2,\boldsymbol{k}}, b_{3,\boldsymbol{k}}, b^{\dagger}_{1,-\boldsymbol{k}}, b^{\dagger}_{2,-\boldsymbol{k}}, b^{\dagger}_{3,-\boldsymbol{k}}\right)$. The Hamiltonian takes the form: $H = \frac{S}{2}\sum_{\boldsymbol{k}} \Psi^{\dagger}_{\boldsymbol{k}} H_{\boldsymbol{k}} \Psi_{\boldsymbol{k}}$ where

$$H_{\boldsymbol{k}} = \begin{pmatrix} A_{\boldsymbol{k}} & B_{\boldsymbol{k}} \\ B_{\boldsymbol{k}} & A^{*}_{\boldsymbol{k}} \end{pmatrix} \tag{S22}$$

Here

$$A_{\boldsymbol{k}} = \begin{pmatrix} 2\left[\Delta^{(0)}_1 + \Delta^{(0)}_2 - \frac{g\mu_B sin(\eta)}{2S} B_z\right] & \Delta_1 cos\,(k_3) + \Delta_2 cos\,(p_3) & \Delta^{*}_1 cos\,(k_2) + \Delta^{*}_2 cos\,(p_2) \\ \Delta^{*}_1 cos\,(k_3) + \Delta^{*}_2 cos\,(p_3) & 2\left[\Delta^{(0)}_1 + \Delta^{(0)}_2 - \frac{g\mu_B sin(\eta)}{2S} B_z\right] & \Delta_1 cos\,(k_3) + \Delta_2 cos\,(p_3) \\ \Delta_1 cos\,(k_2) + \Delta_2 cos\,(p_2) & \Delta^{*}_1 cos\,(k_1) + \Delta^{*}_2 cos\,(p_1) & 2\left[\Delta^{(0)}_1 + \Delta^{(0)}_2 - \frac{g\mu_B sin(\eta)}{2S} B_z\right] \end{pmatrix} \tag{S23}$$

and

$$B_{\boldsymbol{k}} = \begin{pmatrix} 0 & \Delta'_1 cos\,(k_3) + \Delta'_2 cos\,(p_3) & \Delta'_1 cos\,(k_2) + \Delta'_2 cos\,(p_2) \\ \Delta'_1 cos\,(k_3) + \Delta'_2 cos\,(p_3) & 0 & \Delta'_1 cos\,(k_3) + \Delta'_2 cos\,(p_3) \\ \Delta'_1 cos\,(k_2) + \Delta'_2 cos\,(p_2) & \Delta'_1 cos\,(k_1) + \Delta'_2 cos\,(p_1) & 0 \end{pmatrix} \tag{S24}$$

with

$$\Delta^{(0)}_1 = J_1\left[1 - 3sin^2\,(\eta)\right] - \sqrt{3}\left[D_z cos^2\,(\eta) + D_p sin\,(2\eta)\right] \tag{S25}$$

$$\Delta^{(0)}_2 = J_2\left[1 - 3sin^2\,(\eta)\right] \tag{S26}$$

$$\begin{aligned}\Delta_1 = \frac{1}{2}\Big\{&\left[1 - 3sin^2\,(\eta)\right] J_1 + \sqrt{3}\left[1 + sin^2\,(\eta)\right] D_z \\ &-\sqrt{3} sin\,(2\eta)\, D_p\Big\} + i\left[cos\,(\eta)\, D_p + sin\,(\eta)\left(D_z + \sqrt{3} J_1\right)\right]\end{aligned} \tag{S27}$$

$$\Delta_2 = \frac{1}{2}\left[1 - 3sin^2\,(\eta)\right] J_2 + i\sqrt{3} sin\,(\eta)\, J_2 \tag{S28}$$

$$\Delta'_1 = \frac{1}{2}\left[cos^2\,(\eta)\left(\sqrt{3} D_z - 3J_1\right) + \sqrt{3} sin\,(2\eta)\, D_p\right] \tag{S29}$$

$$\Delta'_2 = -\frac{3}{2} cos^2\,(\eta)\, J_2 \tag{S30}$$

the abbreviated notations $k_i = \boldsymbol{k}\cdot\boldsymbol{e}_i$ and $p_i = \boldsymbol{k}\cdot\boldsymbol{e}'_i$ where $\boldsymbol{e}_1 = \left(-\frac{1}{2}, -\frac{\sqrt{3}}{3}\right)$; $\boldsymbol{e}_2 = (1,0)$; $\boldsymbol{e}_3 = \left(-\frac{1}{2}, \frac{\sqrt{3}}{2}\right)$; $\boldsymbol{e}'_1 = \boldsymbol{e}_2 - \boldsymbol{e}_3$; $\boldsymbol{e}'_2 = \boldsymbol{e}_3 - \boldsymbol{e}_1$; $\boldsymbol{e}'_3 = \boldsymbol{e}_1 - \boldsymbol{e}_2$.

The magnetic interaction parameters used in this Hamiltonian for $KFe_3(OH)_6(SO_4)_2$ are $S = 5/2$; $J_1 = 3.18\ meV$; $J_2 = 0.11\ meV$; $D_p = 0.062 J_1$; $D_z = -0.062 J_1$ (9).

C. Berry curvature. We now present a detailed derivation of the Berry curvature expression for magnonic systems discussed in the main text, employing the Berry curvature formula for the bosonic BdG Hamiltonian as given in Refs. (6, 12):

$$\Omega^n_z(\boldsymbol{k}) = i\epsilon_{xy}\left[\boldsymbol{\sigma}_3 \frac{\partial T^{\dagger}(\boldsymbol{k})}{\partial k_x}\boldsymbol{\sigma}_3 \frac{\partial T(\boldsymbol{k})}{\partial k_y}\right]_{nn} \tag{S31}$$

one obtains

$$\begin{aligned}\Omega^n_z(\boldsymbol{k}) &= i\sum_m \left[\boldsymbol{\sigma}_3 \frac{\partial T^{\dagger}(\boldsymbol{k})}{\partial k_x}\right]_{nm}\left[\boldsymbol{\sigma}_3 \frac{\partial T(\boldsymbol{k})}{\partial k_y}\right]_{mn} - i\sum_m \left[\boldsymbol{\sigma}_3 \frac{\partial T^{\dagger}(\boldsymbol{k})}{\partial k_y}\right]_{nm}\left[\boldsymbol{\sigma}_3 \frac{\partial T(\boldsymbol{k})}{\partial k_x}\right]_{mn} \\ &= i\sum_m \sigma^{nn}_3 \frac{\partial\left[T^{\dagger}(\boldsymbol{k})\right]_{nm}}{\partial k_x}\sigma^{mm}_3 \frac{\partial\left[T(\boldsymbol{k})\right]_{mn}}{\partial k_y} - i\sum_m \sigma^{nn}_3 \frac{\partial\left[T^{\dagger}(\boldsymbol{k})\right]_{nm}}{\partial k_y}\sigma^{mm}_3 \frac{\partial\left[T(\boldsymbol{k})\right]_{mn}}{\partial k_x}.\end{aligned} \tag{S32}$$

By defining $|n(\boldsymbol{k})\rangle_m = \left[T(\boldsymbol{k})\right]_{mn}$ as the mth element of a column vector $|n(\boldsymbol{k})\rangle$, so that $\langle n(\boldsymbol{k})|_m = \left[T^{\dagger}(\boldsymbol{k})\right]_{nm}$ is the mth element of a row vector $\langle n(\boldsymbol{k})|$, one has

$$\sum_n \sigma^{nn}_3 |n(\boldsymbol{k})\rangle\boldsymbol{\sigma}_3\langle n(\boldsymbol{k})| = \sum_n \sigma^{nn}_3 |n(\boldsymbol{k})\rangle\langle n(\boldsymbol{k})|\boldsymbol{\sigma}_3 = \mathcal{I}, \tag{S33}$$

which is the completeness relation for the BdG Hamiltonian eigenbasis. Substituting Eq. (S33) into Eq. (S32), yields

$$\begin{aligned}\Omega_z^n(\boldsymbol{k}) &= i\sum_m \sigma_3^{nn}\frac{\partial\langle n(\boldsymbol{k})|_m}{\partial k_x}\sigma_3^{mm}\frac{\partial|n(\boldsymbol{k})\rangle_m}{\partial k_y} - i\sum_m \sigma_3^{nn}\frac{\partial\langle n(\boldsymbol{k})|_m}{\partial k_y}\sigma_3^{mm}\frac{\partial|n(\boldsymbol{k})\rangle_m}{\partial k_x}\\ &= i\sigma_3^{nn}\left\langle\frac{\partial n(\boldsymbol{k})}{\partial k_x}\middle|\boldsymbol{\sigma}_3\middle|\frac{\partial n(\boldsymbol{k})}{\partial k_y}\right\rangle - i\sigma_3^{nn}\left\langle\frac{\partial n(\boldsymbol{k})}{\partial k_y}\middle|\boldsymbol{\sigma}_3\middle|\frac{\partial n(\boldsymbol{k})}{\partial k_x}\right\rangle\\ &= i\sum_{m\neq n}\sigma_3^{nn}\sigma_3^{mm}\left\langle\frac{\partial n(\boldsymbol{k})}{\partial k_x}\middle|\boldsymbol{\sigma}_3\middle|m(\boldsymbol{k})\right\rangle\left\langle m(\boldsymbol{k})\middle|\boldsymbol{\sigma}_3\middle|\frac{\partial n(\boldsymbol{k})}{\partial k_y}\right\rangle - i\sum_{m\neq n}\sigma_3^{nn}\sigma_3^{mm}\left\langle\frac{\partial n(\boldsymbol{k})}{\partial k_y}\middle|\boldsymbol{\sigma}_3\middle|m(\boldsymbol{k})\right\rangle\left\langle m(\boldsymbol{k})\middle|\boldsymbol{\sigma}_3\middle|\frac{\partial n(\boldsymbol{k})}{\partial k_x}\right\rangle,\end{aligned} \tag{S34}$$

leading to

$$\Omega_n^z(\boldsymbol{k}) = i\sum_{m\neq n}\sigma_3^{nn}\sigma_3^{mm}\left\langle\frac{\partial n(\boldsymbol{k})}{\partial k_x}\middle|\boldsymbol{\sigma}_3\middle|m(\boldsymbol{k})\right\rangle\left\langle m(\boldsymbol{k})\middle|\boldsymbol{\sigma}_3\middle|\frac{\partial n(\boldsymbol{k})}{\partial k_y}\right\rangle - (k_x\longleftrightarrow k_y). \tag{S35}$$

By taking the derivative of both sides of Eq. (S17) with respect to k_x, and by using $\langle n(\boldsymbol{k})| = \left[T^\dagger(\boldsymbol{k})\right]_{n\cdots}$ (the nth row of $\left[T^\dagger(\boldsymbol{k})\right]$ matrix) and $|n(\boldsymbol{k})\rangle = [T(\boldsymbol{k})]_{\cdots n}$ (the nth column of $[T(\boldsymbol{k})]$ matrix) we obtain

$$\boldsymbol{\sigma}_3\frac{\partial\hat{H}_{\boldsymbol{k}}}{\partial k_x}|n(\boldsymbol{k})\rangle + \boldsymbol{\sigma}_3\hat{H}_{\boldsymbol{k}}\left|\frac{\partial n(\boldsymbol{k})}{\partial k_x}\right\rangle = \left[\boldsymbol{\sigma}_3\frac{\partial E_{\boldsymbol{k}}}{\partial k_x}\right]_{nn}|n(\boldsymbol{k})\rangle + [\boldsymbol{\sigma}_3 E_{\boldsymbol{k}}]_{nn}\left|\frac{\partial n(\boldsymbol{k})}{\partial k_x}\right\rangle. \tag{S36}$$

Multiplying both sides of Eq. (S36) with $\langle m(\boldsymbol{k})|\boldsymbol{\sigma}_3$ gives

$$\left\langle m(\boldsymbol{k})\middle|\frac{\partial\hat{H}_{\boldsymbol{k}}}{\partial k_x}\middle|n(\boldsymbol{k})\right\rangle + \left\langle m(\boldsymbol{k})\middle|\hat{H}_{\boldsymbol{k}}\middle|\frac{\partial n(\boldsymbol{k})}{\partial k_x}\right\rangle = \left[\boldsymbol{\sigma}_3\frac{\partial E_{\boldsymbol{k}}}{\partial k_x}\right]_{nn}\langle m(\boldsymbol{k})|\boldsymbol{\sigma}_3|n(\boldsymbol{k})\rangle + [\boldsymbol{\sigma}_3 E_{\boldsymbol{k}}]_{nn}\left\langle m(\boldsymbol{k})\middle|\boldsymbol{\sigma}_3\middle|\frac{\partial n(\boldsymbol{k})}{\partial k_x}\right\rangle. \tag{S37}$$

Note that

$$\langle m(\boldsymbol{k})|\boldsymbol{\sigma}_3|n(\boldsymbol{k})\rangle = 0, \tag{S38}$$

with $m\neq n$ and

$$\left\langle m(\boldsymbol{k})\middle|\hat{H}_{\boldsymbol{k}}\middle|\frac{\partial n(\boldsymbol{k})}{\partial k_x}\right\rangle = [\boldsymbol{\sigma}_3 E_{\boldsymbol{k}}]_{mm}\left\langle m(\boldsymbol{k})\middle|\boldsymbol{\sigma}_3\middle|\frac{\partial n(\boldsymbol{k})}{\partial k_x}\right\rangle. \tag{S39}$$

Therefore,

$$\left\langle m(\boldsymbol{k})\middle|\frac{\partial\hat{H}_{\boldsymbol{k}}}{\partial k_x}\middle|n(\boldsymbol{k})\right\rangle = \left\{[\boldsymbol{\sigma}_3 E_{\boldsymbol{k}}]_{nn} - [\boldsymbol{\sigma}_3 E_{\boldsymbol{k}}]_{mm}\right\}\left\langle m(\boldsymbol{k})\middle|\boldsymbol{\sigma}_3\middle|\frac{\partial n(\boldsymbol{k})}{\partial k_x}\right\rangle, \tag{S40}$$

leads to

$$\frac{\left\langle m(\boldsymbol{k})\middle|\frac{\partial\hat{H}_{\boldsymbol{k}}}{\partial k_x}\middle|n(\boldsymbol{k})\right\rangle}{[\boldsymbol{\sigma}_3 E_{\boldsymbol{k}}]_{nn} - [\boldsymbol{\sigma}_3 E_{\boldsymbol{k}}]_{mm}} = \left\langle m(\boldsymbol{k})\middle|\boldsymbol{\sigma}_3\middle|\frac{\partial n(\boldsymbol{k})}{\partial k_x}\right\rangle, \tag{S41}$$

Similarly, we obtain

$$\frac{\left\langle n(\boldsymbol{k})\middle|\frac{\partial\hat{H}_{\boldsymbol{k}}}{\partial k_x}\middle|m(\boldsymbol{k})\right\rangle}{[\boldsymbol{\sigma}_3 E_{\boldsymbol{k}}]_{nn} - [\boldsymbol{\sigma}_3 E_{\boldsymbol{k}}]_{mm}} = \left\langle\frac{\partial n(\boldsymbol{k})}{\partial k_x}\middle|\boldsymbol{\sigma}_3\middle|m(\boldsymbol{k})\right\rangle, \tag{S42}$$

$$\frac{\left\langle m(\boldsymbol{k})\middle|\frac{\partial\hat{H}_{\boldsymbol{k}}}{\partial k_y}\middle|n(\boldsymbol{k})\right\rangle}{[\boldsymbol{\sigma}_3 E_{\boldsymbol{k}}]_{nn} - [\boldsymbol{\sigma}_3 E_{\boldsymbol{k}}]_{mm}} = \left\langle m(\boldsymbol{k})\middle|\boldsymbol{\sigma}_3\middle|\frac{\partial n(\boldsymbol{k})}{\partial k_y}\right\rangle, \tag{S43}$$

$$\frac{\left\langle n(\boldsymbol{k})\middle|\frac{\partial\hat{H}_{\boldsymbol{k}}}{\partial k_y}\middle|m(\boldsymbol{k})\right\rangle}{[\boldsymbol{\sigma}_3 E_{\boldsymbol{k}}]_{nn} - [\boldsymbol{\sigma}_3 E_{\boldsymbol{k}}]_{mm}} = \left\langle\frac{\partial n(\boldsymbol{k})}{\partial k_y}\middle|\boldsymbol{\sigma}_3\middle|m(\boldsymbol{k})\right\rangle. \tag{S44}$$

Combining Eq. (S35) with Eq. (S41)– Eq. (S44), we arrive at the expression for the Berry curvature

$$\begin{aligned}\Omega_z^n(\boldsymbol{k}) &= \sum_{m\neq n} i\sigma_3^{nn}\sigma_3^{mm}\frac{\left\langle n(\boldsymbol{k})\middle|\frac{\partial\hat{H}_{\boldsymbol{k}}}{\partial k_x}\middle|m(\boldsymbol{k})\right\rangle\left\langle m(\boldsymbol{k})\middle|\frac{\partial\hat{H}_{\boldsymbol{k}}}{\partial k_y}\middle|n(\boldsymbol{k})\right\rangle}{\left\{[\boldsymbol{\sigma}_3 E_{\boldsymbol{k}}]_{nn} - [\boldsymbol{\sigma}_3 E_{\boldsymbol{k}}]_{mm}\right\}^2} - (k_x\longleftrightarrow k_y)\\ &= \sum_{m\neq n} i\sigma_3^{nn}\sigma_3^{mm}\frac{\left\langle n(\boldsymbol{k})\middle|\frac{\partial\hat{H}_{\boldsymbol{k}}}{\partial k_x}\middle|m(\boldsymbol{k})\right\rangle\left\langle m(\boldsymbol{k})\middle|\frac{\partial\hat{H}_{\boldsymbol{k}}}{\partial k_y}\middle|n(\boldsymbol{k})\right\rangle}{\left[\sigma_3^{nn}E_{n,\boldsymbol{k}} - \sigma_3^{mm}E_{m,\boldsymbol{k}}\right]^2} - (k_x\longleftrightarrow k_y)\end{aligned} \tag{S45}$$

which can also be generalized into

$$\boldsymbol{\Omega}^n(\boldsymbol{k}) = i\hbar^2 \sum_{m\neq n} \sigma_3^{nn}\sigma_3^{mm} \frac{\langle n(\boldsymbol{k})|\hat{\boldsymbol{v}}_{\boldsymbol{k}}|m(\boldsymbol{k})\rangle \times \langle m(\boldsymbol{k})|\hat{\boldsymbol{v}}_{\boldsymbol{k}}|n(\boldsymbol{k})\rangle}{\left[\sigma_3^{nn}E_{n,\boldsymbol{k}} - \sigma_3^{mm}E_{m,\boldsymbol{k}}\right]^2}, \tag{S46}$$

thereby completing the derivation of Eq. (2) in the main text.

D. Symmetry constraints on Berry curvature. In this section, we analyze the role of inversion (P) symmetry, time-reversal symmetry (TRS), and their combined parity–time symmetry (CPTS) in determining the bosonic BdG Berry curvature. Here, CPTS refers to the simultaneous presence of both P symmetry and TRS. We emphasize that this notion of CPTS differs from the conventional parity–time symmetry ($\mathcal{PT}$), which may be preserved even when P symmetry or TRS is individually broken. As we demonstrate below, a finite magnon Berry curvature necessarily requires the breaking of CPTS.

The inversion symmetry and time-reversal symmetry impose the following constraints on the BdG Hamiltonian:

$$\mathcal{P}\hat{H}_{\boldsymbol{k}}\mathcal{P}^{-1} = \hat{H}_{-\boldsymbol{k}} \tag{S47}$$

$$\mathcal{T}\hat{H}_{\boldsymbol{k}}\mathcal{T}^{-1} = \hat{H}_{-\boldsymbol{k}} \tag{S48}$$

where the inversion operation $\mathcal{P}$ and time reversal operation $\mathcal{T}$ are respectively given by paraunitary matrix:

$$\mathcal{P} = \begin{pmatrix} U_P & 0 \\ 0 & U_P^* \end{pmatrix} \tag{S49}$$

and

$$\mathcal{T} = \begin{pmatrix} U_T & 0 \\ 0 & U_T^* \end{pmatrix} \mathcal{K} \tag{S50}$$

Here $U_{P,T}$ is an $N \times N$ unitary matrix and $\mathcal{K}$ denotes complex conjugation such that the antiunitary time-reversal operator $\mathcal{T}$ satisfies $\mathcal{T}^2 = +1$.

D.1. Effective time-reversal symmetry. Suppose that the bosonic system we consider is invariant under the effective time reversal symmetry, i.e., when the BdG Hamiltonian satisfies

$$\mathcal{T}\hat{H}_{\boldsymbol{k}}\mathcal{T}^{-1} = \hat{H}_{-\boldsymbol{k}}. \tag{S51}$$

leads to

$$\mathcal{D}\hat{H}_{\boldsymbol{k}}^*\mathcal{D}^\dagger = \hat{H}_{-\boldsymbol{k}}. \tag{S52}$$

where

$$\mathcal{D} = \begin{pmatrix} U_T & 0 \\ 0 & U_T^* \end{pmatrix} \tag{S53}$$

Rewrite Eq. (S17) as

$$\boldsymbol{\sigma}_3\hat{H}_{-\boldsymbol{k}}T(-\boldsymbol{k}) = T(-\boldsymbol{k})\boldsymbol{\sigma}_3 E_{-\boldsymbol{k}} \tag{S54}$$

and by inserting Eq. (S52) into Eq. (S54), we obtain

$$\boldsymbol{\sigma}_3\mathcal{D}\hat{H}_{\boldsymbol{k}}^*\mathcal{D}^\dagger T(-\boldsymbol{k}) = T(-\boldsymbol{k})\boldsymbol{\sigma}_3 E_{-\boldsymbol{k}}. \tag{S55}$$

Multiplying both sides of Eq. (S55) by $\mathcal{D}^\dagger$ from the left

$$\mathcal{D}^\dagger\boldsymbol{\sigma}_3\mathcal{D}\hat{H}_{\boldsymbol{k}}^*\mathcal{D}^\dagger T(-\boldsymbol{k}) = \mathcal{D}^\dagger T(-\boldsymbol{k})\boldsymbol{\sigma}_3 E_{-\boldsymbol{k}}, \tag{S56}$$

leads to

$$\boldsymbol{\sigma}_3\hat{H}_{\boldsymbol{k}}^*\mathcal{D}^\dagger T(-\boldsymbol{k}) = \mathcal{D}^\dagger T(-\boldsymbol{k})\boldsymbol{\sigma}_3 E_{-\boldsymbol{k}}. \tag{S57}$$

Taking a complex conjugate of both sides of Eq. (S57) yields

$$\left[\boldsymbol{\sigma}_3\hat{H}_{\boldsymbol{k}}^*\mathcal{D}^\dagger T(-\boldsymbol{k})\right]^* = \left[\mathcal{D}^\dagger T(-\boldsymbol{k})\boldsymbol{\sigma}_3 E_{-\boldsymbol{k}}\right]^*, \tag{S58}$$

Since both $\boldsymbol{\sigma}_3$ and $E_{\boldsymbol{k}}$ are composed of real numbers, we obtain

$$\boldsymbol{\sigma}_3\hat{H}_{\boldsymbol{k}}\mathcal{D}^{\dagger *}T^*(-\boldsymbol{k}) = \mathcal{D}^{\dagger *}T^*(-\boldsymbol{k})\boldsymbol{\sigma}_3 E_{-\boldsymbol{k}}. \tag{S59}$$

Note that the effective time reversal symmetry also imposes $E_{-\boldsymbol{k}} = E_{\boldsymbol{k}}$, so that

$$\boldsymbol{\sigma}_3\hat{H}_{\boldsymbol{k}}\mathcal{D}^{\dagger *}T^*(-\boldsymbol{k}) = \mathcal{D}^{\dagger *}T^*(-\boldsymbol{k})\boldsymbol{\sigma}_3 E_{\boldsymbol{k}}. \tag{S60}$$

One can see that $\mathcal{D}^{\dagger *}T^*(-\boldsymbol{k})$ plays the same role as $T(\boldsymbol{k})$, i.e., it obeys the same eigenvalue equation as $T(\boldsymbol{k})$. This means that they differ only by a phase factor matrix, i.e., a diagonal matrix with phase factor entries. We can ignore this phase factor when considering the Berry curvature (12), therefore, allowing us to write

$$T(\boldsymbol{k}) = \mathcal{D}^{\dagger *}T^*(-\boldsymbol{k}) \tag{S61}$$

Inserting Eq. (S61) into the expression for the Berry curvature written in terms of the paraunitary matrix $T(\boldsymbol{k})$ gives the following.

$$\begin{aligned}\Omega_z^n(\boldsymbol{k}) &= i\epsilon_{xy}\left[\boldsymbol{\sigma}_3\frac{\partial T^\dagger(\boldsymbol{k})}{\partial k_x}\boldsymbol{\sigma}_3\frac{\partial T(\boldsymbol{k})}{\partial k_y}\right]_{nn} = i\epsilon_{xy}\left\{\boldsymbol{\sigma}_3\frac{\partial\left[\mathcal{D}^*T^{\dagger *}(-\boldsymbol{k})\right]}{\partial k_x}\boldsymbol{\sigma}_3\frac{\partial\left[\mathcal{D}^{\dagger *}T^*(-\boldsymbol{k})\right]}{\partial k_y}\right\}_{nn} = i\epsilon_{xy}\left[\boldsymbol{\sigma}_3\frac{\partial T^{\dagger *}(-\boldsymbol{k})}{\partial k_x}\mathcal{D}^*\boldsymbol{\sigma}_3\mathcal{D}^{\dagger *}\frac{\partial T^*(-\boldsymbol{k})}{\partial k_y}\right]_{nn}\\ &= i\epsilon_{xy}\left[\boldsymbol{\sigma}_3\frac{\partial T^{\dagger *}(-\boldsymbol{k})}{\partial k_x}\boldsymbol{\sigma}_3\frac{\partial T^*(-\boldsymbol{k})}{\partial k_y}\right]_{nn} = -i\epsilon_{xy}\left[\boldsymbol{\sigma}_3\frac{\partial T^\dagger(-\boldsymbol{k})}{\partial k_x}\boldsymbol{\sigma}_3\frac{\partial T(-\boldsymbol{k})}{\partial k_y}\right]_{nn} = -\Omega_z^n(-\boldsymbol{k}),\end{aligned} \tag{S62}$$

where we have used $\boldsymbol{\sigma}_3 = \boldsymbol{\sigma}_3^* = \left(\mathcal{D}\boldsymbol{\sigma}_3\mathcal{D}^\dagger\right)^* = \mathcal{D}^{\dagger *}\boldsymbol{\sigma}_3^*\mathcal{D}^* = \mathcal{D}^{\dagger *}\boldsymbol{\sigma}_3\mathcal{D}^*$ together with noticing that $\mathcal{D}$ does not depend on the wave vector $\boldsymbol{k}$.

From Eq. (S62), it follows that when time-reversal symmetry is preserved, the Berry curvature of the bosonic BdG wave function is odd under wavevector inversion.

D.2. Inversion symmetry. Now if we suppose that the bosonic system we consider is invariant under the inversion symmetry, i.e., when the BdG Hamiltonian satisfies

$$\mathcal{P}\hat{H}_{\boldsymbol{k}}\mathcal{P}^{-1} = \hat{H}_{-\boldsymbol{k}}. \tag{S63}$$

where $\mathcal{P}$ is given by Eq. (S49). In the same manner as effective time reversal symmetry, one can easily show that:

$$T(\boldsymbol{k}) = \mathcal{P}^\dagger T(-\boldsymbol{k}) \tag{S64}$$

Substituting Eq. (S64) into the Berry curvature expression gives

$$\Omega_z^n(\boldsymbol{k}) = \Omega_z^n(-\boldsymbol{k}), \tag{S65}$$

indicating that, when the system preserves inversion symmetry, the Berry curvature is even with respect to the wavevector.

D.3. Combined inversion–time-reversal symmetry. We now examine the consequences of the simultaneous presence of inversion symmetry and time-reversal symmetry in bosonic systems on the Berry curvature. For brevity, we refer to this coexistence as the combined parity–time symmetry (CPTS).

In a system possessing CPTS, the Berry curvature must vanish identically. This follows because inversion and time-reversal symmetries impose the conditions

$$\Omega_z^n(\boldsymbol{k}) = -\,\Omega_z^n(-\boldsymbol{k}), \tag{S66}$$

$$\Omega_z^n(\boldsymbol{k}) = \quad\Omega_z^n(-\boldsymbol{k}), \tag{S67}$$

which together imply $\Omega_z^n(\boldsymbol{k}) = 0$ for all bands n. Consequently, a finite Berry curvature and nontrivial magnon topology require CPTS to be broken, either through the breaking of inversion symmetry, time-reversal symmetry, or both.

We again stress that CPTS, as defined here, is distinct from the conventional $\mathcal{PT}$ symmetry. In particular, a system may respect $\mathcal{PT}$ symmetry even when P symmetry or TRS is individually broken, whereas CPTS requires the independent coexistence of both P symmetry and TRS.

S2. Orbital angular moment of magnon

A. Representations of magnon Orbital angular moment in BdG basis. In this section, we derive the expression for magnon orbital angular moment in the magnon Bloch representation used in the main text. This approach allows us to treat the intra-band and inter-band orbital angular moment of magnons on an equal footing.

Magnons exhibit bosonic quasiparticle behavior and can be considered as a motion of a wavepacket. The quasi-velocity operator $\hat{\boldsymbol{v}}$ describing the motion of this wavepacket is given by the Heisenberg equation of motion:

$$\hat{\boldsymbol{v}} = -\frac{i}{\hbar}\left[\hat{\boldsymbol{r}}, \hat{H}_{\boldsymbol{k}}\right] \tag{S68}$$

To obtain the representation of magnon orbital angular moment in the magnon Bloch states, we start with the symmetrized expression of the total orbital angular moment operator for the rotation of a magnon wavepacket that can be written as:

$$\hat{\boldsymbol{L}} = \frac{1}{4}\left(\hat{\boldsymbol{r}} \times \hat{\boldsymbol{v}} - \hat{\boldsymbol{v}} \times \hat{\boldsymbol{r}}\right) \tag{S69}$$

where $\hat{\boldsymbol{r}}$ is the position operator, and the velocity operator is given by Eq. (S68).

The matrix elements of orbital angular moment in the BdG basis representation read:

$$\left\langle m\left(\boldsymbol{k}\right)\left|\hat{L}^{\alpha}\right|n\left(\boldsymbol{k}\right)\right\rangle = \frac{\epsilon_{\beta\gamma}}{4}\left\langle m\left(\boldsymbol{k}\right)\left|\left(\hat{r}_{\beta}\hat{v}_{\gamma}-\hat{v}_{\beta}\hat{r}_{\gamma}\right)\right|n\left(\boldsymbol{k}\right)\right\rangle \tag{S70}$$

$$= -\frac{i\epsilon_{\beta\gamma}}{4\hbar}\left\langle m\left(\boldsymbol{k}\right)\left|\left(\hat{r}_{\beta}\left[\hat{r}_{\gamma},\hat{H}_{\boldsymbol{k}}\right]-\left[\hat{r}_{\beta},\hat{H}_{\boldsymbol{k}}\right]\hat{r}_{\gamma}\right)\right|n\left(\boldsymbol{k}\right)\right\rangle \tag{S71}$$

$$= -\frac{i\epsilon_{\beta\gamma}}{4\hbar}\left\langle m\left(\boldsymbol{k}\right)\left|\left(\hat{r}_{\beta}\hat{r}_{\gamma}\hat{H}_{\boldsymbol{k}}-2\hat{r}_{\beta}\hat{H}_{\boldsymbol{k}}\hat{r}_{\gamma}+\hat{H}_{\boldsymbol{k}}\hat{r}_{\beta}\hat{r}_{\gamma}\right)\right|n\left(\boldsymbol{k}\right)\right\rangle \tag{S72}$$

where $\alpha,\beta,\gamma\equiv x,y,z$. Note that:

$$\hat{H}_{\boldsymbol{k}}^{\dagger}\equiv\hat{H}_{\boldsymbol{k}} \tag{S73}$$

and

$$\left\langle m\left(\boldsymbol{k}\right)\left|\hat{r}_{\beta}\hat{r}_{\gamma}\hat{H}_{\boldsymbol{k}}\right|n\left(\boldsymbol{k}\right)\right\rangle = \left[\boldsymbol{\sigma}_{3}E_{\boldsymbol{k}}\right]_{nn}\left\langle m\left(\boldsymbol{k}\right)\left|\hat{r}_{\beta}\hat{r}_{\gamma}\boldsymbol{\sigma}_{3}\right|n\left(\boldsymbol{k}\right)\right\rangle \tag{S74}$$

$$\left\langle m\left(\boldsymbol{k}\right)\left|\hat{H}_{\boldsymbol{k}}\hat{r}_{\beta}\hat{r}_{\gamma}\right|n\left(\boldsymbol{k}\right)\right\rangle = \left[\boldsymbol{\sigma}_{3}E_{\boldsymbol{k}}\right]_{mm}\left\langle m\left(\boldsymbol{k}\right)\left|\boldsymbol{\sigma}_{3}\hat{r}_{\beta}\hat{r}_{\gamma}\right|n\left(\boldsymbol{k}\right)\right\rangle . \tag{S75}$$

The action of the position operator on the periodic part of the Bloch magnon function is given by

$$\hat{\boldsymbol{r}}\left|n\left(\boldsymbol{k}\right)\right\rangle = i\left|\partial_{\boldsymbol{k}}n\left(\boldsymbol{k}\right)\right\rangle \tag{S76}$$

and because

$$\left[\hat{\boldsymbol{r}},\boldsymbol{\sigma}_{3}\right]=0 \tag{S77}$$

one obtains

$$\left\langle m\left(\boldsymbol{k}\right)\left|\hat{r}_{\beta}\hat{r}_{\gamma}\hat{H}_{\boldsymbol{k}}\right|n\left(\boldsymbol{k}\right)\right\rangle = \left[\boldsymbol{\sigma}_{3}E_{\boldsymbol{k}}\right]_{nn}\left\langle m\left(\boldsymbol{k}\right)\left|\hat{r}_{\beta}\boldsymbol{\sigma}_{3}\hat{r}_{\gamma}\right|n\left(\boldsymbol{k}\right)\right\rangle = -\left[\boldsymbol{\sigma}_{3}E_{\boldsymbol{k}}\right]_{nn}\left\langle \partial_{k_{\beta}}m\left(\boldsymbol{k}\right)\left|\boldsymbol{\sigma}_{3}\right|\partial_{k_{\gamma}}n\left(\boldsymbol{k}\right)\right\rangle \tag{S78}$$

$$\left\langle m\left(\boldsymbol{k}\right)\left|\hat{H}_{\boldsymbol{k}}\hat{r}_{\beta}\hat{r}_{\gamma}\right|n\left(\boldsymbol{k}\right)\right\rangle = \left[\boldsymbol{\sigma}_{3}E_{\boldsymbol{k}}\right]_{mm}\left\langle m\left(\boldsymbol{k}\right)\left|\hat{r}_{\beta}\boldsymbol{\sigma}_{3}\hat{r}_{\gamma}\right|n\left(\boldsymbol{k}\right)\right\rangle = -\left[\boldsymbol{\sigma}_{3}E_{\boldsymbol{k}}\right]_{mm}\left\langle \partial_{k_{\beta}}m\left(\boldsymbol{k}\right)\left|\boldsymbol{\sigma}_{3}\right|\partial_{k_{\gamma}}n\left(\boldsymbol{k}\right)\right\rangle , \tag{S79}$$

which leads to

$$\left\langle m\left(\boldsymbol{k}\right)\left|\hat{L}^{\alpha}\right|n\left(\boldsymbol{k}\right)\right\rangle = -\frac{i\epsilon_{\beta\gamma}}{4\hbar}\left\langle m\left(\boldsymbol{k}\right)\left|\left(\hat{r}_{\beta}\hat{r}_{\gamma}\hat{H}_{\boldsymbol{k}}-2\hat{r}_{\beta}\hat{H}_{\boldsymbol{k}}\hat{r}_{\gamma}+\hat{H}_{\boldsymbol{k}}\hat{r}_{\beta}\hat{r}_{\gamma}\right)\right|n\left(\boldsymbol{k}\right)\right\rangle \tag{S80}$$

$$= \frac{i\epsilon_{\beta\gamma}}{4\hbar}\left\{\left(\left[\boldsymbol{\sigma}_{3}E_{\boldsymbol{k}}\right]_{nn}+\left[\boldsymbol{\sigma}_{3}E_{\boldsymbol{k}}\right]_{mm}\right)\left\langle \partial_{k_{\beta}}m\left(\boldsymbol{k}\right)\right|\boldsymbol{\sigma}_{3}\left|\partial_{k_{\gamma}}n\left(\boldsymbol{k}\right)\right\rangle -2\left\langle \partial_{k_{\beta}}m\left(\boldsymbol{k}\right)\right|\hat{H}_{\boldsymbol{k}}\left|\partial_{k_{\gamma}}n\left(\boldsymbol{k}\right)\right\rangle \right\} . \tag{S81}$$

We recast the above equation as

$$\left\langle m\left(\boldsymbol{k}\right)\left|\hat{\boldsymbol{L}}\right|n\left(\boldsymbol{k}\right)\right\rangle = \frac{i}{2\hbar}\left\langle \partial_{\boldsymbol{k}}m\left(\boldsymbol{k}\right)\right|\times\hat{H}_{\boldsymbol{k}}\left|\partial_{\boldsymbol{k}}n\left(\boldsymbol{k}\right)\right\rangle -\frac{i}{4\hbar}\left(\left[\boldsymbol{\sigma}_{3}E_{\boldsymbol{k}}\right]_{nn}+\left[\boldsymbol{\sigma}_{3}E_{\boldsymbol{k}}\right]_{mm}\right)\left\langle \partial_{\boldsymbol{k}}m\left(\boldsymbol{k}\right)\right|\times\boldsymbol{\sigma}_{3}\left|\partial_{\boldsymbol{k}}n\left(\boldsymbol{k}\right)\right\rangle \tag{S82}$$

For $n\equiv m$ one obtains

$$\left\langle n\left(\boldsymbol{k}\right)\left|\hat{\boldsymbol{L}}\right|n\left(\boldsymbol{k}\right)\right\rangle = \frac{i}{2\hbar}\left\langle \partial_{\boldsymbol{k}}n\left(\boldsymbol{k}\right)\right|\times\left\{\hat{H}_{\boldsymbol{k}}-\left[\boldsymbol{\sigma}_{3}E_{\boldsymbol{k}}\right]_{nn}\boldsymbol{\sigma}_{3}\right\}\left|\partial_{\boldsymbol{k}}n\left(\boldsymbol{k}\right)\right\rangle , \tag{S83}$$

which is the intrinsic orbital angular moment of magnon in the nth-state.

B. Relationship between magnon orbital angular moment and magnon Berry curvature. We now discuss the relationship between orbital angular moment in the magnon Bloch representation and the magnon Berry curvature. To do so, we start with the eigenequation for the magnon system, which reads

$$\boldsymbol{\sigma}_{3}\hat{H}_{\boldsymbol{k}}\left|n\left(\boldsymbol{k}\right)\right\rangle = \left[\boldsymbol{\sigma}_{3}E_{\boldsymbol{k}}\right]_{nn}\left|n\left(\boldsymbol{k}\right)\right\rangle . \tag{S84}$$

Taking the derivative of both sides with respect to $\partial_{\boldsymbol{k}}$, one obtains

$$\boldsymbol{\sigma}_{3}\partial_{\boldsymbol{k}}\hat{H}_{\boldsymbol{k}}\left|n\left(\boldsymbol{k}\right)\right\rangle +\boldsymbol{\sigma}_{3}\hat{H}_{\boldsymbol{k}}\left|\partial_{\boldsymbol{k}}n\left(\boldsymbol{k}\right)\right\rangle = \left[\boldsymbol{\sigma}_{3}\partial_{\boldsymbol{k}}E_{\boldsymbol{k}}\right]_{nn}\left|n\left(\boldsymbol{k}\right)\right\rangle +\left[\boldsymbol{\sigma}_{3}E_{\boldsymbol{k}}\right]_{nn}\left|\partial_{\boldsymbol{k}}n\left(\boldsymbol{k}\right)\right\rangle , \tag{S85}$$

Multiplying both sides with $\left\langle p\left(\boldsymbol{k}\right)\right|\boldsymbol{\sigma}_{3}$ and using $\boldsymbol{\sigma}_{3}\boldsymbol{\sigma}_{3}=\mathcal{I}$, where $\mathcal{I}$ is the identity matrix, one obtains:

$$\left\langle p\left(\boldsymbol{k}\right)\left|\partial_{\boldsymbol{k}}\hat{H}_{\boldsymbol{k}}\right|n\left(\boldsymbol{k}\right)\right\rangle +\left\langle p\left(\boldsymbol{k}\right)\left|\hat{H}_{\boldsymbol{k}}\right|\partial_{\boldsymbol{k}}n\left(\boldsymbol{k}\right)\right\rangle = \left[\boldsymbol{\sigma}_{3}\partial_{\boldsymbol{k}}E_{\boldsymbol{k}}\right]_{nn}\left\langle p\left(\boldsymbol{k}\right)\left|\boldsymbol{\sigma}_{3}\right|n\left(\boldsymbol{k}\right)\right\rangle +\left[\boldsymbol{\sigma}_{3}E_{\boldsymbol{k}}\right]_{nn}\left\langle p\left(\boldsymbol{k}\right)\left|\boldsymbol{\sigma}_{3}\right|\partial_{\boldsymbol{k}}n\left(\boldsymbol{k}\right)\right\rangle . \tag{S86}$$

Note that $\left\langle p\left(\boldsymbol{k}\right)\left|\boldsymbol{\sigma}_{3}\right|n\left(\boldsymbol{k}\right)\right\rangle =\left\langle n\left(\boldsymbol{k}\right)\left|\boldsymbol{\sigma}_{3}\right|n\left(\boldsymbol{k}\right)\right\rangle \delta_{p,n}=\sigma_{3}^{nn}\delta_{p,n}$ and

$$\left\langle p\left(\boldsymbol{k}\right)\left|\hat{H}_{\boldsymbol{k}}\right|\partial_{\boldsymbol{k}}n\left(\boldsymbol{k}\right)\right\rangle = \left[\boldsymbol{\sigma}_{3}E_{\boldsymbol{k}}\right]_{pp}\left\langle p\left(\boldsymbol{k}\right)\left|\boldsymbol{\sigma}_{3}\right|\partial_{\boldsymbol{k}}n\left(\boldsymbol{k}\right)\right\rangle \tag{S87}$$

so that, for $n\equiv p$, one gets:

$$\sigma_{3}^{nn}\left[\boldsymbol{\sigma}_{3}\partial_{\boldsymbol{k}}E_{\boldsymbol{k}}\right]_{nn} = \left\langle n\left(\boldsymbol{k}\right)\left|\partial_{\boldsymbol{k}}\hat{H}_{\boldsymbol{k}}\right|n\left(\boldsymbol{k}\right)\right\rangle , \tag{S88}$$

which is the well-known Hellmann-Feynman theorem. For the case $n \neq p$, one has

$$\left\langle p\left(\boldsymbol{k}\right)\left|\partial_{\boldsymbol{k}}\hat{H}_{\boldsymbol{k}}\right|n\left(\boldsymbol{k}\right)\right\rangle = \left\{\left[\boldsymbol{\sigma}_3 E_{\boldsymbol{k}}\right]_{nn} - \left[\boldsymbol{\sigma}_3 E_{\boldsymbol{k}}\right]_{pp}\right\}\left\langle p\left(\boldsymbol{k}\right)\left|\boldsymbol{\sigma}_3\right|\partial_{\boldsymbol{k}} n\left(\boldsymbol{k}\right)\right\rangle, \tag{S89}$$

which leads to

$$\left\langle p\left(\boldsymbol{k}\right)\left|\boldsymbol{\sigma}_3\right|\partial_{\boldsymbol{k}} n\left(\boldsymbol{k}\right)\right\rangle = \frac{\left\langle p\left(\boldsymbol{k}\right)\left|\partial_{\boldsymbol{k}}\hat{H}_{\boldsymbol{k}}\right|n\left(\boldsymbol{k}\right)\right\rangle}{\left[\boldsymbol{\sigma}_3 E_{\boldsymbol{k}}\right]_{nn} - \left[\boldsymbol{\sigma}_3 E_{\boldsymbol{k}}\right]_{pp}}. \tag{S90}$$

Multiplying both sides with $\sigma_3^{pp}\left|m\left(\boldsymbol{k}\right)\right\rangle$ and taking a sum over all p ($p \neq n$), one has:

$$\sum_{p\neq n}\sigma_3^{pp}\left|p\left(\boldsymbol{k}\right)\right\rangle\left\langle p\left(\boldsymbol{k}\right)\left|\boldsymbol{\sigma}_3\right|\partial_{\boldsymbol{k}} n\left(\boldsymbol{k}\right)\right\rangle = \sum_{p\neq n}\sigma_3^{pp}\left|p\left(\boldsymbol{k}\right)\right\rangle\frac{\left\langle p\left(\boldsymbol{k}\right)\left|\partial_{\boldsymbol{k}}\hat{H}_{\boldsymbol{k}}\right|n\left(\boldsymbol{k}\right)\right\rangle}{\left[\boldsymbol{\sigma}_3 E_{\boldsymbol{k}}\right]_{nn} - \left[\boldsymbol{\sigma}_3 E_{\boldsymbol{k}}\right]_{pp}} \tag{S91}$$

$$\left[\sum_{p\neq n}\sigma_3^{pp}\left|p\left(\boldsymbol{k}\right)\right\rangle\left\langle p\left(\boldsymbol{k}\right)\right|\boldsymbol{\sigma}_3\right]\left|\partial_{\boldsymbol{k}} n\left(\boldsymbol{k}\right)\right\rangle = \sum_{p\neq n}\sigma_3^{pp}\left|p\left(\boldsymbol{k}\right)\right\rangle\frac{\left\langle p\left(\boldsymbol{k}\right)\left|\partial_{\boldsymbol{k}}\hat{H}_{\boldsymbol{k}}\right|n\left(\boldsymbol{k}\right)\right\rangle}{\left[\boldsymbol{\sigma}_3 E_{\boldsymbol{k}}\right]_{nn} - \left[\boldsymbol{\sigma}_3 E_{\boldsymbol{k}}\right]_{pp}}. \tag{S92}$$

Using the completeness equation of the BdG Hamiltonian $\sum_p \sigma_3^{pp}\left|p\left(\boldsymbol{k}\right)\right\rangle\left\langle p\left(\boldsymbol{k}\right)\right|\boldsymbol{\sigma}_3 = \mathcal{I}$, one obtains:

$$\left(-i\mathcal{A}_n + \partial_{\boldsymbol{k}}\right)\left|n\left(\boldsymbol{k}\right)\right\rangle = \sum_{p\neq n}\sigma_3^{pp}\frac{\left\langle p\left(\boldsymbol{k}\right)\left|\partial_{\boldsymbol{k}}\hat{H}_{\boldsymbol{k}}\right|n\left(\boldsymbol{k}\right)\right\rangle}{\left[\boldsymbol{\sigma}_3 E_{\boldsymbol{k}}\right]_{nn} - \left[\boldsymbol{\sigma}_3 E_{\boldsymbol{k}}\right]_{pp}}\left|p\left(\boldsymbol{k}\right)\right\rangle \tag{S93}$$

where $\mathcal{A}_n = i\sigma_3^{nn}\left\langle n\left(\boldsymbol{k}\right)\left|\boldsymbol{\sigma}_3\right|\partial_{\boldsymbol{k}} n\left(\boldsymbol{k}\right)\right\rangle$ is the Berry connection. A gauge choice of $\mathcal{A}_n = 0$ can be applied, which leads to:

$$\left|\partial_{\boldsymbol{k}} n\left(\boldsymbol{k}\right)\right\rangle = \sum_{p\neq n}\sigma_3^{pp}\frac{\left\langle p\left(\boldsymbol{k}\right)\left|\partial_{\boldsymbol{k}}\hat{H}_{\boldsymbol{k}}\right|n\left(\boldsymbol{k}\right)\right\rangle}{\left[\boldsymbol{\sigma}_3 E_{\boldsymbol{k}}\right]_{nn} - \left[\boldsymbol{\sigma}_3 E_{\boldsymbol{k}}\right]_{pp}}\left|p\left(\boldsymbol{k}\right)\right\rangle \tag{S94}$$

In the same manner, one has

$$\left\langle\partial_{\boldsymbol{k}} m\left(\boldsymbol{k}\right)\right| = \sum_{l\neq m}\sigma_3^{ll}\frac{\left\langle m\left(\boldsymbol{k}\right)\left|\partial_{\boldsymbol{k}}\hat{H}_{\boldsymbol{k}}\right|l\left(\boldsymbol{k}\right)\right\rangle}{\left[\boldsymbol{\sigma}_3 E_{\boldsymbol{k}}\right]_{mm} - \left[\boldsymbol{\sigma}_3 E_{\boldsymbol{k}}\right]_{ll}}\left\langle l\left(\boldsymbol{k}\right)\right|. \tag{S95}$$

Inserting the above relations into the expression of the following term:

$$\begin{aligned}
&\left\langle\partial_{\boldsymbol{k}} m\left(\boldsymbol{k}\right)\right| \times \hat{H}_{\boldsymbol{k}}\left|\partial_{\boldsymbol{k}} n\left(\boldsymbol{k}\right)\right\rangle \\
&= \sum_{l\neq m}\sigma_3^{ll}\frac{\left\langle m\left(\boldsymbol{k}\right)\left|\partial_{\boldsymbol{k}}\hat{H}_{\boldsymbol{k}}\right|l\left(\boldsymbol{k}\right)\right\rangle}{\left[\boldsymbol{\sigma}_3 E_{\boldsymbol{k}}\right]_{mm} - \left[\boldsymbol{\sigma}_3 E_{\boldsymbol{k}}\right]_{ll}}\left\langle l\left(\boldsymbol{k}\right)\right| \times \hat{H}_{\boldsymbol{k}}\sum_{p\neq n}\sigma_3^{pp}\frac{\left\langle p\left(\boldsymbol{k}\right)\left|\partial_{\boldsymbol{k}}\hat{H}_{\boldsymbol{k}}\right|n\left(\boldsymbol{k}\right)\right\rangle}{\left[\boldsymbol{\sigma}_3 E_{\boldsymbol{k}}\right]_{nn} - \left[\boldsymbol{\sigma}_3 E_{\boldsymbol{k}}\right]_{pp}}\left|p\left(\boldsymbol{k}\right)\right\rangle && \text{[S96]} \\
&= \sum_{l\neq m}\sigma_3^{ll}\frac{\left\langle m\left(\boldsymbol{k}\right)\left|\partial_{\boldsymbol{k}}\hat{H}_{\boldsymbol{k}}\right|l\left(\boldsymbol{k}\right)\right\rangle}{\left[\boldsymbol{\sigma}_3 E_{\boldsymbol{k}}\right]_{mm} - \left[\boldsymbol{\sigma}_3 E_{\boldsymbol{k}}\right]_{ll}}\left\langle l\left(\boldsymbol{k}\right)\right| \times \sum_{p\neq n}\sigma_3^{pp}\frac{\left\langle p\left(\boldsymbol{k}\right)\left|\partial_{\boldsymbol{k}}\hat{H}_{\boldsymbol{k}}\right|n\left(\boldsymbol{k}\right)\right\rangle}{\left[\boldsymbol{\sigma}_3 E_{\boldsymbol{k}}\right]_{nn} - \left[\boldsymbol{\sigma}_3 E_{\boldsymbol{k}}\right]_{pp}}\hat{H}_{\boldsymbol{k}}\left|p\left(\boldsymbol{k}\right)\right\rangle && \text{[S97]} \\
&= \sum_{l\neq m}\sigma_3^{ll}\frac{\left\langle m\left(\boldsymbol{k}\right)\left|\partial_{\boldsymbol{k}}\hat{H}_{\boldsymbol{k}}\right|l\left(\boldsymbol{k}\right)\right\rangle}{\left[\boldsymbol{\sigma}_3 E_{\boldsymbol{k}}\right]_{mm} - \left[\boldsymbol{\sigma}_3 E_{\boldsymbol{k}}\right]_{ll}}\left\langle l\left(\boldsymbol{k}\right)\right| \times \sum_{p\neq n}\sigma_3^{pp}\frac{\left\langle p\left(\boldsymbol{k}\right)\left|\partial_{\boldsymbol{k}}\hat{H}_{\boldsymbol{k}}\right|n\left(\boldsymbol{k}\right)\right\rangle}{\left[\boldsymbol{\sigma}_3 E_{\boldsymbol{k}}\right]_{nn} - \left[\boldsymbol{\sigma}_3 E_{\boldsymbol{k}}\right]_{pp}}\boldsymbol{\sigma}_3\left[\boldsymbol{\sigma}_3 E_{\boldsymbol{k}}\right]_{pp}\left|p\left(\boldsymbol{k}\right)\right\rangle && \text{[S98]} \\
&= \sum_{l\neq m}\sigma_3^{ll}\frac{\left\langle m\left(\boldsymbol{k}\right)\left|\partial_{\boldsymbol{k}}\hat{H}_{\boldsymbol{k}}\right|l\left(\boldsymbol{k}\right)\right\rangle}{\left[\boldsymbol{\sigma}_3 E_{\boldsymbol{k}}\right]_{mm} - \left[\boldsymbol{\sigma}_3 E_{\boldsymbol{k}}\right]_{ll}}\left\langle l\left(\boldsymbol{k}\right)\right| \times \sum_{p\neq n}\sigma_3^{pp}\left[\boldsymbol{\sigma}_3 E\left(\boldsymbol{k}\right)\right]_{pp}\frac{\left\langle p\left(\boldsymbol{k}\right)\left|\partial_{\boldsymbol{k}}\hat{H}_{\boldsymbol{k}}\right|n\left(\boldsymbol{k}\right)\right\rangle}{\left[\boldsymbol{\sigma}_3 E_{\boldsymbol{k}}\right]_{nn} - \left[\boldsymbol{\sigma}_3 E_{\boldsymbol{k}}\right]_{pp}}\boldsymbol{\sigma}_3\left|p\left(\boldsymbol{k}\right)\right\rangle && \text{[S99]} \\
&= \sum_{l\neq m}\sum_{p\neq n}\sigma_3^{ll}\sigma_3^{pp}\left[\boldsymbol{\sigma}_3 E_{\boldsymbol{k}}\right]_{pp}\frac{\left\langle m\left(\boldsymbol{k}\right)\left|\partial_{\boldsymbol{k}}\hat{H}_{\boldsymbol{k}}\right|l\left(\boldsymbol{k}\right)\right\rangle \times \left\langle p\left(\boldsymbol{k}\right)\left|\partial_{\boldsymbol{k}}\hat{H}_{\boldsymbol{k}}\right|n\left(\boldsymbol{k}\right)\right\rangle}{\left\{\left[\boldsymbol{\sigma}_3 E_{\boldsymbol{k}}\right]_{mm} - \left[\boldsymbol{\sigma}_3 E_{\boldsymbol{k}}\right]_{ll}\right\}\left\{\left[\boldsymbol{\sigma}_3 E_{\boldsymbol{k}}\right]_{nn} - \left[\boldsymbol{\sigma}_3 E_{\boldsymbol{k}}\right]_{pp}\right\}}\left\langle l\left(\boldsymbol{k}\right)\right|\boldsymbol{\sigma}_3\left|p\left(\boldsymbol{k}\right)\right\rangle && \text{[S100]} \\
&= \hbar^2\sum_{l\neq m}\sum_{p\neq n}\sigma_3^{ll}\sigma_3^{pp}\left[\boldsymbol{\sigma}_3 E_{\boldsymbol{k}}\right]_{pp}\frac{\left\langle m\left(\boldsymbol{k}\right)\left|\boldsymbol{v}\right|l\left(\boldsymbol{k}\right)\right\rangle \times \left\langle p\left(\boldsymbol{k}\right)\left|\boldsymbol{v}\right|n\left(\boldsymbol{k}\right)\right\rangle}{\left\{\left[\boldsymbol{\sigma}_3 E_{\boldsymbol{k}}\right]_{mm} - \left[\boldsymbol{\sigma}_3 E_{\boldsymbol{k}}\right]_{ll}\right\}\left\{\left[\boldsymbol{\sigma}_3 E_{\boldsymbol{k}}\right]_{nn} - \left[\boldsymbol{\sigma}_3 E_{\boldsymbol{k}}\right]_{pp}\right\}}\left\langle l\left(\boldsymbol{k}\right)\right|\boldsymbol{\sigma}_3\left|p\left(\boldsymbol{k}\right)\right\rangle. && \text{[S101]}
\end{aligned}$$

Similarly, one obtains

$$\begin{aligned}
&\langle \partial_{\boldsymbol{k}} m(\boldsymbol{k})| \times \boldsymbol{\sigma}_3 |\partial_{\boldsymbol{k}} n(\boldsymbol{k})\rangle \\
&= \sum_{l\neq m} \sigma_3^{ll} \frac{\left\langle m(\boldsymbol{k}) \left|\partial_{\boldsymbol{k}} \hat{H}_{\boldsymbol{k}}\right| l(\boldsymbol{k})\right\rangle}{[\boldsymbol{\sigma}_3 E_{\boldsymbol{k}}]_{mm} - [\boldsymbol{\sigma}_3 E_{\boldsymbol{k}}]_{ll}} \langle l(\boldsymbol{k})| \times \boldsymbol{\sigma}_3 \sum_{p\neq n} \sigma_3^{pp} \frac{\left\langle p(\boldsymbol{k}) \left|\partial_{\boldsymbol{k}} \hat{H}_{\boldsymbol{k}}\right| n(\boldsymbol{k})\right\rangle}{[\boldsymbol{\sigma}_3 E_{\boldsymbol{k}}]_{nn} - [\boldsymbol{\sigma}_3 E_{\boldsymbol{k}}]_{pp}} |p(\boldsymbol{k})\rangle \qquad \text{[S102]} \\
&= \sum_{l\neq m}\sum_{p\neq n} \sigma_3^{ll}\sigma_3^{pp} \frac{\left\langle m(\boldsymbol{k}) \left|\partial_{\boldsymbol{k}} \hat{H}_{\boldsymbol{k}}\right| l(\boldsymbol{k})\right\rangle}{[\boldsymbol{\sigma}_3 E_{\boldsymbol{k}}]_{mm} - [\boldsymbol{\sigma}_3 E_{\boldsymbol{k}}]_{ll}} \langle l(\boldsymbol{k})| \times \boldsymbol{\sigma}_3 \frac{\left\langle p(\boldsymbol{k}) \left|\partial_{\boldsymbol{k}} \hat{H}_{\boldsymbol{k}}\right| n(\boldsymbol{k})\right\rangle}{[\boldsymbol{\sigma}_3 E_{\boldsymbol{k}}]_{nn} - [\boldsymbol{\sigma}_3 E_{\boldsymbol{k}}]_{pp}} |p(\boldsymbol{k})\rangle \qquad \text{[S103]} \\
&= \sum_{l\neq m}\sum_{p\neq n} \sigma_3^{ll}\sigma_3^{pp} \frac{\left\langle m(\boldsymbol{k}) \left|\partial_{\boldsymbol{k}} \hat{H}_{\boldsymbol{k}}\right| l(\boldsymbol{k})\right\rangle \times \left\langle p(\boldsymbol{k}) \left|\partial_{\boldsymbol{k}} \hat{H}_{\boldsymbol{k}}\right| n(\boldsymbol{k})\right\rangle}{\left\{[\boldsymbol{\sigma}_3 E_{\boldsymbol{k}}]_{mm} - [\boldsymbol{\sigma}_3 E_{\boldsymbol{k}}]_{ll}\right\}\left\{[\boldsymbol{\sigma}_3 E_{\boldsymbol{k}}]_{nn} - [\boldsymbol{\sigma}_3 E_{\boldsymbol{k}}]_{pp}\right\}} \langle l(\boldsymbol{k})| \boldsymbol{\sigma}_3 |p(\boldsymbol{k})\rangle \qquad \text{[S104]} \\
&= \hbar^2 \sum_{l\neq m}\sum_{p\neq n} \sigma_3^{ll}\sigma_3^{pp} \frac{\langle m(\boldsymbol{k})|\hat{\boldsymbol{v}}_{\boldsymbol{k}}| l(\boldsymbol{k})\rangle \times \langle p(\boldsymbol{k})|\hat{\boldsymbol{v}}_{\boldsymbol{k}}| n(\boldsymbol{k})\rangle}{\left\{[\boldsymbol{\sigma}_3 E_{\boldsymbol{k}}]_{mm} - [\boldsymbol{\sigma}_3 E_{\boldsymbol{k}}]_{ll}\right\}\left\{[\boldsymbol{\sigma}_3 E_{\boldsymbol{k}}]_{nn} - [\boldsymbol{\sigma}_3 E_{\boldsymbol{k}}]_{pp}\right\}} \langle l(\boldsymbol{k})| \boldsymbol{\sigma}_3 |p(\boldsymbol{k})\rangle \qquad \text{[S105]}
\end{aligned}$$

where

$$\hat{\boldsymbol{v}}_{\boldsymbol{k}} = \frac{1}{\hbar}\partial_{\boldsymbol{k}} \hat{H}_{\boldsymbol{k}} \qquad \text{[S106]}$$

is the velocity operator. Note that $\langle l(\boldsymbol{k})| \boldsymbol{\sigma}_3 |p(\boldsymbol{k})\rangle = \langle p(\boldsymbol{k})| \boldsymbol{\sigma}_3 |p(\boldsymbol{k})\rangle \delta_{p,l}$. Therefore, one gets:

$$\begin{aligned}
&\langle \partial_{\boldsymbol{k}} m(\boldsymbol{k})| \times \boldsymbol{\sigma}_3 |\partial_{\boldsymbol{k}} n(\boldsymbol{k})\rangle \\
&= \hbar^2 \sum_{p\neq m}\sum_{p\neq n} \sigma_3^{pp}\sigma_3^{pp} \frac{\langle m(\boldsymbol{k})|\hat{\boldsymbol{v}}_{\boldsymbol{k}}| p(\boldsymbol{k})\rangle \times \langle p(\boldsymbol{k})|\hat{\boldsymbol{v}}_{\boldsymbol{k}}| n(\boldsymbol{k})\rangle}{\left\{[\boldsymbol{\sigma}_3 E_{\boldsymbol{k}}]_{mm} - [\boldsymbol{\sigma}_3 E_{\boldsymbol{k}}]_{pp}\right\}\left\{[\boldsymbol{\sigma}_3 E_{\boldsymbol{k}}]_{nn} - [\boldsymbol{\sigma}_3 E_{\boldsymbol{k}}]_{pp}\right\}} \langle p(\boldsymbol{k})| \boldsymbol{\sigma}_3 |p(\boldsymbol{k})\rangle \qquad \text{[S107]} \\
&= \hbar^2 \sum_{p\neq m,n} \sigma_3^{pp} \frac{\langle m(\boldsymbol{k})|\hat{\boldsymbol{v}}_{\boldsymbol{k}}| p(\boldsymbol{k})\rangle \times \langle p(\boldsymbol{k})|\hat{\boldsymbol{v}}_{\boldsymbol{k}}| n(\boldsymbol{k})\rangle}{\left\{[\boldsymbol{\sigma}_3 E_{\boldsymbol{k}}]_{mm} - [\boldsymbol{\sigma}_3 E_{\boldsymbol{k}}]_{pp}\right\}\left\{[\boldsymbol{\sigma}_3 E_{\boldsymbol{k}}]_{nn} - [\boldsymbol{\sigma}_3 E_{\boldsymbol{k}}]_{pp}\right\}} \qquad \text{[S108]}
\end{aligned}$$

leads to

$$\langle \partial_{\boldsymbol{k}} m(\boldsymbol{k})| \times \boldsymbol{\sigma}_3 |\partial_{\boldsymbol{k}} n(\boldsymbol{k})\rangle = \hbar^2 \sum_{p\neq m,n} \sigma_3^{pp} \frac{\langle m(\boldsymbol{k})|\hat{\boldsymbol{v}}_{\boldsymbol{k}}| p(\boldsymbol{k})\rangle \times \langle p(\boldsymbol{k})|\hat{\boldsymbol{v}}_{\boldsymbol{k}}| n(\boldsymbol{k})\rangle}{\left\{[\boldsymbol{\sigma}_3 E_{\boldsymbol{k}}]_{mm} - [\boldsymbol{\sigma}_3 E_{\boldsymbol{k}}]_{pp}\right\}\left\{[\boldsymbol{\sigma}_3 E_{\boldsymbol{k}}]_{nn} - [\boldsymbol{\sigma}_3 E_{\boldsymbol{k}}]_{pp}\right\}} \qquad \text{[S109]}$$

where we have used $\sigma_3^{pp}\sigma_3^{pp} = 1$ and $\langle p(\boldsymbol{k})| \boldsymbol{\sigma}_3 |p(\boldsymbol{k})\rangle = \sigma_3^{pp}$.

Similarly, one obtains:

$$\langle \partial_{\boldsymbol{k}} m(\boldsymbol{k})| \times \hat{H}_{\boldsymbol{k}} |\partial_{\boldsymbol{k}} n(\boldsymbol{k})\rangle = \hbar^2 \sum_{p\neq m,n} \sigma_3^{pp} [\boldsymbol{\sigma}_3 E_{\boldsymbol{k}}]_{pp} \frac{\langle m(\boldsymbol{k})|\hat{\boldsymbol{v}}_{\boldsymbol{k}}| p(\boldsymbol{k})\rangle \times \langle p(\boldsymbol{k})|\hat{\boldsymbol{v}}_{\boldsymbol{k}}| n(\boldsymbol{k})\rangle}{\left\{[\boldsymbol{\sigma}_3 E_{\boldsymbol{k}}]_{mm} - [\boldsymbol{\sigma}_3 E_{\boldsymbol{k}}]_{pp}\right\}\left\{[\boldsymbol{\sigma}_3 E_{\boldsymbol{k}}]_{nn} - [\boldsymbol{\sigma}_3 E_{\boldsymbol{k}}]_{pp}\right\}} \qquad \text{[S110]}$$

Inserting the above relations into the expression of the magnon orbital angular moment, we obtain:

$$\begin{aligned}
\left\langle m(\boldsymbol{k}) \left|\hat{\boldsymbol{L}}\right| n(\boldsymbol{k})\right\rangle &= \frac{i\hbar^2}{2\hbar} \left\{ \sum_{p\neq m,n} \sigma_3^{pp} [\boldsymbol{\sigma}_3 E_{\boldsymbol{k}}]_{pp} \frac{\langle m(\boldsymbol{k})|\hat{\boldsymbol{v}}_{\boldsymbol{k}}| p(\boldsymbol{k})\rangle \times \langle p(\boldsymbol{k})|\hat{\boldsymbol{v}}_{\boldsymbol{k}}| n(\boldsymbol{k})\rangle}{\left\{[\boldsymbol{\sigma}_3 E_{\boldsymbol{k}}]_{mm} - [\boldsymbol{\sigma}_3 E_{\boldsymbol{k}}]_{pp}\right\}\left\{[\boldsymbol{\sigma}_3 E_{\boldsymbol{k}}]_{nn} - [\boldsymbol{\sigma}_3 E_{\boldsymbol{k}}]_{pp}\right\}} \right\} \qquad \text{[S111]} \\
&- \frac{i\hbar^2}{4\hbar} \left\{ \sum_{p\neq m,n} \sigma_3^{pp} \left([\boldsymbol{\sigma}_3 E_{\boldsymbol{k}}]_{nn} + [\boldsymbol{\sigma}_3 E_{\boldsymbol{k}}]_{mm}\right) \frac{\langle m(\boldsymbol{k})|\hat{\boldsymbol{v}}_{\boldsymbol{k}}| p(\boldsymbol{k})\rangle \times \langle p(\boldsymbol{k})|\hat{\boldsymbol{v}}_{\boldsymbol{k}}| n(\boldsymbol{k})\rangle}{\left\{[\boldsymbol{\sigma}_3 E_{\boldsymbol{k}}]_{mm} - [\boldsymbol{\sigma}_3 E_{\boldsymbol{k}}]_{pp}\right\}\left\{[\boldsymbol{\sigma}_3 E_{\boldsymbol{k}}]_{nn} - [\boldsymbol{\sigma}_3 E_{\boldsymbol{k}}]_{pp}\right\}} \right\} \qquad \text{[S112]} \\
&= -\frac{i\hbar}{4} \left\{ \sum_{p\neq m,n} \frac{\sigma_3^{pp} \left([\boldsymbol{\sigma}_3 E_{\boldsymbol{k}}]_{nn} + [\boldsymbol{\sigma}_3 E_{\boldsymbol{k}}]_{mm} - 2[\boldsymbol{\sigma}_3 E_{\boldsymbol{k}}]_{pp}\right) \langle m(\boldsymbol{k})|\hat{\boldsymbol{v}}_{\boldsymbol{k}}| p(\boldsymbol{k})\rangle \times \langle p(\boldsymbol{k})|\hat{\boldsymbol{v}}_{\boldsymbol{k}}| n(\boldsymbol{k})\rangle}{\left\{[\boldsymbol{\sigma}_3 E_{\boldsymbol{k}}]_{mm} - [\boldsymbol{\sigma}_3 E_{\boldsymbol{k}}]_{pp}\right\}\left\{[\boldsymbol{\sigma}_3 E_{\boldsymbol{k}}]_{nn} - [\boldsymbol{\sigma}_3 E_{\boldsymbol{k}}]_{pp}\right\}} \right\} \qquad \text{[S113]} \\
&= -\frac{i\hbar}{4} \left\{ \sum_{p\neq m,n} \sigma_3^{pp} \left(\frac{1}{[\boldsymbol{\sigma}_3 E_{\boldsymbol{k}}]_{mm} - [\boldsymbol{\sigma}_3 E_{\boldsymbol{k}}]_{pp}} + \frac{1}{[\boldsymbol{\sigma}_3 E_{\boldsymbol{k}}]_{nn} - [\boldsymbol{\sigma}_3 E_{\boldsymbol{k}}]_{pp}} \right) \langle m(\boldsymbol{k})|\hat{\boldsymbol{v}}_{\boldsymbol{k}}| p(\boldsymbol{k})\rangle \times \langle p(\boldsymbol{k})|\hat{\boldsymbol{v}}_{\boldsymbol{k}}| n(\boldsymbol{k})\rangle \right\} \qquad \text{[S114]}
\end{aligned}$$

which can be recast as

$$\boldsymbol{L}_{mn}(\boldsymbol{k}) = \left\langle m(\boldsymbol{k}) \left|\hat{\boldsymbol{L}}\right| n(\boldsymbol{k})\right\rangle = -i\hbar \boldsymbol{\mathcal{N}}_{mn} \qquad \text{[S115]}$$

where

$$\begin{aligned}
\boldsymbol{\mathcal{N}}_{mn} = \frac{1}{4} \sum_{p\neq m,n} \sigma_3^{pp} &\left(\frac{1}{[\boldsymbol{\sigma}_3 E_{\boldsymbol{k}}]_{mm} - [\boldsymbol{\sigma}_3 E_{\boldsymbol{k}}]_{pp}} + \frac{1}{[\boldsymbol{\sigma}_3 E_{\boldsymbol{k}}]_{nn} - [\boldsymbol{\sigma}_3 E_{\boldsymbol{k}}]_{pp}} \right) \times \\
&\times \langle m(\boldsymbol{k})|\hat{\boldsymbol{v}}_{\boldsymbol{k}}| p(\boldsymbol{k})\rangle \times \langle p(\boldsymbol{k})|\hat{\boldsymbol{v}}_{\boldsymbol{k}}| n(\boldsymbol{k})\rangle . \qquad \text{[S116]}
\end{aligned}$$

The intra-band magnon orbital angular moment is given by:

$$\boldsymbol{L}_{nn}(\boldsymbol{k}) = -i\hbar\boldsymbol{\mathcal{N}}_{nn} \tag{S117}$$

where

$$\boldsymbol{\mathcal{N}}_{nn} = \frac{1}{2}\sum_{p\neq n}\sigma_3^{pp}\frac{\langle n(\boldsymbol{k})|\hat{\boldsymbol{v}}_{\boldsymbol{k}}|p(\boldsymbol{k})\rangle \times \langle p(\boldsymbol{k})|\hat{\boldsymbol{v}}_{\boldsymbol{k}}|n(\boldsymbol{k})\rangle}{[\boldsymbol{\sigma}_3 E_{\boldsymbol{k}}]_{nn} - [\boldsymbol{\sigma}_3 E_{\boldsymbol{k}}]_{pp}} \tag{S118}$$

thereby completing the derivation of Eq. (4), which shows the deep connections to the magnon Berry curvature in Eq. (2) in the main text.

The connection between intra-band magnon orbital angular moment and Berry curvature offers a fascinating shortcut. Much like Berry curvature, intra-band magnon orbital angular moment exhibits analogous behaviors under combined parity time symmetry (CPTS) and effective time reversal symmetry (TRS) operations. In this context, CPTS imposes a constraint, rendering the intra-band magnon orbital angular moment zero, while TRS introduces an intriguing peculiarity: the intra-band magnon orbital angular moment becomes an odd function with respect to wavevector (13). This phenomenon is particularly noteworthy in systems such as the 2D honeycomb antiferromagnetic structure with Néel order. Here, intra-band magnon orbital angular moment can manifest even in the absence of Dzyaloshinskii-Moriya interaction, courtesy of the self-broken CPTS arising from the lack of an inversion center [see Fig. S1(b)]. In contrast, the Zigzag pattern's presence of CPTS due to the existence of the inversion center I_c, as presented in Fig. S1(c), underscores the indispensability of DMI for observing nonvanishing intra-band magnon orbital angular moment. Hence, we see that DMI is essential to the observation of nontrivial intra-band magnon orbital angular moment in systems exhibiting Zigzag order.

The odd parity of intra-band magnon orbital angular moment with respect to the wavevector in 2D honeycomb systems with Néel order results in zero contribution to electric polarization in the absence of DMI. Similarly, in the 2D honeycomb antiferromagnetic structure with Zigzag order, the lack of DMI causes the intra-band magnon orbital angular moment to vanish, thereby leading to zero intra-band magnon orbital angular moment induced electric polarization. Consequently, we see that DMI plays a crucial role in enabling magnon OAM to contribute to electric polarization in 2D honeycomb AFMs with either Néel or Zigzag magnetic configuration, as discussed in the main text.

In a continued analogy to Berry curvature, intra-band magnon orbital angular moment increases at anti-crossing points or band extrema. This suggests that materials with enhanced hybridization between different bands would exhibit substantial intra-band magnon orbital angular moment and magnon ONE, consequently resulting in a larger observable quantity such as electric polarization.

Finally, the total magnon orbital angular moment tensor $\boldsymbol{L}$, which encompasses both intra- and inter-band orbital angular momentum, is expressed as

$$\boldsymbol{L}(\boldsymbol{k}) = -i\hbar\boldsymbol{\mathcal{N}} \tag{S119}$$

where $\boldsymbol{\mathcal{N}}$ is a rank 3 tensor whose components and elements are given by Eq. (S116). The expression Eq. (S119) serves as the foundation for computing the magnon orbital Berry curvature, the magnon orbital Nernst current, and the magnon induced electric polarization, as fully derived in the subsequent sections through the application of linear response theory and perturbation theory.

S3. Magnon-induced electric polarization

A. Electric polarization induced by magnons in equilibrium: : A perturbation theory approach. In this section we provide a comprehensive derivation of the formula used in the main text for electric polarization induced by motions of magnon wave packet. This idea stems from the duality between electric and magnetic fields, offering a shortcut from electron-based mechanisms to those involving magnons (14, 15). Notably, the orbital moment of electrons is known to contribute to magnetization (16–18). Building upon this understanding, it is reasonable to anticipate that the orbital moment of magnons, along with their finite magnetic dipoles, could similarly influence the electric polarization. This insight opens avenues for detecting the orbital angular moment of magnons and exploring phenomena such as the Orbital Nernst effect of magnons, which are the focus of our study.

We now employ standard perturbation theory to derive the formula for the magnon-induced electric polarization discussed in the main text. To do so, we suppose that the system is in the ground states and calculate the energy correction due to a uniform electric field. We consider noninteracting magnons in which the grand-canonical partition function is given by

$$\Omega = E - TS + \mu N \tag{S120}$$

where E is the energy density, T is the temperature and S is the entropy of the system, μ is the chemical potential and N is the total number of particles.

The electric polarization is given by

$$\boldsymbol{P} = -\frac{1}{V}\left(\frac{\partial\Omega}{\partial\boldsymbol{\Xi}}\right)_T. \tag{S121}$$

Because the zero-temperature electric polarization

$$\tilde{\boldsymbol{P}} = -\frac{1}{V}\left(\frac{\partial E}{\partial\boldsymbol{\Xi}}\right)_T \tag{S122}$$

is related to the finite temperature electric polarization through the relationship

$$\tilde{\boldsymbol{P}} = \frac{\partial(\beta \boldsymbol{P})}{\partial \beta} \tag{S123}$$

where $\beta = \frac{1}{k_B T}$, in the following we only compute $\tilde{\boldsymbol{P}}$ and then infer $\boldsymbol{P}$ from relationship Eq. (S123). To derive the expression for $\tilde{\boldsymbol{P}}$ involving the quantum mechanical wavefunction and energy dispersion, we represent the relation Eq. (S122) as

$$\delta E = \int d\boldsymbol{r} \delta E(\boldsymbol{r}) = -\int d\boldsymbol{r} \tilde{\boldsymbol{P}}(\boldsymbol{r}) \boldsymbol{\Xi}(\boldsymbol{r}) \tag{S124}$$

where

$$\delta E(\boldsymbol{r}) = \tilde{\boldsymbol{P}}(\boldsymbol{r}) \boldsymbol{\Xi}(\boldsymbol{r}) \tag{S125}$$

is the local change of the energy induced by external electric field.

We start from the single-particle Hamiltonian:

$$\hat{H} = \hat{H}^0 + \hat{V}_{\boldsymbol{\Xi}} \tag{S126}$$

where $\hat{H}_0$ is the unperturbed Hamiltonian that yields the band dispersion $E_{n,\boldsymbol{k}}$ and corresponding Bloch wave function $\psi_{n,\boldsymbol{k}}(\boldsymbol{r}) = \langle \boldsymbol{r} | \psi_{n,\boldsymbol{k}} \rangle = e^{i\boldsymbol{k}.\boldsymbol{r}} u_{n,\boldsymbol{k}}(\boldsymbol{r})$.

We will now calculate the perturbed electric potential energy of the magnons $\hat{V}_{\boldsymbol{\Xi}}$. The local charge polarization induced by a magnon wavepacket with velocity $\boldsymbol{v}$ carrying magnetic dipole moment $\boldsymbol{m} = g\mu_B \boldsymbol{S}$ is described by the following operator (15):

$$\hat{\mathbf{p}} = \frac{\hat{\boldsymbol{v}} \times \hat{\boldsymbol{m}} - \hat{\boldsymbol{m}} \times \hat{\boldsymbol{v}}}{2Vc^2} \tag{S127}$$

where V represents the volume of the system, and c is the speed of light in vacuum. Under an externally applied electric field $\boldsymbol{\Xi}$ which is generally non-uniform, the perturbing electric potential energy of the magnon wave packet at position $\boldsymbol{r}$ associated with this charge polarization is expressed as:

$$\hat{V}_{\boldsymbol{\Xi}} = \frac{g\mu_B}{V^2c^2} \int_0^r \left(\hat{\boldsymbol{v}} \times \hat{\boldsymbol{S}} - \hat{\boldsymbol{S}} \times \hat{\boldsymbol{v}}\right) \cdot \boldsymbol{\Xi} d\boldsymbol{r} = \frac{g\mu_B}{V^2c^2} \int_0^r \left[\hat{\boldsymbol{v}} \cdot \left(\hat{\boldsymbol{S}} \times \hat{\boldsymbol{e}}_{\boldsymbol{\Xi}}\right) - \left(\hat{\boldsymbol{e}}_{\boldsymbol{\Xi}} \times \hat{\boldsymbol{S}}\right) \cdot \hat{\boldsymbol{v}}\right] \Xi d\boldsymbol{r} \tag{S128}$$

Here he have set the zero potential energy at the origin $\boldsymbol{r} = 0$; $\hat{\boldsymbol{e}}_{\boldsymbol{\Xi}}$ is the unit vector along $\boldsymbol{\Xi}$ direction; $\hat{\boldsymbol{v}} = -\frac{i}{\hbar}\left[\hat{H}, \hat{\boldsymbol{r}}\right]$ is the velocity operator, $\hat{\boldsymbol{S}}$ is the spin operator.

Assuming that the motion of a magnon wave packet is driven by a temperature gradient along the x-axis, we will now calculate the electric polarization induced by magnon transport in the y-direction. In principle, one could evaluate the electric polarization using standard quantum mechanical perturbation theory to calculate the energy correction from a uniform electric field. However, this method encounters difficulties due to the nonlocal nature of the electric polarization operator with Bloch wave functions. To circumvent this issue, we consider an external electric field along the y-direction with an infinitely slow in-plane spatial variation given by:

$$\boldsymbol{\Xi} = \Xi_0 \, cos(q_y y) \, \hat{\boldsymbol{y}} \tag{S129}$$

with q_y being small. This leads to

$$\hat{\boldsymbol{S}} \times \hat{\boldsymbol{e}}_{\boldsymbol{\Xi}} = -\hat{S}^z \hat{\boldsymbol{x}} + \hat{S}^x \hat{\boldsymbol{z}} \tag{S130}$$

where $\hat{\boldsymbol{x}}$, $\hat{\boldsymbol{y}}$ and $\hat{\boldsymbol{z}}$ are, respectively, the unit vectors along the x-axis, y-axis and z-axis.

Since the external electric field varies slowly in space, the corrections due to changes in the wave function under this variation are of a higher order and can be neglected. This allows us to obtain the perturbing potential of the magnon wave packet at position y by inserting Eq. (S129) into Eq. (S128) which leads to

$$\hat{V}_{\boldsymbol{\Xi}} = -\frac{g\mu_B \Xi_0}{W_y V c^2} \left[\hat{\boldsymbol{x}}\left(\hat{\boldsymbol{v}}\hat{S}^z + \hat{S}^z\hat{\boldsymbol{v}}\right) - \hat{\boldsymbol{z}}\left(\hat{\boldsymbol{v}}\hat{S}^x + \hat{S}^x\hat{\boldsymbol{v}}\right)\right] \int_0^y cos(q_y y) \, dy \tag{S131}$$

$$= -\frac{g\mu_B \Xi_0 sin(q_y y)\, \hat{\boldsymbol{x}}}{q_y W_y V c^2} \left(\hat{\boldsymbol{v}}\hat{S}^z + \hat{S}^z\hat{\boldsymbol{v}}\right) + \frac{g\mu_B \Xi_0 sin(q_y y)\, \hat{\boldsymbol{z}}}{q_y W_y V c^2} \left(\hat{\boldsymbol{v}}\hat{S}^x + \hat{S}^x\hat{\boldsymbol{v}}\right) \tag{S132}$$

$$= \hat{V}_{\boldsymbol{\Xi}}^{(1)} + \hat{V}_{\boldsymbol{\Xi}}^{(2)} \tag{S133}$$

where

$$\hat{V}_{\boldsymbol{\Xi}}^{(1)} = -\frac{g\mu_B \Xi_0 sin(q_y y)\, \hat{\boldsymbol{x}}}{q_y W_y V c^2} \left(\hat{\boldsymbol{v}}\hat{S}^z + \hat{S}^z\hat{\boldsymbol{v}}\right) \tag{S134}$$

$$\hat{V}_{\boldsymbol{\Xi}}^{(2)} = \frac{g\mu_B \Xi_0 sin(q_y y)\, \hat{\boldsymbol{z}}}{q_y W_y V c^2} \left(\hat{\boldsymbol{v}}\hat{S}^x + \hat{S}^x\hat{\boldsymbol{v}}\right) \tag{S135}$$

and W_y represent the length of the system along the y-direction.

The grand-canonical ensemble energy density

$$E\left(\boldsymbol{r}\right)=\sum_{n,\boldsymbol{k}}\rho_{n,\boldsymbol{k}}\sigma_3^{nn}Re\left\{\psi_{n,\boldsymbol{k}}^{*}\left(\boldsymbol{r}\right)\hat{H}\psi_{n,\boldsymbol{k}}\left(\boldsymbol{r}\right)\right\} \tag{S136}$$

where $\rho_{n,\boldsymbol{k}}=[e^{E_{n,\boldsymbol{k}}/k_BT}-1]^{-1}$ is the Bose-Einstein distribution function that describes the occupation number of single magnon states of band index n and momentum $\boldsymbol{k}$. The variation in total energy δE up to the first order is given by

$$\begin{aligned}\delta E\left(\boldsymbol{r}\right)=&\sum_{n,\boldsymbol{k}}\left\{\delta\rho_{n,\boldsymbol{k}}\sigma_3^{nn}\psi_{n,\boldsymbol{k}}^{*}\left(\boldsymbol{r}\right)\hat{H}^0\psi_{n,\boldsymbol{k}}\left(\boldsymbol{r}\right)+\rho_{n,\boldsymbol{k}}\sigma_3^{nn}\psi_{n,\boldsymbol{k}}^{*}\left(\boldsymbol{r}\right)\hat{V}_{\boldsymbol{\Xi}}\psi_{n,\boldsymbol{k}}\left(\boldsymbol{r}\right)\right.\\&\left.+\rho_{n,\boldsymbol{k}}\sigma_3^{nn}\left[\delta\psi_{n,\boldsymbol{k}}^{*}\left(\boldsymbol{r}\right)\hat{H}^0\psi_{n,\boldsymbol{k}}\left(\boldsymbol{r}\right)+\psi_{n,\boldsymbol{k}}^{*}\left(\boldsymbol{r}\right)\hat{H}^0\delta\psi_{n,\boldsymbol{k}}\left(\boldsymbol{r}\right)\right]\right\}.\end{aligned} \tag{S137}$$

The first two terms vanish so that

$$\delta E\left(\boldsymbol{r}\right)=\sum_{n,\boldsymbol{k}}\rho_{n,\boldsymbol{k}}\sigma_3^{nn}\left[\delta\psi_{n,\boldsymbol{k}}^{*}\left(\boldsymbol{r}\right)\hat{H}^0\psi_{n,\boldsymbol{k}}\left(\boldsymbol{r}\right)+\psi_{n,\boldsymbol{k}}^{*}\left(\boldsymbol{r}\right)\hat{H}^0\delta\psi_{n,\boldsymbol{k}}\left(\boldsymbol{r}\right)\right]. \tag{S138}$$

in another words, only the change in the wave function will contribute to the electric polarization.

In the same spirit as Eq. (S94), one obtains

$$\begin{aligned}\left|\delta\psi_{n,\boldsymbol{k}}\right\rangle=&\sum_{p\neq n,\boldsymbol{k}'}\sigma_3^{pp}\frac{\left\langle\psi_{p,\boldsymbol{k}'}\left|\delta\hat{H}\right|\psi_{n,\boldsymbol{k}}\right\rangle}{\left[\boldsymbol{\sigma}_3E_{\boldsymbol{k}}\right]_{nn}-\left[\boldsymbol{\sigma}_3E_{\boldsymbol{k}'}\right]_{pp}}\left|\psi_{p,\boldsymbol{k}'}\right\rangle+\sum_{n,\boldsymbol{k}'\neq\boldsymbol{k}}\sigma_3^{nn}\frac{\left\langle\psi_{n,\boldsymbol{k}'}\left|\delta\hat{H}\right|\psi_{n,\boldsymbol{k}}\right\rangle}{\left[\boldsymbol{\sigma}_3E_{\boldsymbol{k}}\right]_{nn}-\left[\boldsymbol{\sigma}_3E_{\boldsymbol{k}'}\right]_{nn}}\left|\psi_{p,\boldsymbol{k}'}\right\rangle\\=&\sum_{p\neq n,\boldsymbol{k}'}\sigma_3^{pp}\frac{\left\langle\psi_{p,\boldsymbol{k}'}\left|\hat{V}_{\boldsymbol{\Xi}}\right|\psi_{n,\boldsymbol{k}}\right\rangle}{\left[\boldsymbol{\sigma}_3E_{\boldsymbol{k}}\right]_{nn}-\left[\boldsymbol{\sigma}_3E_{\boldsymbol{k}'}\right]_{pp}}\left|\psi_{p,\boldsymbol{k}'}\right\rangle+\sum_{n,\boldsymbol{k}'\neq\boldsymbol{k}}\sigma_3^{nn}\frac{\left\langle\psi_{n,\boldsymbol{k}'}\left|\hat{V}_{\boldsymbol{\Xi}}\right|\psi_{n,\boldsymbol{k}}\right\rangle}{\left[\boldsymbol{\sigma}_3E_{\boldsymbol{k}}\right]_{nn}-\left[\boldsymbol{\sigma}_3E_{\boldsymbol{k}'}\right]_{nn}}\left|\psi_{p,\boldsymbol{k}'}\right\rangle.\end{aligned} \tag{S139}$$

The matrix elements of the perturbation $\hat{V}_{\boldsymbol{\Xi}}$ read:

$$\begin{aligned}&\left\langle\psi_{p,\boldsymbol{k}'}\left|\hat{V}_{\boldsymbol{\Xi}}\right|\psi_{n,\boldsymbol{k}}\right\rangle=\frac{1}{V}\int d\boldsymbol{r}\psi_{p,\boldsymbol{k}'}^{*}\left(\boldsymbol{r}\right)\hat{V}_{\boldsymbol{\Xi}}\psi_{n,\boldsymbol{k}}\left(\boldsymbol{r}\right)=\frac{1}{V_0}\int d\boldsymbol{r}e^{i(\boldsymbol{k}+\boldsymbol{q}-\boldsymbol{k}')\boldsymbol{r}}u_{p,\boldsymbol{k}'}^{*}\left(\boldsymbol{r}\right)\hat{V}_{\boldsymbol{\Xi}}u_{n,\boldsymbol{k}}\left(\boldsymbol{r}\right)\\&=-\frac{g\mu_B\Xi_0\hat{\boldsymbol{x}}}{4iq_yV^2W_yc^2}\int d\boldsymbol{r}\left[e^{i(\boldsymbol{k}+\boldsymbol{q}-\boldsymbol{k}')\boldsymbol{r}}-e^{-i(\boldsymbol{k}-\boldsymbol{q}-\boldsymbol{k}')\boldsymbol{r}}\right]u_{p,\boldsymbol{k}'}\left(\boldsymbol{r}\right)\left(\hat{\boldsymbol{v}}_{\boldsymbol{k}'}\boldsymbol{\sigma}_3\hat{S}^z+\hat{S}^z\boldsymbol{\sigma}_3\hat{\boldsymbol{v}}_{\boldsymbol{k}}\right)u_{n,\boldsymbol{k}}\left(\boldsymbol{r}\right)-(x\leftrightarrow z)\\&=-\frac{g\mu_B\Xi_0\hat{\boldsymbol{x}}}{4iq_yV^2W_yc^2}\int d\boldsymbol{r}\left[e^{i(\boldsymbol{k}+\boldsymbol{q}-\boldsymbol{k}')\boldsymbol{r}}u_{p,\boldsymbol{k}'}\left(\boldsymbol{r}\right)\left(\hat{\boldsymbol{v}}_{\boldsymbol{k}'}\boldsymbol{\sigma}_3\hat{S}^z+\hat{S}^z\boldsymbol{\sigma}_3\hat{\boldsymbol{v}}_{\boldsymbol{k}}\right)u_{n,\boldsymbol{k}}\left(\boldsymbol{r}\right)-(\boldsymbol{q}\rightarrow-\boldsymbol{q})\right]-(x\leftrightarrow z)\\&=-\frac{g\mu_B\Xi_0\hat{\boldsymbol{x}}}{4iq_yW_yVc^2}\left[\delta_{\boldsymbol{k}',\boldsymbol{k}+\boldsymbol{q}}\left\langle u_{p,\boldsymbol{k}'}\left|\left(\hat{\boldsymbol{v}}_{\boldsymbol{k}'}\boldsymbol{\sigma}_3\hat{S}^z+\hat{S}^z\boldsymbol{\sigma}_3\hat{\boldsymbol{v}}_{\boldsymbol{k}}\right)\right|u_{n,\boldsymbol{k}}\right\rangle-(\boldsymbol{q}\rightarrow-\boldsymbol{q})\right]-(x\leftrightarrow z)\end{aligned} \tag{S140}$$

where we have used $sin\left(q_yy\right)=sin\left(\boldsymbol{qr}\right)=\frac{e^{i\boldsymbol{qr}}-e^{-i\boldsymbol{qr}}}{2i}$ with $\boldsymbol{q}=[0,q_y,0]^T$, i.e the wave vector $\boldsymbol{q}$ is along the y-direction and $\left\langle u_{p,\boldsymbol{k}'}\left|\left(\hat{\boldsymbol{v}}_{\boldsymbol{k}'}\boldsymbol{\sigma}_3\hat{S}^z+\hat{S}^z\boldsymbol{\sigma}_3\hat{\boldsymbol{v}}_{\boldsymbol{k}}\right)\right|u_{n,\boldsymbol{k}}\right\rangle=\frac{1}{V_0}\int d\boldsymbol{r}\ u_{p,\boldsymbol{k}'}\left(\boldsymbol{r}\right)\left(\hat{\boldsymbol{v}}_{\boldsymbol{k}'}\boldsymbol{\sigma}_3\hat{S}^z+\hat{S}^z\boldsymbol{\sigma}_3\hat{\boldsymbol{v}}_{\boldsymbol{k}}\right)u_{n,\boldsymbol{k}}\left(\boldsymbol{r}\right)$. From this one obtains

$$\begin{aligned}&\sum_{p\neq n,\boldsymbol{k}'}\sigma_3^{pp}\frac{\left\langle\psi_{p,\boldsymbol{k}'}\left|\hat{V}_{\boldsymbol{\Xi}}\right|\psi_{n,\boldsymbol{k}}\right\rangle}{\left[\boldsymbol{\sigma}_3E_{\boldsymbol{k}}\right]_{nn}-\left[\boldsymbol{\sigma}_3E_{\boldsymbol{k}'}\right]_{pp}}\left|\psi_{p,\boldsymbol{k}'}\right\rangle\\&=-\frac{g\mu_B\Xi_0\hat{\boldsymbol{x}}}{4iq_yW_yVc^2}\sum_{p\neq n,\boldsymbol{k}'}\sigma_3^{pp}\left[\delta_{\boldsymbol{k}',\boldsymbol{k}+\boldsymbol{q}}\frac{\left\langle u_{p,\boldsymbol{k}'}\left|\left(\hat{\boldsymbol{v}}_{\boldsymbol{k}'}\boldsymbol{\sigma}_3\hat{S}^z+\hat{S}^z\boldsymbol{\sigma}_3\hat{\boldsymbol{v}}_{\boldsymbol{k}}\right)\right|u_{n,\boldsymbol{k}}\right\rangle}{\left[\boldsymbol{\sigma}_3E_{\boldsymbol{k}}\right]_{nn}-\left[\boldsymbol{\sigma}_3E_{\boldsymbol{k}'}\right]_{pp}}\left|\psi_{p,\boldsymbol{k}'}\right\rangle-(\boldsymbol{q}\rightarrow-\boldsymbol{q})\right]-(x\leftrightarrow z)\\&=-\frac{g\mu_B\Xi_0\hat{\boldsymbol{x}}}{4iq_yW_yVc^2}\sum_{p\neq n}\sigma_3^{pp}\left[\frac{\left\langle u_{p,\boldsymbol{k}+\boldsymbol{q}}\left|\left(\hat{\boldsymbol{v}}_{\boldsymbol{k}+\boldsymbol{q}}\boldsymbol{\sigma}_3\hat{S}^z+\hat{S}^z\boldsymbol{\sigma}_3\hat{\boldsymbol{v}}_{\boldsymbol{k}}\right)\right|u_{n,\boldsymbol{k}}\right\rangle}{\left[\boldsymbol{\sigma}_3E_{\boldsymbol{k}}\right]_{nn}-\left[\boldsymbol{\sigma}_3E_{\boldsymbol{k}+\boldsymbol{q}}\right]_{pp}}\left|\psi_{p,\boldsymbol{k}+\boldsymbol{q}}\right\rangle-(\boldsymbol{q}\rightarrow-\boldsymbol{q})\right]-(x\leftrightarrow z)\end{aligned} \tag{S141}$$

Similarly, one gets

$$\begin{aligned}&\sum_{n,\boldsymbol{k}'\neq\boldsymbol{k}}\sigma_3^{nn}\frac{\left\langle\psi_{n,\boldsymbol{k}'}\left|\hat{V}_{\boldsymbol{\Xi}}\right|\psi_{n,\boldsymbol{k}}\right\rangle}{\left[\boldsymbol{\sigma}_3E_{\boldsymbol{k}}\right]_{nn}-\left[\boldsymbol{\sigma}_3E_{\boldsymbol{k}'}\right]_{nn}}\left|\psi_{n,\boldsymbol{k}'}\right\rangle\\&=-\frac{g\mu_B\Xi_0\hat{\boldsymbol{x}}}{4iq_yW_yVc^2}\sum_{n}\sigma_3^{nn}\left[\frac{\left\langle u_{n,\boldsymbol{k}+\boldsymbol{q}}\left|\left(\hat{\boldsymbol{v}}_{\boldsymbol{k}+\boldsymbol{q}}\boldsymbol{\sigma}_3\hat{S}^z+\hat{S}^z\boldsymbol{\sigma}_3\hat{\boldsymbol{v}}_{\boldsymbol{k}}\right)\right|u_{n,\boldsymbol{k}}\right\rangle}{\left[\boldsymbol{\sigma}_3E_{\boldsymbol{k}}\right]_{nn}-\left[\boldsymbol{\sigma}_3E_{\boldsymbol{k}+\boldsymbol{q}}\right]_{nn}}\left|\psi_{n,\boldsymbol{k}+\boldsymbol{q}}\right\rangle-(\boldsymbol{q}\rightarrow-\boldsymbol{q})\right]-(x\leftrightarrow z)\end{aligned} \tag{S142}$$

so that

$$\left|\delta\psi_{n,\boldsymbol{k}}\right\rangle=-\frac{g\mu_B\Xi_0\hat{\boldsymbol{x}}}{4iq_yW_yVc^2}\sum_{p}\sigma_3^{pp}\left[\left|\psi_{p,\boldsymbol{k}+\boldsymbol{q}}\right\rangle\frac{\left\langle u_{p,\boldsymbol{k}+\boldsymbol{q}}\left|\left(\hat{\boldsymbol{v}}_{\boldsymbol{k}+\boldsymbol{q}}\boldsymbol{\sigma}_3\hat{S}^z+\hat{S}^z\boldsymbol{\sigma}_3\hat{\boldsymbol{v}}_{\boldsymbol{k}}\right)\right|u_{n,\boldsymbol{k}}\right\rangle}{\left[\boldsymbol{\sigma}_3E_{\boldsymbol{k}}\right]_{nn}-\left[\boldsymbol{\sigma}_3E_{\boldsymbol{k}+\boldsymbol{q}}\right]_{pp}}-(\boldsymbol{q}\rightarrow-\boldsymbol{q})\right]-(x\leftrightarrow z). \tag{S143}$$

The first order perturbation to the wave function now reads:

$$\delta\psi_{n,\boldsymbol{k}}(\boldsymbol{r}) = \langle \boldsymbol{r} | \delta\psi_{n,\boldsymbol{k}} \rangle \tag{S144}$$

$$= -\frac{g\mu_B \Xi_0 \hat{\boldsymbol{x}}}{4iq_y W_y V c^2} \sum_p \sigma_3^{pp} \left[\langle \boldsymbol{r} | \psi_{p,\boldsymbol{k}+\boldsymbol{q}} \rangle \frac{\left\langle u_{p,\boldsymbol{k}+\boldsymbol{q}} \middle| \left(\hat{\boldsymbol{v}}_{\boldsymbol{k}+\boldsymbol{q}} \boldsymbol{\sigma}_3 \hat{S}^z + \hat{S}^z \boldsymbol{\sigma}_3 \hat{\boldsymbol{v}}_{\boldsymbol{k}} \right) \middle| u_{n,\boldsymbol{k}} \right\rangle}{[\boldsymbol{\sigma}_3 E_{\boldsymbol{k}}]_{nn} - [\boldsymbol{\sigma}_3 E_{\boldsymbol{k}+\boldsymbol{q}}]_{pp}} - (\boldsymbol{q} \to -\boldsymbol{q}) \right] - (x \leftrightarrow z)$$

$$= -\frac{g\mu_B \Xi_0 \hat{\boldsymbol{x}}}{4iq_y W_y V c^2} \sum_p \sigma_3^{pp} \left[\psi_{p,\boldsymbol{k}+\boldsymbol{q}}(\boldsymbol{r}) \frac{\left\langle u_{p,\boldsymbol{k}+\boldsymbol{q}} \middle| \left(\hat{\boldsymbol{v}}_{\boldsymbol{k}+\boldsymbol{q}} \boldsymbol{\sigma}_3 \hat{S}^z + \hat{S}^z \boldsymbol{\sigma}_3 \hat{\boldsymbol{v}}_{\boldsymbol{k}} \right) \middle| u_{n,\boldsymbol{k}} \right\rangle}{[\boldsymbol{\sigma}_3 E_{\boldsymbol{k}}]_{nn} - [\boldsymbol{\sigma}_3 E_{\boldsymbol{k}+\boldsymbol{q}}]_{pp}} - (\boldsymbol{q} \to -\boldsymbol{q}) \right] - (x \leftrightarrow z). \tag{S145}$$

The variation of total energy can now be given by

$$\delta E(\boldsymbol{r}) \tag{S146}$$

$$= -\frac{g\mu_B \Xi_0 \hat{\boldsymbol{x}}}{4iq_y W_y V c^2} \sum_{n,p,\boldsymbol{k}} \rho_{n,\boldsymbol{k}} \sigma_3^{nn} \sigma_3^{pp} \left[\psi^*_{n,\boldsymbol{k}}(\boldsymbol{r}) \hat{H}^0 \psi_{p,\boldsymbol{k}+\boldsymbol{q}}(\boldsymbol{r}) \frac{\left\langle u_{p,\boldsymbol{k}+\boldsymbol{q}} \middle| \left(\hat{\boldsymbol{v}}_{\boldsymbol{k}+\boldsymbol{q}} \boldsymbol{\sigma}_3 \hat{S}^z + \hat{S}^z \boldsymbol{\sigma}_3 \hat{\boldsymbol{v}}_{\boldsymbol{k}} \right) \middle| u_{n,\boldsymbol{k}} \right\rangle}{[\boldsymbol{\sigma}_3 E_{\boldsymbol{k}}]_{nn} - [\boldsymbol{\sigma}_3 E_{\boldsymbol{k}+\boldsymbol{q}}]_{pp}} - (\boldsymbol{q} \to -\boldsymbol{q}) \right]$$

$$+ c.c. - (x \leftrightarrow z) \tag{S147}$$

Because

$$\psi^*_{n,\boldsymbol{k}}(\boldsymbol{r}) \hat{H}^0 \psi_{p,\boldsymbol{k}+\boldsymbol{q}}(\boldsymbol{r}) = [\boldsymbol{\sigma}_3 E_{\boldsymbol{k}}]_{nn} e^{i\boldsymbol{q}.\boldsymbol{r}} u^*_{n,\boldsymbol{k}}(\boldsymbol{r}) \boldsymbol{\sigma}_3 u_{p,\boldsymbol{k}+\boldsymbol{q}}(\boldsymbol{r}), \tag{S148}$$

one obtains

$$\delta E(\boldsymbol{r}) = -\frac{g\mu_B \Xi_0 \hat{\boldsymbol{x}}}{4iq_y W_y V c^2} \sum_{n,p,\boldsymbol{k}} \rho_{n,\boldsymbol{k}} \sigma_3^{nn} \sigma_3^{pp} \left[e^{i\boldsymbol{q}.\boldsymbol{r}} u^*_{n,\boldsymbol{k}}(\boldsymbol{r}) \boldsymbol{\sigma}_3 u_{p,\boldsymbol{k}+\boldsymbol{q}}(\boldsymbol{r}) \left\{ \frac{[\boldsymbol{\sigma}_3 E_{\boldsymbol{k}}]_{nn}}{[\boldsymbol{\sigma}_3 E_{\boldsymbol{k}}]_{nn} - [\boldsymbol{\sigma}_3 E_{\boldsymbol{k}+\boldsymbol{q}}]_{pp}} \right\} \times \right.$$

$$\left. \times \left\langle u_{p,\boldsymbol{k}+\boldsymbol{q}} \middle| \left(\hat{\boldsymbol{v}}_{\boldsymbol{k}+\boldsymbol{q}} \boldsymbol{\sigma}_3 \hat{S}^z + \hat{S}^z \boldsymbol{\sigma}_3 \hat{\boldsymbol{v}}_{\boldsymbol{k}} \right) \middle| u_{n,\boldsymbol{k}} \right\rangle - (\boldsymbol{q} \to -\boldsymbol{q}) \right] + c.c. - (x \leftrightarrow z) \tag{S149}$$

Using Eq. (S125), the zero-temperature total electric polarization is obtained from the Fourier component of the local energy $\delta E(\boldsymbol{r})$ taking the limit $q_y \to 0$:

$$\tilde{\boldsymbol{P}} = -\frac{2}{\Xi_0 V} \lim_{q_y \to 0} \int \delta E(\boldsymbol{r}) \cos(q_y y) \, d\boldsymbol{r}. \tag{S150}$$

Inserting Eq. (S149) into Eq. (S150) and using $\frac{1}{V_0} \int u^*_{n,\boldsymbol{k}}(\boldsymbol{r}) \boldsymbol{\sigma}_3 u_{p,\boldsymbol{k}+\boldsymbol{q}}(\boldsymbol{r}) \, d\boldsymbol{r} = \langle u_{n,\boldsymbol{k}} | \boldsymbol{\sigma}_3 | u_{p,\boldsymbol{k}+\boldsymbol{q}} \rangle$, which is $\boldsymbol{r}$-independent, one can do integration by parts

$$\frac{1}{V} \int \cos(\boldsymbol{q}.\boldsymbol{r}) e^{i\boldsymbol{q}\boldsymbol{r}} \left[u^*_{n,\boldsymbol{k}}(\boldsymbol{r}) \boldsymbol{\sigma}_3 u_{p,\boldsymbol{k}+\boldsymbol{q}}(\boldsymbol{r}) \right] d\boldsymbol{r}$$

$$= \cos(\boldsymbol{q}.\boldsymbol{r}) e^{i\boldsymbol{q}\boldsymbol{r}} \langle u_{n,\boldsymbol{k}} | \boldsymbol{\sigma}_3 | u_{p,\boldsymbol{k}+\boldsymbol{q}} \rangle - \int \langle u_{n,\boldsymbol{k}} | \boldsymbol{\sigma}_3 | u_{p,\boldsymbol{k}+\boldsymbol{q}} \rangle [q \, sin(\boldsymbol{q}\boldsymbol{r}) + iq \, cos(\boldsymbol{q}\boldsymbol{r})] e^{i\boldsymbol{q}\boldsymbol{r}} d\boldsymbol{r}$$

$$= \cos(\boldsymbol{q}.\boldsymbol{r}) e^{i\boldsymbol{q}\boldsymbol{r}} \langle u_{n,\boldsymbol{k}} | \boldsymbol{\sigma}_3 | u_{p,\boldsymbol{k}+\boldsymbol{q}} \rangle - \langle u_{n,\boldsymbol{k}} | \boldsymbol{\sigma}_3 | u_{p,\boldsymbol{k}+\boldsymbol{q}} \rangle \int [sin(\boldsymbol{q}\boldsymbol{r}) + i \, cos(\boldsymbol{q}\boldsymbol{r})] e^{i\boldsymbol{q}\boldsymbol{r}} d(\boldsymbol{q}\boldsymbol{r})$$

$$= \cos(\boldsymbol{q}.\boldsymbol{r}) e^{i\boldsymbol{q}\boldsymbol{r}} \langle u_{n,\boldsymbol{k}} | \boldsymbol{\sigma}_3 | u_{p,\boldsymbol{k}+\boldsymbol{q}} \rangle - i\boldsymbol{q}\boldsymbol{r} \langle u_{n,\boldsymbol{k}} | \boldsymbol{\sigma}_3 | u_{p,\boldsymbol{k}+\boldsymbol{q}} \rangle \tag{S151}$$

Because $\boldsymbol{q}$ is an infinitesimal vector,

$$e^{i\boldsymbol{q}\boldsymbol{r}} \approx 1 + i\boldsymbol{q}\boldsymbol{r} \tag{S152}$$

and $cos(\boldsymbol{q}\boldsymbol{r}) \approx 1$ leads to

$$\frac{1}{V} \int \cos(\boldsymbol{q}.\boldsymbol{r}) e^{i\boldsymbol{q}\boldsymbol{r}} \left[u^*_{n,\boldsymbol{k}}(\boldsymbol{r}) \boldsymbol{\sigma}_3 u_{p,\boldsymbol{k}+\boldsymbol{q}}(\boldsymbol{r}) \right] d\boldsymbol{r} = \langle u_{n,\boldsymbol{k}} | \boldsymbol{\sigma}_3 | u_{p,\boldsymbol{k}+\boldsymbol{q}} \rangle. \tag{S153}$$

Therefore, the electric polarization reads

$$\tilde{P}_y = -\lim_{q_y \to 0} \frac{g\mu_B \hat{\boldsymbol{x}}}{2iq_y W_y V c^2} \sum_{n,p,\boldsymbol{k}} \sigma_3^{nn} \sigma_3^{pp} \rho_{n,\boldsymbol{k}} [\boldsymbol{\sigma}_3 E_{\boldsymbol{k}}]_{nn} \times$$

$$\times \left\{ \frac{\left\langle u_{p,\boldsymbol{k}+\boldsymbol{q}} \middle| \left(\hat{\boldsymbol{v}}_{\boldsymbol{k}+\boldsymbol{q}} \boldsymbol{\sigma}_3 \hat{S}^z + \hat{S}^z \boldsymbol{\sigma}_3 \hat{\boldsymbol{v}}_{\boldsymbol{k}} \right) \middle| u_{n,\boldsymbol{k}} \right\rangle \langle u_{n,\boldsymbol{k}} | \boldsymbol{\sigma}_3 | u_{p,\boldsymbol{k}+\boldsymbol{q}} \rangle}{[\boldsymbol{\sigma}_3 E_{\boldsymbol{k}}]_{nn} - [\boldsymbol{\sigma}_3 E_{\boldsymbol{k}+\boldsymbol{q}}]_{pp}} - (\boldsymbol{q} \to -\boldsymbol{q}) \right\} + c.c. - (x \leftrightarrow z)$$

$$= -\lim_{q_y \to 0} \frac{g\mu_B \hat{\boldsymbol{x}}}{2iq_y W_y V c^2} \sum_{n,p,\boldsymbol{k}} \left([\boldsymbol{\sigma}_3 E_{\boldsymbol{k}}]_{nn} \rho_{n,\boldsymbol{k}} - [\boldsymbol{\sigma}_3 E_{\boldsymbol{k}+\boldsymbol{q}}]_{pp} \rho_{p,\boldsymbol{k}+\boldsymbol{q}} \right) \sigma_3^{nn} \sigma_3^{pp} \times$$

$$\times \left\{ \frac{\left\langle u_{p,\boldsymbol{k}+\boldsymbol{q}} \middle| \left(\hat{\boldsymbol{v}}_{\boldsymbol{k}+\boldsymbol{q}} \boldsymbol{\sigma}_3 \hat{S}^z + \hat{S}^z \boldsymbol{\sigma}_3 \hat{\boldsymbol{v}}_{\boldsymbol{k}} \right) \middle| u_{n,\boldsymbol{k}} \right\rangle}{[\boldsymbol{\sigma}_3 E_{\boldsymbol{k}}]_{nn} - [\boldsymbol{\sigma}_3 E_{\boldsymbol{k}+\boldsymbol{q}}]_{pp}} \langle u_{n,\boldsymbol{k}} | \boldsymbol{\sigma}_3 | u_{p,\boldsymbol{k}+\boldsymbol{q}} \rangle \right\} + c.c. - (x \leftrightarrow z) \tag{S154}$$

Using $\langle u_{n,\boldsymbol{k}}|\,\boldsymbol{\sigma}_3\,|u_{p,\boldsymbol{k}}\rangle = \sigma_3^{nn}\delta_{p,n}$ where $\delta_{p,n}$ here is the Kronecker delta function and implementing the limit in Eq. (S154), one obtains for $p \neq n$

$$\tilde{P}_y^{(1)} = -\lim_{q_y\to 0}\frac{g\mu_B\hat{\boldsymbol{x}}}{2iq_yW_yVc^2}\sum_{p\neq n,\boldsymbol{k}}\left([\boldsymbol{\sigma}_3E_{\boldsymbol{k}}]_{nn}\,\rho_{n,\boldsymbol{k}} - [\boldsymbol{\sigma}_3E_{\boldsymbol{k}+\boldsymbol{q}}]_{pp}\,\rho_{p,\boldsymbol{k}+\boldsymbol{q}}\right)\sigma_3^{nn}\sigma_3^{pp}\times$$

$$\times\left\{\frac{\left\langle u_{p,\boldsymbol{k}+\boldsymbol{q}}\left|\left(\hat{\boldsymbol{v}}_{\boldsymbol{k}+\boldsymbol{q}}\boldsymbol{\sigma}_3\hat{S}^z + \hat{S}^z\boldsymbol{\sigma}_3\hat{\boldsymbol{v}}_{\boldsymbol{k}}\right)\right|u_{n,\boldsymbol{k}}\right\rangle}{[\boldsymbol{\sigma}_3E_{\boldsymbol{k}}]_{nn} - [\boldsymbol{\sigma}_3E_{\boldsymbol{k}+\boldsymbol{q}}]_{pp}}\langle u_{n,\boldsymbol{k}}|\,\boldsymbol{\sigma}_3\,|u_{p,\boldsymbol{k}+\boldsymbol{q}}\rangle\right\} + c.c. - (x\leftrightarrow z) \quad [S155]$$

$$= -\frac{g\mu_B\hat{\boldsymbol{x}}}{2iW_yVc^2}\sum_{p\neq n,\boldsymbol{k}}\left([\boldsymbol{\sigma}_3E_{\boldsymbol{k}}]_{nn}\,\rho_{n,\boldsymbol{k}} - [\boldsymbol{\sigma}_3E_{\boldsymbol{k}}]_{pp}\,\rho_{p,\boldsymbol{k}}\right)\sigma_3^{nn}\sigma_3^{pp}\times$$

$$\times\left\{\frac{\left\langle u_{p,\boldsymbol{k}}\left|\left(\hat{\boldsymbol{v}}_{\boldsymbol{k}}\boldsymbol{\sigma}_3\hat{S}^z + \hat{S}^z\boldsymbol{\sigma}_3\hat{\boldsymbol{v}}_{\boldsymbol{k}}\right)\right|u_{n,\boldsymbol{k}}\right\rangle}{[\boldsymbol{\sigma}_3E_{\boldsymbol{k}}]_{nn} - [\boldsymbol{\sigma}_3E_{\boldsymbol{k}}]_{pp}}\langle u_{n,\boldsymbol{k}}|\,\boldsymbol{\sigma}_3\left|\partial_{k_y}u_{p,\boldsymbol{k}}\right\rangle\right\} + c.c. - (x\leftrightarrow z) \quad [S156]$$

$$= -\frac{i\hbar g\mu_B}{2W_yVc^2}\sum_{n\neq p,\boldsymbol{k}}\sigma_3^{nn}\sigma_3^{pp}\left([\boldsymbol{\sigma}_3E_{\boldsymbol{k}}]_{nn}\,\rho_{n,\boldsymbol{k}} - [\boldsymbol{\sigma}_3E_{\boldsymbol{k}}]_{pp}\,\rho_{p,\boldsymbol{k}}\right)\times$$

$$\times\frac{\left\langle u_{p,\boldsymbol{k}}\left|\left(\hat{v}_x\boldsymbol{\sigma}_3\hat{S}^z + \hat{S}^z\boldsymbol{\sigma}_3\hat{v}_x\right)\right|u_{n,\boldsymbol{k}}\right\rangle\langle u_{n,\boldsymbol{k}}\,|\hat{v}_y|\,u_{p,\boldsymbol{k}}\rangle}{\left\{[\boldsymbol{\sigma}_3E_{\boldsymbol{k}}]_{nn} - [\boldsymbol{\sigma}_3E_{\boldsymbol{k}}]_{pp}\right\}^2} + c.c. - (x\leftrightarrow z) \quad [S157]$$

$$= -\frac{g\mu_B}{\hbar W_yVc^2}\sum_{n\neq p,\boldsymbol{k}} Im\left(2\hbar^2\sigma_3^{nn}\sigma_3^{pp}\frac{\left\langle u_{p,\boldsymbol{k}}\left|\left(\hat{v}_x\boldsymbol{\sigma}_3\hat{S}^z + \hat{S}^z\boldsymbol{\sigma}_3\hat{v}_x\right)\right|u_{n,\boldsymbol{k}}\right\rangle\langle u_{n,\boldsymbol{k}}\,|\hat{v}_y|\,u_{p,\boldsymbol{k}}\rangle}{\left\{[\boldsymbol{\sigma}_3E_{\boldsymbol{k}}]_{nn} - [\boldsymbol{\sigma}_3E_{\boldsymbol{k}}]_{pp}\right\}^2}\right)[\boldsymbol{\sigma}_3E_{\boldsymbol{k}}]_{nn}\,\rho_{n,\boldsymbol{k}} -$$

$$-(x\leftrightarrow z) \quad [S158]$$

where we have used

$$\langle u_{n,\boldsymbol{k}}\,|\hat{v}_{\boldsymbol{k}}|\,u_{p,\boldsymbol{k}}\rangle = \frac{1}{\hbar}\left[(\boldsymbol{\sigma}_3E_{\boldsymbol{k}})_{pp} - (\boldsymbol{\sigma}_3E_{\boldsymbol{k}})_{nn}\right]\langle u_{n,\boldsymbol{k}}|\,\boldsymbol{\sigma}_3\left|\partial_{k_y}u_{p,\boldsymbol{k}}\right\rangle \quad [S159]$$

Noting that

$$\sum_{p\neq n} Im\left(2\hbar^2\sigma_3^{nn}\sigma_3^{pp}\frac{\left\langle u_{p,\boldsymbol{k}}\left|\left(\hat{v}_x\boldsymbol{\sigma}_3\hat{S}^z + \hat{S}^z\boldsymbol{\sigma}_3\hat{v}_x\right)\right|u_{n,\boldsymbol{k}}\right\rangle\langle u_{n,\boldsymbol{k}}\,|\hat{v}_y|\,u_{p,\boldsymbol{k}}\rangle}{\left\{[\boldsymbol{\sigma}_3E_{\boldsymbol{k}}]_{nn} - [\boldsymbol{\sigma}_3E_{\boldsymbol{k}}]_{pp}\right\}^2}\right) \equiv \Omega_{xy}^{S^z,n}(\boldsymbol{k}) \quad [S160]$$

is the magnon spin Berry curvature of nth-band (13), therefore one obtains

$$\tilde{P}_y^{(1)} = -\frac{g\mu_B}{\hbar W_yVc^2}\sum_{n,\boldsymbol{k}}\Omega_{xy}^{S^z,n}(\boldsymbol{k})\,[\boldsymbol{\sigma}_3E_{\boldsymbol{k}}]_{nn}\,\rho_{n,\boldsymbol{k}} - (x\leftrightarrow z) \quad [S161]$$

$$= -\frac{g\mu_B}{\hbar W_yVc^2}\sum_{n,\boldsymbol{k}}\left[\Omega_{xy}^{S^z,n}(\boldsymbol{k}) - \Omega_{zy}^{S^x,n}(\boldsymbol{k})\right][\boldsymbol{\sigma}_3E_{\boldsymbol{k}}]_{nn}\,\rho_{n,\boldsymbol{k}} \quad [S162]$$

For $p \equiv n$, one gets

$$\tilde{P}_y^{(2)} = -\frac{g\mu_B\hat{\boldsymbol{x}}}{2iW_yVc^2}\sum_{n,\boldsymbol{k}}\left(\rho_{n,\boldsymbol{k}} + [\boldsymbol{\sigma}_3E_{\boldsymbol{k}}]_{nn}\,\rho'_{n,\boldsymbol{k}}\right)\left[\left\langle\partial_{k_y}u_{n,\boldsymbol{k}}\left|\left(\hat{\boldsymbol{v}}_{\boldsymbol{k}}\boldsymbol{\sigma}_3\hat{S}^z + \hat{S}^z\boldsymbol{\sigma}_3\hat{\boldsymbol{v}}_{\boldsymbol{k}}\right)\right|u_{n,\boldsymbol{k}}\right\rangle\langle u_{n,\boldsymbol{k}}|\,\boldsymbol{\sigma}_3\,|u_{n,\boldsymbol{k}}\rangle +\right.$$

$$+\left\langle u_{n,\boldsymbol{k}}\left|\left(\partial_{k_y}\hat{\boldsymbol{v}}_{\boldsymbol{k}}\right)\boldsymbol{\sigma}_3\hat{S}^z\right|u_{n,\boldsymbol{k}}\right\rangle\langle u_{n,\boldsymbol{k}}|\,\boldsymbol{\sigma}_3\,|u_{n,\boldsymbol{k}}\rangle$$

$$\left.+\left\langle u_{n,\boldsymbol{k}}\left|\left(\hat{\boldsymbol{v}}_{\boldsymbol{k}}\boldsymbol{\sigma}_3\hat{S}^z + \hat{S}^z\boldsymbol{\sigma}_3\hat{\boldsymbol{v}}_{\boldsymbol{k}}\right)\right|u_{n,\boldsymbol{k}}\right\rangle\langle u_{n,\boldsymbol{k}}|\,\boldsymbol{\sigma}_3\left|\partial_{k_y}u_{n,\boldsymbol{k}}\right\rangle\right] + c.c. - (x\leftrightarrow z) \quad [S163]$$

$$= -\frac{g\mu_B}{W_yVc^2}\sum_{n,\boldsymbol{k}}\left(\rho_{n,\boldsymbol{k}} + [\boldsymbol{\sigma}_3E_{\boldsymbol{k}}]_{nn}\,\rho'_{n,\boldsymbol{k}}\right)Im\left[\left\langle\partial_{k_y}u_{n,\boldsymbol{k}}\left|\left(\hat{v}_x\boldsymbol{\sigma}_3\hat{S}^z + \hat{S}^z\boldsymbol{\sigma}_3\hat{v}_x\right)\right|u_{n,\boldsymbol{k}}\right\rangle\langle u_{n,\boldsymbol{k}}|\,\boldsymbol{\sigma}_3\,|u_{n,\boldsymbol{k}}\rangle +\right.$$

$$+\left\langle u_{n,\boldsymbol{k}}\left|\left(\partial_{k_y}\hat{v}_x\right)\boldsymbol{\sigma}_3\hat{S}^z\right|u_{n,\boldsymbol{k}}\right\rangle\langle u_{n,\boldsymbol{k}}|\,\boldsymbol{\sigma}_3\,|u_{n,\boldsymbol{k}}\rangle$$

$$\left.+\left\langle u_{n,\boldsymbol{k}}\left|\left(\hat{v}_x\boldsymbol{\sigma}_3\hat{S}^z + \hat{S}^z\boldsymbol{\sigma}_3\hat{v}_x\right)\right|u_{n,\boldsymbol{k}}\right\rangle\langle u_{n,\boldsymbol{k}}|\,\boldsymbol{\sigma}_3\left|\partial_{k_y}u_{n,\boldsymbol{k}}\right\rangle\right] - (x\leftrightarrow z) \quad [S164]$$

At finite temperature, the electric polarization is given by:

$$P_y = \frac{1}{\beta}\int\tilde{P}_y d\beta = P_y^{(1)} + P_y^{(2)} \quad [S165]$$

where

$$P_y^{(1)} = \frac{1}{\beta}\int\tilde{P}_y^{(1)}d\beta \quad [S166]$$

$$P_y^{(2)} = \frac{1}{\beta}\int\tilde{P}_y^{(2)}d\beta \quad [S167]$$

After performing the integration, one obtains

$$P_y^{(1)} = -\frac{g\mu_B}{\hbar W_y V c^2}\sum_{n,\boldsymbol{k}}\left[\Omega_{xy}^{S^z,n}(\boldsymbol{k}) - \Omega_{zy}^{S^x,n}(\boldsymbol{k})\right] ln\left|e^{-\frac{E_{n,\boldsymbol{k}}}{k_BT}} - 1\right| k_BT \tag{S168}$$

and

$$\begin{aligned} P_y^{(2)} = -\frac{g\mu_B}{W_y V c^2}\sum_{n,\boldsymbol{k}} \rho_{n,\boldsymbol{k}} Im\Big[&\left\langle \partial_{k_y} u_{n,\boldsymbol{k}}\right| \left(\hat{v}_x\boldsymbol{\sigma}_3\hat{S}^z + \hat{S}^z\boldsymbol{\sigma}_3\hat{v}_x\right)\left|u_{n,\boldsymbol{k}}\right\rangle \left\langle u_{n,\boldsymbol{k}}\right|\boldsymbol{\sigma}_3\left|u_{n,\boldsymbol{k}}\right\rangle + \\ &+\left\langle u_{n,\boldsymbol{k}}\right|\left(\partial_{k_y}\hat{v}_x\right)\boldsymbol{\sigma}_3\hat{S}^z\left|u_{n,\boldsymbol{k}}\right\rangle \left\langle u_{n,\boldsymbol{k}}\right|\boldsymbol{\sigma}_3\left|u_{n,\boldsymbol{k}}\right\rangle \\ &+\left\langle u_{n,\boldsymbol{k}}\right|\left(\hat{v}_x\boldsymbol{\sigma}_3\hat{S}^z + \hat{S}^z\boldsymbol{\sigma}_3\hat{v}_x\right)\left|u_{n,\boldsymbol{k}}\right\rangle \left\langle u_{n,\boldsymbol{k}}\right|\boldsymbol{\sigma}_3\left|\partial_{k_y}u_{n,\boldsymbol{k}}\right\rangle\Big] - (x\leftrightarrow z) \end{aligned} \tag{S169}$$

Here, we have used the relation

$$\frac{d}{d\beta}\left[\beta\rho_{n,\boldsymbol{k}}\right] = \rho_{n,\boldsymbol{k}} + \left[\boldsymbol{\sigma}_3 E_{\boldsymbol{k}}\right]_{nn}\rho'_{n,\boldsymbol{k}} \tag{S170}$$

along with the integral identity:

$$\int\frac{dx}{e^x-1} = ln\left|e^x-1\right| - x = ln\left|e^x-1\right| + ln\left(e^{-x}\right) = ln\left|e^{-x}-1\right| \tag{S171}$$

where we have used the logarithmic identity $ln(A.B) = ln(A) + ln(B)$ and set the integration constant to zero.

Eq. (S168) and Eq. (S169) provide a microscopic framework to compute the electric polarization induced by magnon transport in both 3D and 2D magnetic materials. Eq. (S168) reveals the contribution of magnon spin current to the electric polarization through the magnon spin Berry curvatures $\Omega_{xy}^{S^z,n}(\boldsymbol{k})$ and $\Omega_{zy}^{S^x,n}(\boldsymbol{k})$ (13). Meanwhile, the $P_y^{(2)}$ term in Eq. (S169) is difficult to analyze at this stage. However, one can infer that this term is related to the orbital angular moment of the magnon, $\hat{\boldsymbol{L}} = \frac{1}{4}\left(\hat{\boldsymbol{r}}\times\boldsymbol{v} - \hat{\boldsymbol{v}}\times\hat{\boldsymbol{r}}\right)$ defined in Eq. (S69). This is because $\langle\partial_{\boldsymbol{k}}u_{n,\boldsymbol{k}}| \equiv \langle u_{n,\boldsymbol{k}}|\boldsymbol{r}$, ($\boldsymbol{r}$ is the position operator) appears in a multiplication with the velocity operator $\hat{\boldsymbol{v}}_{\boldsymbol{k}}$ as shown in Eq. (S169).

For those reasons, we relabel the expressions Eq. (S168) and Eq. (S169) as follows:

$$P_y^{(S)} = -\frac{g\mu_B}{\hbar W_y V c^2}\sum_{n,\boldsymbol{k}}\left[\Omega_{xy}^{S^z,n}(\boldsymbol{k}) - \Omega_{zy}^{S^x,n}(\boldsymbol{k})\right] ln\left|e^{-\frac{E_{n,\boldsymbol{k}}}{k_BT}} - 1\right| k_BT \tag{S172}$$

and

$$\begin{aligned} P_y^{(O)} = -\frac{g\mu_B}{W_y V c^2}\sum_{n,\boldsymbol{k}} \rho_{n,\boldsymbol{k}} Im\Big[&\left\langle \partial_{k_y} u_{n,\boldsymbol{k}}\right| \left(\hat{v}_x\boldsymbol{\sigma}_3\hat{S}^z + \hat{S}^z\boldsymbol{\sigma}_3\hat{v}_x\right)\left|u_{n,\boldsymbol{k}}\right\rangle \left\langle u_{n,\boldsymbol{k}}\right|\boldsymbol{\sigma}_3\left|u_{n,\boldsymbol{k}}\right\rangle + \\ &+\left\langle u_{n,\boldsymbol{k}}\right|\left(\partial_{k_y}\hat{v}_x\right)\boldsymbol{\sigma}_3\hat{S}^z\left|u_{n,\boldsymbol{k}}\right\rangle \left\langle u_{n,\boldsymbol{k}}\right|\boldsymbol{\sigma}_3\left|u_{n,\boldsymbol{k}}\right\rangle \\ &+\left\langle u_{n,\boldsymbol{k}}\right|\left(\hat{v}_x\boldsymbol{\sigma}_3\hat{S}^z + \hat{S}^z\boldsymbol{\sigma}_3\hat{v}_x\right)\left|u_{n,\boldsymbol{k}}\right\rangle \left\langle u_{n,\boldsymbol{k}}\right|\boldsymbol{\sigma}_3\left|\partial_{k_y}u_{n,\boldsymbol{k}}\right\rangle\Big] - (x\leftrightarrow z) \end{aligned} \tag{S173}$$

These labels S and O indicate the contributions from the spin Berry curvature and orbital moment to the electric polarization, respectively. Nevertheless, in principle, one can compute numerically the finite-temperature electric polarization $P_y = P_y^S + P_y^O$ for general 2D or 3D systems by using the following relations:

$$\left\langle\partial_{k_y}u_{n,\boldsymbol{k}}\right| = i\mathcal{A}_n^y\left\langle u_{n,\boldsymbol{k}}\right| + \sum_{q\neq n}\sigma_3^{qq}\frac{\left\langle u_{n,\boldsymbol{k}}\right|\partial_{k_y}\hat{H}_{\boldsymbol{k}}^0\left|u_{q,\boldsymbol{k}}\right\rangle}{\left[\boldsymbol{\sigma}_3E_{\boldsymbol{k}}\right]_{nn} - \left[\boldsymbol{\sigma}_3E_{\boldsymbol{k}}\right]_{qq}}\left\langle u_{q,\boldsymbol{k}}\right| \tag{S174}$$

where $\mathcal{A}_n^y = i\sigma_3^{nn}\left\langle u_{n,\boldsymbol{k}}\right|\boldsymbol{\sigma}_3\left|\partial_{k_y}u_{n,\boldsymbol{k}}\right\rangle$.

Inserting Eq. (S174) to Eq. (S173), one obtains:

$$\begin{aligned} P_y^{(O)} = -\frac{g\mu_B}{W_y V c^2}\sum_{n,\boldsymbol{k}} \rho_{n,\boldsymbol{k}} Im\Big[&\left\langle u_{n,\boldsymbol{k}}\right|\left(\partial_{k_y}\hat{v}_x\right)\boldsymbol{\sigma}_3\hat{S}^z\left|u_{n,\boldsymbol{k}}\right\rangle \left\langle u_{n,\boldsymbol{k}}\right|\boldsymbol{\sigma}_3\left|u_{n,\boldsymbol{k}}\right\rangle + \\ &+\sum_{q\neq n}\sigma_3^{qq}\frac{\left\langle u_{n,\boldsymbol{k}}\right|\partial_{k_y}\hat{H}_{\boldsymbol{k}}^0\left|u_{q,\boldsymbol{k}}\right\rangle}{\left[\boldsymbol{\sigma}_3E_{\boldsymbol{k}}\right]_{nn} - \left[\boldsymbol{\sigma}_3E_{\boldsymbol{k}}\right]_{qq}}\left\langle u_{q,\boldsymbol{k}}\right|\left(\hat{v}_x\boldsymbol{\sigma}_3\hat{S}^z + \hat{S}^z\boldsymbol{\sigma}_3\hat{v}_x\right)\left|u_{n,\boldsymbol{k}}\right\rangle \left\langle u_{n,\boldsymbol{k}}\right|\boldsymbol{\sigma}_3\left|u_{n,\boldsymbol{k}}\right\rangle \\ &+i\mathcal{A}_n^y\left\langle u_{n,\boldsymbol{k}}\right|\left(\hat{v}_x\boldsymbol{\sigma}_3\hat{S}^z + \hat{S}^z\boldsymbol{\sigma}_3\hat{v}_x\right)\left|u_{n,\boldsymbol{k}}\right\rangle\sigma_3^{nn} + \left\langle u_{n,\boldsymbol{k}}\right|\left(\hat{v}_x\boldsymbol{\sigma}_3\hat{S}^z + \hat{S}^z\boldsymbol{\sigma}_3\hat{v}_x\right)\left|u_{n,\boldsymbol{k}}\right\rangle \left\langle u_{n,\boldsymbol{k}}\right|\boldsymbol{\sigma}_3\left|\partial_{k_y}u_{n,\boldsymbol{k}}\right\rangle\Big] \\ &-(x\leftrightarrow z) \end{aligned} \tag{S175}$$

This leads to:

$$\begin{aligned} P_y^{(O)} = -\frac{g\mu_B}{W_y V c^2}\sum_{n,\boldsymbol{k}} \rho_{n,\boldsymbol{k}} Im\Big[&\left\langle u_{n,\boldsymbol{k}}\right|\left(\partial_{k_y}\hat{v}_x\right)\boldsymbol{\sigma}_3\hat{S}^z\left|u_{n,\boldsymbol{k}}\right\rangle \left\langle u_{n,\boldsymbol{k}}\right|\boldsymbol{\sigma}_3\left|u_{n,\boldsymbol{k}}\right\rangle + \\ &+\sum_{q\neq n}\sigma_3^{qq}\frac{\left\langle u_{n,\boldsymbol{k}}\right|\partial_{k_y}\hat{H}_{\boldsymbol{k}}^0\left|u_{q,\boldsymbol{k}}\right\rangle}{\left[\boldsymbol{\sigma}_3E_{\boldsymbol{k}}\right]_{nn} - \left[\boldsymbol{\sigma}_3E_{\boldsymbol{k}}\right]_{qq}}\left\langle u_{q,\boldsymbol{k}}\right|\left(\hat{v}_x\boldsymbol{\sigma}_3\hat{S}^z + \hat{S}^z\boldsymbol{\sigma}_3\hat{v}_x\right)\left|u_{n,\boldsymbol{k}}\right\rangle \left\langle u_{n,\boldsymbol{k}}\right|\boldsymbol{\sigma}_3\left|u_{n,\boldsymbol{k}}\right\rangle\Big] - (x\leftrightarrow z) \end{aligned} \tag{S176}$$

or

$$P_y^{(O)} = -\frac{g\mu_B}{W_y V c^2}\sum_{n,\boldsymbol{k}}\rho_{n,\boldsymbol{k}}\sigma_3^{nn} Im\left[\left\langle u_{n,\boldsymbol{k}}\right|\left(\partial_{k_y}\hat{v}_x\right)\boldsymbol{\sigma}_3\hat{S}^z\left|u_{n,\boldsymbol{k}}\right\rangle + \right.$$
$$\left. + 4\sum_{q\neq n}\sigma_3^{qq}\frac{\left\langle u_{n,\boldsymbol{k}}\right|\partial_{k_y}\hat{H}^0_{\boldsymbol{k}}\left|u_{q,\boldsymbol{k}}\right\rangle}{\left[\boldsymbol{\sigma}_3 E_{\boldsymbol{k}}\right]_{nn}-\left[\boldsymbol{\sigma}_3 E_{\boldsymbol{k}}\right]_{qq}}\left\langle u_{q,\boldsymbol{k}}\right|\hat{j}_x^{S^z}\left|u_{n,\boldsymbol{k}}\right\rangle\right] - (x\leftrightarrow z) \tag{S177}$$

where

$$\hat{j}_x^{S^z} = \frac{1}{4}\left(\hat{v}_x\boldsymbol{\sigma}_3\hat{S}^z + \hat{S}^z\boldsymbol{\sigma}_3\hat{v}_x\right) \tag{S178}$$

is the spin current operator. Eq. (S177) captures the contributions to the net electric polarization P_y likely arising from both inter-band and intra-band magnon orbital angular moment.

Given that our focus in this work is on 2D systems, we set $v_z = 0$. Consequently, the contribution of the S^x term and thus the $\hat{V}^{(2)}_{\boldsymbol{\Xi}}$ in Eq. (S133) vanishes. This reduction simplifies Eq. (S172) and Eq. (S173) to

$$P_y^{(S)} = -\frac{g\mu_B}{\hbar W_y V c^2}\sum_{n,\boldsymbol{k}}\Omega_{xy}^{S^z,n}\left(\boldsymbol{k}\right) ln\left|e^{-\frac{E_{n,\boldsymbol{k}}}{k_B T}}-1\right| k_B T \tag{S179}$$

and

$$P_y^{(O)} = -\frac{g\mu_B}{W_y V c^2}\sum_{n,\boldsymbol{k}}\rho_{n,\boldsymbol{k}} Im\left[\left\langle\partial_{k_y}u_{n,\boldsymbol{k}}\right|\left(\hat{v}_x\boldsymbol{\sigma}_3\hat{S}^z + \hat{S}^z\boldsymbol{\sigma}_3\hat{v}_x\right)\left|u_{n,\boldsymbol{k}}\right\rangle\left\langle u_{n,\boldsymbol{k}}\right|\boldsymbol{\sigma}_3\left|u_{n,\boldsymbol{k}}\right\rangle + \right.$$
$$+\left\langle u_{n,\boldsymbol{k}}\right|\left(\partial_{k_y}\hat{v}_x\right)\boldsymbol{\sigma}_3\hat{S}^z\left|u_{n,\boldsymbol{k}}\right\rangle\left\langle u_{n,\boldsymbol{k}}\right|\boldsymbol{\sigma}_3\left|u_{n,\boldsymbol{k}}\right\rangle$$
$$\left.+\left\langle u_{n,\boldsymbol{k}}\right|\left(\hat{v}_x\boldsymbol{\sigma}_3\hat{S}^z + \hat{S}^z\boldsymbol{\sigma}_3\hat{v}_x\right)\left|u_{n,\boldsymbol{k}}\right\rangle\left\langle u_{n,\boldsymbol{k}}\right|\boldsymbol{\sigma}_3\left|\partial_{k_y}u_{n,\boldsymbol{k}}\right\rangle\right] \tag{S180}$$

Furthermore, in order to gain a deeper understanding of the physical implications of the magnon orbital moment on polarization, we focus on scenarios where spin is conserved. This approach is valid in this work because the z-component of the total spin should be a good quantum number under the DMI. This allows for simplification, reducing the complexity of relation Eq. (S180) to:

$$P_y^{O} = -\frac{2g\mu_B}{W_y V c^2}\sum_{n,\boldsymbol{k}}\rho_{n,\boldsymbol{k}}\sigma_3^{nn}S^z_{nn}\ Im\left[\left\langle\partial_{k_y}u_{n,\boldsymbol{k}}\right|\hat{v}_x\left|u_{n,\boldsymbol{k}}\right\rangle\left\langle u_{n,\boldsymbol{k}}\right|\boldsymbol{\sigma}_3\left|u_{n,\boldsymbol{k}}\right\rangle + \right.$$
$$+\frac{1}{2}\left\langle u_{n,\boldsymbol{k}}\right|\left(\partial_{k_y}\hat{v}_x\right)\left|u_{n,\boldsymbol{k}}\right\rangle\left\langle u_{n,\boldsymbol{k}}\right|\boldsymbol{\sigma}_3\left|u_{n,\boldsymbol{k}}\right\rangle$$
$$\left.+\left\langle u_{n,\boldsymbol{k}}\right|\hat{v}_x\left|u_{n,\boldsymbol{k}}\right\rangle\left\langle u_{n,\boldsymbol{k}}\right|\boldsymbol{\sigma}_3\left|\partial_{k_y}u_{n,\boldsymbol{k}}\right\rangle\right] \tag{S181}$$

leads to

$$P_y^{O} = -\frac{2g\mu_B}{\hbar W_y V c^2}\sum_{n,\boldsymbol{k}}\rho_{n,\boldsymbol{k}}\sigma_3^{nn}S^z_{nn} Im\left\{\left\langle\partial_{k_y}u_{n,\boldsymbol{k}}\right|\left[\left(\boldsymbol{\sigma}_3 E_{\boldsymbol{k}}\right)_{nn}\boldsymbol{\sigma}_3 - \hat{H}^0_{\boldsymbol{k}}\right]\left|\partial_{k_x}u_{n,\boldsymbol{k}}\right\rangle\right\} \tag{S182}$$

Finally, one obtains

$$P_y = P_y^S + P_y^O = -\frac{g\mu_B}{\hbar W_y V c^2}\sum_{n,\boldsymbol{k}}\left[\Omega_{xy}^{S^z,n}\left(\boldsymbol{k}\right) ln\left|e^{-\frac{E_{n,\boldsymbol{k}}}{k_B T}}-1\right| k_B T + 2\hbar\sigma_3^{nn}S^z_{nn}L^z_{nn}\left(\boldsymbol{k}\right)\rho_{n,\boldsymbol{k}}\right] \tag{S183}$$

where

$$L^z_{nn}\left(\boldsymbol{k}\right) = \frac{1}{\hbar}Im\left\{\left\langle\partial_{k_y}u_{n,\boldsymbol{k}}\right|\left[\left(\boldsymbol{\sigma}_3 E_{\boldsymbol{k}}\right)_{nn}\boldsymbol{\sigma}_3 - \hat{H}^0_{\boldsymbol{k}}\right]\left|\partial_{k_x}u_{n,\boldsymbol{k}}\right\rangle\right\} \tag{S184}$$
$$\equiv \frac{1}{\hbar}Im\left\{\left\langle\partial_{k_y}n\left(\boldsymbol{k}\right)\right|\left[\left(\boldsymbol{\sigma}_3 E_{\boldsymbol{k}}\right)_{nn}\boldsymbol{\sigma}_3 - \hat{H}^0_{\boldsymbol{k}}\right]\left|\partial_{k_x}n\left(\boldsymbol{k}\right)\right\rangle\right\} \tag{S185}$$

is the intra-band orbital angular moment of the magnon in the nth state as presented in Eq. (S83). Here we have used $u_{n,\boldsymbol{k}} \equiv n\left(\boldsymbol{k}\right)$.

$$P_y^S = -\frac{g\mu_B}{\hbar W_y V c^2}\sum_{n,\boldsymbol{k}}\Omega_{xy}^{S^z,n}\left(\boldsymbol{k}\right) ln\left|e^{-\frac{E_{n,\boldsymbol{k}}}{k_B T}}-1\right| k_B T \tag{S186}$$

and

$$P_y^O = -\frac{2g\mu_B}{W_y V c^2}\sum_{n,\boldsymbol{k}}\sigma_3^{nn}S^z_{nn}L^z_{nn}\left(\boldsymbol{k}\right)\rho_{n,\boldsymbol{k}} \tag{S187}$$

thereby completing the derivation of Eq. (15) and Eq. (16) in the main text. The electric polarization induced by the motion of the magnon wave packets has two distinct contributions:

1. P_y^S, arising from the spin current through the spin-Berry curvature $\Omega_{xy}^{S^z,n}$ accounts for the accumulation of spin angular momentum along y-direction due to, for example the magnon spin Nernst current carried by magnons under a temperature gradient along the x-direction.

2. P_y^O, which results from the intra-band orbital angular moment $L_{nn}^z(\boldsymbol{k})$ of the magnons.

We note that our derivation presented in this part is based on perturbation theory within the thermodynamic limit, assuming an infinite x-dimension and the system is not too far away from equilibrium. For the magnon Nernst effect, this condition is satisfied when $\Delta_x T \ll T$. The electric polarization P_y in Eq. (S188) is the zeroth-order term in the expansion of electric polarization in terms of the temperature gradient $\partial_x T$

$$P_y = P_y^0 + P_y^1 \partial_x T + ... \tag{S188}$$

The zeroth order P_y^0 as given in Eq. (S188) is associated with the electric dipole moment, which depends on the temperature T but is independent of $\partial_x T$. The first-order term $P_y^1 \partial_x T$ corresponds to the electric quadrupole moment and indicates the induced electric polarization due to the temperature gradient $\partial_x T$. In this work, for the sake of simplification, we focus on the zeroth-order term and leave the contribution from higher-order terms for future investigation. However, we emphasise that the higher-order term respects the system's symmetry. This means that in the absence of DMI, the higher-order term must vanish to ensure that the total net electric polarization is zero, as previously discussed.

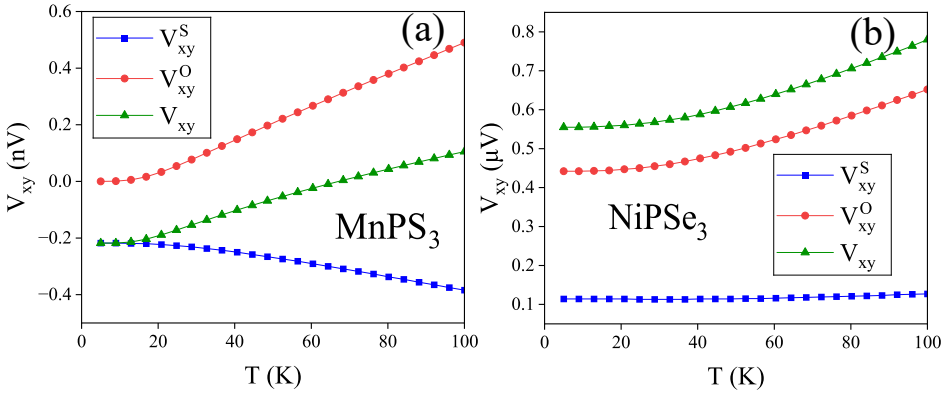

Fig. S3. The transverse voltage V_{xy} induced by the finite net electric polarization, along with its individual contributions from the orbital angular moment (V_{xy}^O) and spin Berry curvature (V_{xy}^S), in $MnPS_3$ (a) and $NiPSe_3$ (b) as a function of the average temperature T. The calculations are carried out under an applied out-of-plane magnetic field of $B_z = 1$ T.

B. Transverse voltage generated by finite net electric polarization. A finite net electric polarization induced by magnons gives rise to a transverse voltage V_{xy}. Specifically, the electric field Ξ_y along the y-direction, generated by the finite net electric polarization P_y, is given by:

$$\Xi_y = \frac{P_y}{\varepsilon_0 \chi} \tag{S189}$$

where ε_0 is the electric permittivity of free space and χ is the electric susceptibility. Therefore, the transverse voltage is given by

$$\begin{aligned} V_{xy} &= -\int_0^{W_y} \Xi_y dy = \frac{g\mu_B}{\hbar \varepsilon_0 \chi c^2 V} \sum_{n,\boldsymbol{k}} \left\{ \left[\Omega_{xy}^{S^z,n}(\boldsymbol{k}) - \Omega_{zy}^{S^x,n}(\boldsymbol{k}) \right] ln \left| e^{-\frac{E_{n,\boldsymbol{k}}}{k_B T}} - 1 \right| k_B T \right. \\ &+ \left. \hbar \sigma_3^{nn} Im \left[\left\langle n(\boldsymbol{k}) \left| \left(\partial_{k_y} \hat{v}_x \right) \boldsymbol{\sigma}_3 \hat{S}^z \right| n(\boldsymbol{k}) \right\rangle + 4 \sum_{q \neq n} \sigma_3^{qq} \frac{\left\langle n(\boldsymbol{k}) \left| \partial_{k_y} \hat{H}_{\boldsymbol{k}} \right| q(\boldsymbol{k}) \right\rangle}{[\boldsymbol{\sigma}_3 E_{\boldsymbol{k}}]_{nn} - [\boldsymbol{\sigma}_3 E_{\boldsymbol{k}}]_{qq}} \left\langle q(\boldsymbol{k}) \left| \hat{j}_x^{S^z} \right| n(\boldsymbol{k}) \right\rangle - (x \leftrightarrow z) \right] \rho_{n,\boldsymbol{k}} \right\} \\ &= V_{xy}^S + V_{xy}^O \end{aligned} \tag{S190}$$

where

$$\hat{j}_x^{S^z} = \frac{\hat{v}_x \boldsymbol{\sigma}_3 \hat{S}^z + \hat{S}^z \boldsymbol{\sigma}_3 \hat{v}_x}{4}; \tag{S191}$$

is the spin current operator;

$$V_{xy}^S = \frac{g\mu_B}{\hbar \varepsilon_0 \chi c^2 V} \sum_{n,\boldsymbol{k}} \left[\Omega_{xy}^{S^z,n}(\boldsymbol{k}) - \Omega_{zy}^{S^x,n}(\boldsymbol{k}) \right] ln \left| e^{-\frac{E_{n,\boldsymbol{k}}}{k_B T}} - 1 \right| k_B T; \tag{S192}$$

and

$$V_{xy}^{O}=\frac{g\mu_B}{\varepsilon_0\chi c^2 V}\sum_{n,\boldsymbol{k}}\sigma_3^{nn}Im\left[\left\langle n\left(\boldsymbol{k}\right)\left|\left(\partial_{k_y}\hat{v}_x\right)\boldsymbol{\sigma}_3\hat{S}^z\right|n\left(\boldsymbol{k}\right)\right\rangle+4\sum_{q\neq n}\sigma_3^{qq}\frac{\left\langle n\left(\boldsymbol{k}\right)\left|\partial_{k_y}\hat{H}_{\boldsymbol{k}}\right|q\left(\boldsymbol{k}\right)\right\rangle}{\left[\boldsymbol{\sigma}_3E_{\boldsymbol{k}}\right]_{nn}-\left[\boldsymbol{\sigma}_3E_{\boldsymbol{k}}\right]_{qq}}\left\langle q\left(\boldsymbol{k}\right)\left|\hat{j}_x^{S^z}\right|n\left(\boldsymbol{k}\right)\right\rangle-(x\leftrightarrow z)\right]\rho_{n,\boldsymbol{k}} \tag{S193}$$

We note that while the electric polarizations P_y directly depend on the width along y-direction of the sample, the resulting transverse voltage V_{xy} does not. Indeed, when the $\boldsymbol{k}$-point sampling is sufficiently dense, the discrete sum over momentum can be replaced by a continuous integral according to

$$\frac{1}{V}\sum_{\boldsymbol{k}}\rightarrow\frac{1}{(2\pi)^D}\int d\boldsymbol{k}. \tag{S194}$$

where D is the dimension of the sample. As a result, the expressions on the right-hand side of Eq. (S168) and Eq. (S169) decrease with the width W_y, whereas the transverse voltage in Eq. (S190) remains independent of W_y. We note that, in general, both the electric polarization and the transverse voltage could exhibit a dependence on the sample size, since in small systems the finite size of the sample may affect the band dispersion and the wavefunctions. Such size effects can modify quantities like the spin Berry curvature and the orbital moment, leading to variations in the resulting polarization and voltage. However, in this study, we assume that the system is sufficiently large such that finite-size effects on the band structure and wavefunctions can be neglected.

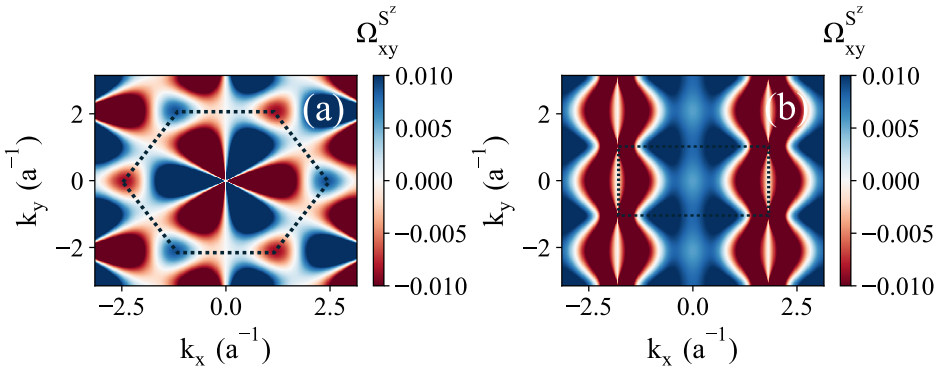

Fig. S4. The spin Berry curvature as a function of in-plane wave vector (k_x, k_y). Calculations are performed with applied magnetic field for the left-handed magnon mode of $MnPS_3$ (a), which has Néel magnetic order, and $NiPSe_3$ (b), which exhibits Zigzag magnetic order.

Furthermore, our analysis focuses on two-dimensional antiferromagnets: (i) collinear antiferromagnets on honeycomb lattices and (ii) noncollinear antiferromagnets on Kagome lattices. The results presented here apply specifically to the monolayer limit of these materials. In realistic experimental settings, however, multilayer samples are often used, which introduces additional thickness dependence in both the electric polarization and the transverse voltage. For instance, in the case of 2D honeycomb antiferromagnets such as those based on van der Waals materials with weak interlayer coupling, one may expect an approximately linear dependence of the polarization and transverse voltage on sample thickness for multilayers with A–A stacking. However, in thick samples, the emergence of out-of-plane temperature gradients may further influence the measured signals, suggesting that the sample thickness should be carefully controlled to minimize such effects. In this regard, $FePS_3$, a 2D antiferromagnet with Zigzag order known to exist in a stable monolayer form (19), emerges as a promising candidate for experimentally exploring the phenomena proposed in this work.

For the 2D honeycomb antiferromagnet with well-defined spin alignment along the z-direction considered in this work, the expression for the transverse voltage is given by:

$$V_{xy}=\frac{g\mu_B}{\hbar\varepsilon_0\chi c^2 V}\sum_{n,\boldsymbol{k}}\left[\Omega_{xy}^{S^z,n}\left(\boldsymbol{k}\right)ln\left|e^{-\frac{E_{n,\boldsymbol{k}}}{k_BT}}-1\right|k_BT+\hbar\sigma_3^{nn}S_{nn}^zL_{nn}^z\left(\boldsymbol{k}\right)\rho_{n,\boldsymbol{k}}\right] \tag{S195}$$

In Fig.S3, we present the transverse voltage V_{xy} as a function of average temperature T for $MnPS_3$ in panel (a) and $NiPSe_3$ in panel (b), along with the respective contributions from the orbital angular moment (V_{xy}^O) and spin Berry curvature (V_{xy}^S). In $NiPSe_3$, the orbital angular moment contribution dominates over the spin Berry curvature across the entire temperature range. In contrast, for $MnPS_3$, the spin Berry curvature is the dominant contributor at low temperatures. As the temperature increases, the contribution from the orbital angular moment becomes more significant, and at $T = 100$K, the orbital angular moment and spin Berry curvature contributions become comparable in magnitude. This behavior can be attributed to the symmetry properties of the system. Specifically, at low temperatures, i.e $T \rightarrow 0$, one finds that:

$$\rho_{n,\boldsymbol{k}}=\frac{1}{e^{E_{n,\boldsymbol{k}}/k_BT}-1}\rightarrow 0\quad when\quad E_{n,\boldsymbol{k}}>0 \tag{S196}$$

$$\rho_{n,\boldsymbol{k}} = \frac{1}{e^{E_{n,\boldsymbol{k}}/k_BT} - 1} \to -1 \quad when \quad E_{n,\boldsymbol{k}} < 0 \tag{S197}$$

Therefore, the second term in the square brackets of Eq. (S195) vanishes at low temperature when summing over all wave vectors, provided that the correlation function $\langle L^z S^z \rangle^n = S^z_{nn} L^z_{nn}(\boldsymbol{k})$ is odd with respect to the wave vector $\boldsymbol{k}$. This is indeed the case for $MnPS_3$, as shown in Fig.7(d) of the main text. As a result, the contribution from the orbital angular moment, V^O_{xy}, to the transverse voltage in $MnPS_3$ vanishes at low temperature, as illustrated in Fig.S3(a). In contrast, the correlation function in $NiPSe_3$ is even with respect to $\boldsymbol{k}$ and therefore remains finite at low temperature, as evident from Fig.S3(b). On the other hand, the contribution from the spin Berry curvature remains finite in both materials even as $T \to 0$, because when $T \to 0$

$$ln\left|e^{-\frac{E_{n,\boldsymbol{k}}}{k_BT}} - 1\right| k_BT \to ln\,(1)\, k_BT \quad \equiv \quad 0 \quad when \quad E_{n,\boldsymbol{k}} > 0 \tag{S198}$$

$$ln\left|e^{-\frac{E_{n,\boldsymbol{k}}}{k_BT}} - 1\right| k_BT \to \quad ln\left|e^{-\frac{E_{n,\boldsymbol{k}}}{k_BT}}\right| k_BT \quad \equiv \quad -E_{n,\boldsymbol{k}} \quad when \quad E_{n,\boldsymbol{k}} < 0 \tag{S199}$$

Therefore, although the spin Berry curvature in $MnPS_3$ exhibits odd behavior with respect to the wave vector [see Fig. S4(a)], its contribution to the transverse voltage remains finite due to $E_{n,\boldsymbol{k}} \neq E_{n,-\boldsymbol{k}}$ in the presence of Dzyaloshinskii–Moriya interaction. In $NiPSe_3$, the spin Berry curvature is even in $\boldsymbol{k}$ and also gives a finite contribution, as shown in Fig. S4(b).

Overall, the transverse voltage induced by magnon transport in $MnPS_3$ is dominated by the spin Berry curvature contribution at low temperatures, while at higher temperatures, both the spin Berry curvature and orbital angular moment contribute. In contrast, $NiPSe_3$ exhibits a dominant orbital angular moment contribution to the transverse voltage across the entire temperature range considered here.

S4. Linear response theory of the magnon orbital Nernst effect

We now turn to the description of the linear response theory for magnon orbital transport discussed in the main text. In the following, we shall elucidate the derivation of the continuity equation for magnon orbital angular moment density and introduce the corresponding orbital angular moment current operator being used in the linear response theory to compute the magnon orbital current in 2D collinear AFMs under a temperature gradient.

A. Orbital angular moment current operator. We start from the time evolution equation for the local angular moment density $L^\alpha(\boldsymbol{r}) = \frac{1}{2}\Psi^\dagger(\boldsymbol{r})\hat{L}^\alpha\Psi(\boldsymbol{r})$ $(\alpha = x, y, z)$, where the following commutators of the bosonic wavefunctions hold:

$$\left[\Psi^\dagger_m(\boldsymbol{r}), \Psi_n(\boldsymbol{r}')\right] = \sigma_3^{mn}\delta_{\boldsymbol{r},\boldsymbol{r}'} \tag{S200}$$

$$\left[\Psi_m(\boldsymbol{r}), \Psi_n(\boldsymbol{r}')\right] = i\sigma_2^{mn}\delta_{\boldsymbol{r},\boldsymbol{r}'} \tag{S201}$$

$$\left[\Psi^\dagger_m(\boldsymbol{r}), \Psi^\dagger_n(\boldsymbol{r}')\right] = -i\sigma_2^{mn}\delta_{\boldsymbol{r},\boldsymbol{r}'} \tag{S202}$$

with $\boldsymbol{\sigma}_i$ $(i = 1, 2, 3)$ Pauli matrices acting on particle-hole space. The Heisenberg equation of motion for the angular momentum operator is then:

$$\frac{\partial L^\alpha(\boldsymbol{r})}{\partial t} = i\left[\hat{H}, \hat{L}^\alpha(\boldsymbol{r})\right] \tag{S203}$$

where the total Hamiltonian can be expressed as $H = \frac{1}{2}\int d\boldsymbol{r}\tilde{\Psi}^\dagger(\boldsymbol{r})\hat{H}\tilde{\Psi}(\boldsymbol{r})$ with $\hat{H} = \sum_{\boldsymbol{\delta}}\hat{H}_{\boldsymbol{\delta}}e^{i\hat{\boldsymbol{p}}\cdot\boldsymbol{\delta}}$, $\mathcal{T}_{\boldsymbol{\delta}} = e^{i\hat{\boldsymbol{p}}\cdot\boldsymbol{\delta}}$ is the translation operator that satisfies $\mathcal{T}_{\boldsymbol{\delta}}f(\boldsymbol{r}) = e^{i\hat{\boldsymbol{p}}\cdot\boldsymbol{\delta}}f(\boldsymbol{r}) = f(\boldsymbol{r}+\boldsymbol{\delta})$, $\boldsymbol{\delta}$ is the vector shift between unit cells, and $\tilde{\Psi}(\boldsymbol{r}) = \left(1 + \boldsymbol{r}.\frac{\nabla\chi}{2}\right)\Psi(\boldsymbol{r}) = \xi(\boldsymbol{r})\Psi(\boldsymbol{r})$ with $\nabla\chi$ the temperature gradient.

To simplify the notation, we adopt the Einstein summation convention in which repeated Roman indices imply summation over the BdG field operator indices, which range from $-N, -N+1, ... -1, 1, ..., N-1, N$. Additionally, we introduce the notation $C_{A,B} = AB - BA = [A, B]$ representing the commutator of operators A and B and we set the Planck constant $\hbar = 1$. With these conventions in place, the continuity equation can be expressed as follows

$$\frac{\partial L^\alpha(\boldsymbol{r})}{\partial t} = i\left[\hat{H}, \hat{L}^\alpha(\boldsymbol{r})\right] = i\left[\frac{1}{2}\sum_{\boldsymbol{\delta}}\int d\boldsymbol{r}'\tilde{\Psi}^\dagger(\boldsymbol{r}')\hat{H}_{\boldsymbol{\delta}}\tilde{\Psi}(\boldsymbol{r}'+\boldsymbol{\delta}), \frac{1}{2}\Psi^\dagger(\boldsymbol{r})\hat{L}^\alpha\Psi(\boldsymbol{r})\right] \tag{S204}$$

$$= -\frac{i}{4}\sum_{\boldsymbol{\delta}}\int d\boldsymbol{r}'\left[\Psi^\dagger_n(\boldsymbol{r})\hat{L}^\alpha_{nn'}\Psi_{n'}(\boldsymbol{r})\tilde{\Psi}^\dagger_m(\boldsymbol{r}')\left(\hat{H}_{\boldsymbol{\delta}}\right)_{mk}\tilde{\Psi}_k(\boldsymbol{r}'+\boldsymbol{\delta})\right.$$

$$\left.-\tilde{\Psi}^\dagger_m(\boldsymbol{r}')\left(\hat{H}_{\boldsymbol{\delta}}\right)_{mk}\tilde{\Psi}_k(\boldsymbol{r}'+\boldsymbol{\delta})\Psi^\dagger_n(\boldsymbol{r})\hat{L}^\alpha_{nn'}\Psi_{n'}(\boldsymbol{r})\right] \tag{S205}$$

$$= -\frac{i}{2}\sum_{\boldsymbol{\delta}}\left\{\Psi^\dagger_n(\boldsymbol{r})\hat{L}^\alpha_{nn'}\sigma_3^{n'm}\left[\xi(\boldsymbol{r})\hat{H}_{\boldsymbol{\delta}}\xi(\boldsymbol{r}+\boldsymbol{\delta})\right]_{mk}\Psi_k(\boldsymbol{r}+\boldsymbol{\delta})\right.$$

$$\left.-\Psi^\dagger_m(\boldsymbol{r}-\boldsymbol{\delta})\left[\xi(\boldsymbol{r}-\boldsymbol{\delta})\hat{H}_{\boldsymbol{\delta}}\xi(\boldsymbol{\delta})\right]_{mk}\sigma_3^{kn}\hat{L}^\alpha_{nn'}\Psi_{n'}(\boldsymbol{r})\right\}. \tag{S206}$$

Using

$$\hat{L}^{\alpha}\xi\left(\boldsymbol{r}\right)=C_{\hat{L}^{\alpha},\xi(\boldsymbol{r})}+\xi\left(\boldsymbol{r}\right)\hat{L}^{\alpha} \tag{S207}$$

one has

$$\frac{\partial L^{\alpha}\left(\boldsymbol{r}\right)}{\partial t}=-\frac{i}{2}\sum_{\boldsymbol{\delta}}\left[\tilde{\Psi}^{\dagger}\left(\boldsymbol{r}\right)\hat{L}^{\alpha}\boldsymbol{\sigma}_{3}\hat{H}_{\boldsymbol{\delta}}\tilde{\Psi}\left(\boldsymbol{r}+\boldsymbol{\delta}\right)-\tilde{\Psi}^{\dagger}\left(\boldsymbol{r}-\boldsymbol{\delta}\right)\hat{H}_{\boldsymbol{\delta}}\boldsymbol{\sigma}_{3}\hat{L}^{\alpha}\tilde{\Psi}\left(\boldsymbol{r}\right)\right]-\mathcal{O}_{1} \tag{S208}$$

where

$$\mathcal{O}_{1}=\frac{i}{2}\sum_{\boldsymbol{\delta}}\left\{\Psi^{\dagger}\left(\boldsymbol{r}\right)C_{\hat{L}^{\alpha},\xi(\boldsymbol{r})}\boldsymbol{\sigma}_{3}\hat{H}_{\boldsymbol{\delta}}\xi\left(\boldsymbol{r}+\boldsymbol{\delta}\right)\Psi\left(\boldsymbol{r}+\boldsymbol{\delta}\right)+\Psi^{\dagger}\left(\boldsymbol{r}-\boldsymbol{\delta}\right)\xi\left(\boldsymbol{r}-\boldsymbol{\delta}\right)\hat{H}_{\boldsymbol{\delta}}\boldsymbol{\sigma}_{3}C_{\hat{L}^{\alpha},\xi(\boldsymbol{r})}\Psi\left(\boldsymbol{r}\right)\right\}. \tag{S209}$$

Using the approximations $\tilde{\Psi}\left(\boldsymbol{r}\pm\boldsymbol{\delta}\right)=\tilde{\Psi}\left(\boldsymbol{r}\right)\pm\boldsymbol{\delta}\cdot\boldsymbol{\nabla}\tilde{\Psi}\left(\boldsymbol{r}\right)$ and $\tilde{\Psi}\left(\boldsymbol{r}\right)=\tilde{\Psi}\left(\boldsymbol{r}\pm\boldsymbol{\delta}\right)\mp\boldsymbol{\delta}\cdot\boldsymbol{\nabla}\tilde{\Psi}\left(\boldsymbol{r}\pm\boldsymbol{\delta}\right)$, one gets:

$$-\frac{i}{2}\sum_{\boldsymbol{\delta}}\tilde{\Psi}^{\dagger}\left(\boldsymbol{r}\right)\hat{L}^{\alpha}\boldsymbol{\sigma}_{3}\hat{H}_{\boldsymbol{\delta}}\tilde{\Psi}\left(\boldsymbol{r}+\boldsymbol{\delta}\right)=-\frac{i}{4}\sum_{\boldsymbol{\delta}}\tilde{\Psi}^{\dagger}\left(\boldsymbol{r}\right)\hat{L}^{\alpha}\boldsymbol{\sigma}_{3}\hat{H}_{\boldsymbol{\delta}}\tilde{\Psi}\left(\boldsymbol{r}+\boldsymbol{\delta}\right)-\frac{i}{4}\sum_{\boldsymbol{\delta}}\tilde{\Psi}^{\dagger}\left(\boldsymbol{r}\right)\hat{L}^{\alpha}\boldsymbol{\sigma}_{3}\hat{H}_{\boldsymbol{\delta}}\tilde{\Psi}\left(\boldsymbol{r}+\boldsymbol{\delta}\right) \tag{S210}$$

$$=-\frac{i}{4}\sum_{\boldsymbol{\delta}}\left[\tilde{\Psi}^{\dagger}\left(\boldsymbol{r}-\boldsymbol{\delta}\right)+\boldsymbol{\delta}\cdot\boldsymbol{\nabla}\tilde{\Psi}^{\dagger}\left(\boldsymbol{r}\right)\right]\hat{L}^{\alpha}\boldsymbol{\sigma}_{3}\hat{H}_{\boldsymbol{\delta}}\tilde{\Psi}\left(\boldsymbol{r}+\boldsymbol{\delta}\right)-\frac{i}{4}\sum_{\boldsymbol{\delta}}\tilde{\Psi}^{\dagger}\left(\boldsymbol{r}\right)\hat{L}^{\alpha}\boldsymbol{\sigma}_{3}\hat{H}_{\boldsymbol{\delta}}\left[\tilde{\Psi}\left(\boldsymbol{r}\right)+\boldsymbol{\delta}\cdot\boldsymbol{\nabla}\tilde{\Psi}\left(\boldsymbol{r}+\boldsymbol{\delta}\right)\right] \tag{S211}$$

$$=-\frac{i}{4}\sum_{\boldsymbol{\delta}}\left[\boldsymbol{\delta}\cdot\boldsymbol{\nabla}\tilde{\Psi}^{\dagger}\left(\boldsymbol{r}\right)\hat{L}^{\alpha}\boldsymbol{\sigma}_{3}\hat{H}_{\boldsymbol{\delta}}\tilde{\Psi}\left(\boldsymbol{r}+\boldsymbol{\delta}\right)+\tilde{\Psi}^{\dagger}\left(\boldsymbol{r}\right)\hat{L}^{\alpha}\boldsymbol{\sigma}_{3}\hat{H}_{\boldsymbol{\delta}}\boldsymbol{\delta}\cdot\boldsymbol{\nabla}\tilde{\Psi}\left(\boldsymbol{r}+\boldsymbol{\delta}\right)\right] \tag{S212}$$

$$-\frac{i}{4}\sum_{\boldsymbol{\delta}}\left[\tilde{\Psi}^{\dagger}\left(\boldsymbol{r}-\boldsymbol{\delta}\right)\hat{L}^{\alpha}\boldsymbol{\sigma}_{3}\hat{H}_{\boldsymbol{\delta}}\tilde{\Psi}\left(\boldsymbol{r}+\boldsymbol{\delta}\right)+\tilde{\Psi}^{\dagger}\left(\boldsymbol{r}\right)\hat{L}^{\alpha}\boldsymbol{\sigma}_{3}\hat{H}_{\boldsymbol{\delta}}\tilde{\Psi}\left(\boldsymbol{r}\right)\right] \tag{S213}$$

$$=-\frac{i}{4}\sum_{\boldsymbol{\delta}}\boldsymbol{\delta}\cdot\boldsymbol{\nabla}\left[\tilde{\Psi}^{\dagger}\left(\boldsymbol{r}\right)\hat{L}^{\alpha}\boldsymbol{\sigma}_{3}\hat{H}_{\boldsymbol{\delta}}\tilde{\Psi}\left(\boldsymbol{r}+\boldsymbol{\delta}\right)\right]-\frac{i}{2}\sum_{\boldsymbol{\delta}}\tilde{\Psi}^{\dagger}\left(\boldsymbol{r}\right)\hat{L}^{\alpha}\boldsymbol{\sigma}_{3}\hat{H}_{\boldsymbol{\delta}}\tilde{\Psi}\left(\boldsymbol{r}\right)$$

$$+\frac{i}{4}\sum_{\boldsymbol{\delta}}\tilde{\Psi}^{\dagger}\left(\boldsymbol{r}\right)C_{\hat{L}^{\alpha},\mathcal{T}_{-\boldsymbol{\delta}}}\boldsymbol{\sigma}_{3}\hat{H}_{\boldsymbol{\delta}}e^{i\hat{\boldsymbol{p}}\cdot\boldsymbol{\delta}}\tilde{\Psi}\left(\boldsymbol{r}\right) \tag{S214}$$

$$=-\boldsymbol{\nabla}\frac{1}{4}\left[\tilde{\Psi}^{\dagger}\left(\boldsymbol{r}\right)\hat{L}^{\alpha}\boldsymbol{\sigma}_{3}\hat{\boldsymbol{v}}\tilde{\Psi}\left(\boldsymbol{r}\right)\right]-\frac{i}{2}\sum_{\boldsymbol{\delta}}\tilde{\Psi}^{\dagger}\left(\boldsymbol{r}\right)\hat{L}^{\alpha}\boldsymbol{\sigma}_{3}\hat{H}_{\boldsymbol{\delta}}\tilde{\Psi}\left(\boldsymbol{r}\right)+\frac{i}{4}\sum_{\boldsymbol{\delta}}\tilde{\Psi}^{\dagger}\left(\boldsymbol{r}\right)C_{\hat{L}^{\alpha},\mathcal{T}_{-\boldsymbol{\delta}}}e^{i\hat{\boldsymbol{p}}\cdot\boldsymbol{\delta}}\boldsymbol{\sigma}_{3}\hat{H}_{\boldsymbol{\delta}}\tilde{\Psi}\left(\boldsymbol{r}\right) \tag{S215}$$

where $\hat{\boldsymbol{v}}=i\left[\hat{H},\hat{\boldsymbol{r}}\right]=i\sum_{\boldsymbol{\delta}}\boldsymbol{\delta}\cdot\hat{H}_{\boldsymbol{\delta}}e^{i\hat{\boldsymbol{p}}\boldsymbol{\delta}}$ is the velocity operator. Similarly:

$$\frac{i}{2}\sum_{\boldsymbol{\delta}}\tilde{\Psi}^{\dagger}\left(\boldsymbol{r}-\boldsymbol{\delta}\right)\hat{H}_{\boldsymbol{\delta}}\boldsymbol{\sigma}_{3}\hat{L}^{\alpha}\tilde{\Psi}\left(\boldsymbol{r}\right)=\frac{i}{4}\sum_{\boldsymbol{\delta}}\tilde{\Psi}^{\dagger}\left(\boldsymbol{r}-\boldsymbol{\delta}\right)\hat{H}_{\boldsymbol{\delta}}\boldsymbol{\sigma}_{3}\hat{L}^{\alpha}\tilde{\Psi}\left(\boldsymbol{r}\right)+\frac{i}{4}\sum_{\boldsymbol{\delta}}\tilde{\Psi}^{\dagger}\left(\boldsymbol{r}-\boldsymbol{\delta}\right)\hat{H}_{\boldsymbol{\delta}}\boldsymbol{\sigma}_{3}\hat{L}^{\alpha}\tilde{\Psi}\left(\boldsymbol{r}\right) \tag{S216}$$

$$=\frac{i}{4}\sum_{\boldsymbol{\delta}}\left[\tilde{\Psi}^{\dagger}\left(\boldsymbol{r}\right)-\boldsymbol{\delta}\cdot\boldsymbol{\nabla}\tilde{\Psi}^{\dagger}\left(\boldsymbol{r}-\boldsymbol{\delta}\right)\right]\hat{H}_{\boldsymbol{\delta}}\boldsymbol{\sigma}_{3}\hat{L}^{\alpha}\tilde{\Psi}\left(\boldsymbol{r}\right)+\frac{i}{4}\sum_{\boldsymbol{\delta}}\tilde{\Psi}^{\dagger}\left(\boldsymbol{r}-\boldsymbol{\delta}\right)\hat{H}_{\boldsymbol{\delta}}\boldsymbol{\sigma}_{3}\hat{L}^{\alpha}\left[\tilde{\Psi}\left(\boldsymbol{r}+\boldsymbol{\delta}\right)-\boldsymbol{\delta}\cdot\boldsymbol{\nabla}\tilde{\Psi}\left(\boldsymbol{r}\right)\right] \tag{S217}$$

$$=-\frac{i}{4}\sum_{\boldsymbol{\delta}}\left[\boldsymbol{\delta}\cdot\boldsymbol{\nabla}\tilde{\Psi}^{\dagger}\left(\boldsymbol{r}-\boldsymbol{\delta}\right)\hat{H}_{\boldsymbol{\delta}}\boldsymbol{\sigma}_{3}\hat{L}^{\alpha}\tilde{\Psi}\left(\boldsymbol{r}\right)+\tilde{\Psi}^{\dagger}\left(\boldsymbol{r}-\boldsymbol{\delta}\right)\hat{H}_{\boldsymbol{\delta}}\boldsymbol{\sigma}_{3}\hat{L}^{\alpha}\boldsymbol{\delta}\cdot\boldsymbol{\nabla}\tilde{\Psi}\left(\boldsymbol{r}\right)\right] \tag{S218}$$

$$+\frac{i}{4}\left[\tilde{\Psi}^{\dagger}\left(\boldsymbol{r}\right)\hat{H}_{\boldsymbol{\delta}}\boldsymbol{\sigma}_{3}\hat{L}^{\alpha}\tilde{\Psi}\left(\boldsymbol{r}\right)+\tilde{\Psi}^{\dagger}\left(\boldsymbol{r}-\boldsymbol{\delta}\right)\hat{H}_{\boldsymbol{\delta}}\boldsymbol{\sigma}_{3}\hat{L}^{\alpha}\tilde{\Psi}\left(\boldsymbol{r}+\boldsymbol{\delta}\right)\right] \tag{S219}$$

$$=-\frac{i}{4}\sum_{\boldsymbol{\delta}}\boldsymbol{\delta}\cdot\boldsymbol{\nabla}\left[\tilde{\Psi}^{\dagger}\left(\boldsymbol{r}-\boldsymbol{\delta}\right)\hat{H}_{\boldsymbol{\delta}}\boldsymbol{\sigma}_{3}\hat{L}^{\alpha}\tilde{\Psi}\left(\boldsymbol{r}\right)\right]+\frac{i}{2}\tilde{\Psi}^{\dagger}\left(\boldsymbol{r}\right)\hat{H}_{\boldsymbol{\delta}}\boldsymbol{\sigma}_{3}\hat{L}^{\alpha}\tilde{\Psi}\left(\boldsymbol{r}\right)-\frac{i}{4}\sum_{\boldsymbol{\delta}}\tilde{\Psi}^{\dagger}\left(\boldsymbol{r}\right)\hat{H}_{\boldsymbol{\delta}}\boldsymbol{\sigma}_{3}C_{\hat{L}^{\alpha},\mathcal{T}_{-\boldsymbol{\delta}}}e^{i\hat{\boldsymbol{p}}\cdot\boldsymbol{\delta}}\tilde{\Psi}\left(\boldsymbol{r}\right) \tag{S220}$$

$$=-\boldsymbol{\nabla}\frac{1}{4}\left[\tilde{\Psi}^{\dagger}\left(\boldsymbol{r}\right)\hat{\boldsymbol{v}}\boldsymbol{\sigma}_{3}\hat{L}^{\alpha}\tilde{\Psi}\left(\boldsymbol{r}\right)\right]+\frac{i}{2}\tilde{\Psi}^{\dagger}\left(\boldsymbol{r}\right)\hat{H}_{\boldsymbol{\delta}}\boldsymbol{\sigma}_{3}\hat{L}^{\alpha}\tilde{\Psi}\left(\boldsymbol{r}\right)-\frac{i}{4}\sum_{\boldsymbol{\delta}}\tilde{\Psi}^{\dagger}\left(\boldsymbol{r}\right)\hat{H}_{\boldsymbol{\delta}}\boldsymbol{\sigma}_{3}C_{\hat{L}^{\alpha},\mathcal{T}_{-\boldsymbol{\delta}}}e^{i\hat{\boldsymbol{p}}\cdot\boldsymbol{\delta}}\tilde{\Psi}\left(\boldsymbol{r}\right). \tag{S221}$$

Consequently

$$\begin{aligned}\frac{\partial L^{\alpha}\left(\boldsymbol{r}\right)}{\partial t}&=-\boldsymbol{\nabla}\left[\tilde{\Psi}^{\dagger}\left(\boldsymbol{r}\right)\frac{\left(\hat{L}^{\alpha}\boldsymbol{\sigma}_{3}\hat{\boldsymbol{v}}+\hat{\boldsymbol{v}}\boldsymbol{\sigma}_{3}\hat{L}^{\alpha}\right)}{4}\tilde{\Psi}\left(\boldsymbol{r}\right)\right]-\frac{1}{2}\tilde{\Psi}^{\dagger}\left(\boldsymbol{r}\right)\left(\hat{L}^{\alpha}\boldsymbol{\sigma}_{3}\hat{H}_{\boldsymbol{\delta}}-\hat{H}_{\boldsymbol{\delta}}\boldsymbol{\sigma}_{3}\hat{L}^{\alpha}\right)\tilde{\Psi}\left(\boldsymbol{r}\right)+\mathcal{O}_{1}+\mathcal{O}_{2}\\&=-\boldsymbol{\nabla}\boldsymbol{j}^{L^{\alpha}}+\boldsymbol{S}^{L^{\alpha}}\end{aligned} \tag{S222}$$

where

$$\mathcal{O}_{2}=\frac{i}{4}\sum_{\boldsymbol{\delta}}\tilde{\Psi}^{\dagger}\left(\boldsymbol{r}\right)C_{\hat{L}^{\alpha},\mathcal{T}_{-\boldsymbol{\delta}}}e^{i\hat{\boldsymbol{p}}\cdot\boldsymbol{\delta}}\boldsymbol{\sigma}_{3}\hat{H}_{\boldsymbol{\delta}}\tilde{\Psi}\left(\boldsymbol{r}\right)-\frac{i}{4}\sum_{\boldsymbol{\delta}}\tilde{\Psi}^{\dagger}\left(\boldsymbol{r}\right)\hat{H}_{\boldsymbol{\delta}}\boldsymbol{\sigma}_{3}C_{\hat{L}^{\alpha},\mathcal{T}_{-\boldsymbol{\delta}}}e^{i\hat{\boldsymbol{p}}\cdot\boldsymbol{\delta}}\tilde{\Psi}\left(\boldsymbol{r}\right) \tag{S223}$$

and

$$\boldsymbol{S}^{L^{\alpha}}=-\frac{1}{2}\tilde{\Psi}^{\dagger}\left(\boldsymbol{r}\right)\left(\hat{L}^{\alpha}\boldsymbol{\sigma}_{3}\hat{H}_{\boldsymbol{\delta}}-\hat{H}_{\boldsymbol{\delta}}\boldsymbol{\sigma}_{3}\hat{L}^{\alpha}\right)\tilde{\Psi}\left(\boldsymbol{r}\right)+\mathcal{O}_{1}+\mathcal{O}_{2} \tag{S224}$$

is the orbital source density corresponding to the orbital torque density (20) and

$$\boldsymbol{j}^{L^\alpha} = \tilde{\Psi}^\dagger(\boldsymbol{r}) \frac{\left(\hat{L}^\alpha \boldsymbol{\sigma}_3 \hat{\boldsymbol{v}} + \hat{\boldsymbol{v}} \boldsymbol{\sigma}_3 \hat{L}^\alpha\right)}{4} \tilde{\Psi}(\boldsymbol{r}) \tag{S225}$$

is the local orbital current density. The orbital angular moment current operator can be defined as $\hat{\boldsymbol{j}}^{L^\alpha} = \frac{1}{4}\left(\hat{L}^\alpha \boldsymbol{\sigma}_3 \hat{\boldsymbol{v}} + \hat{\boldsymbol{v}} \boldsymbol{\sigma}_3 \hat{L}^\alpha\right)$.

We note that in addition to the conventional source term $-\frac{1}{2}\tilde{\Psi}^\dagger(\boldsymbol{r})\left(\hat{L}^\alpha \boldsymbol{\sigma}_3 \hat{H}_{\boldsymbol{\delta}} - \hat{H}_{\boldsymbol{\delta}} \boldsymbol{\sigma}_3 \hat{L}^\alpha\right)\tilde{\Psi}(\boldsymbol{r})$, Eq. (S224) also incorporates the terms $\mathcal{O}_1$ and $\mathcal{O}_2$ arising due to the nonzero commutator $\left[\hat{\boldsymbol{L}}, \hat{\boldsymbol{r}}\right] \neq 0$. This indicates that even in a scenario where $-\frac{1}{2}\tilde{\Psi}^\dagger(\boldsymbol{r})\left(\hat{L}^\alpha \boldsymbol{\sigma}_3 \hat{H}_{\boldsymbol{\delta}} - \hat{H}_{\boldsymbol{\delta}} \boldsymbol{\sigma}_3 \hat{L}^\alpha\right)\tilde{\Psi}(\boldsymbol{r}) = 0$, the conservation of the orbital angular moment current is not guaranteed. Additional considerations such as source density and magnon orbital torque are beyond the scope of this study. Instead, our focus will be exclusively on the orbital current term. The inclusion of a source term will result in some dissipation; nevertheless, our findings remain valid within the orbital relaxation time.

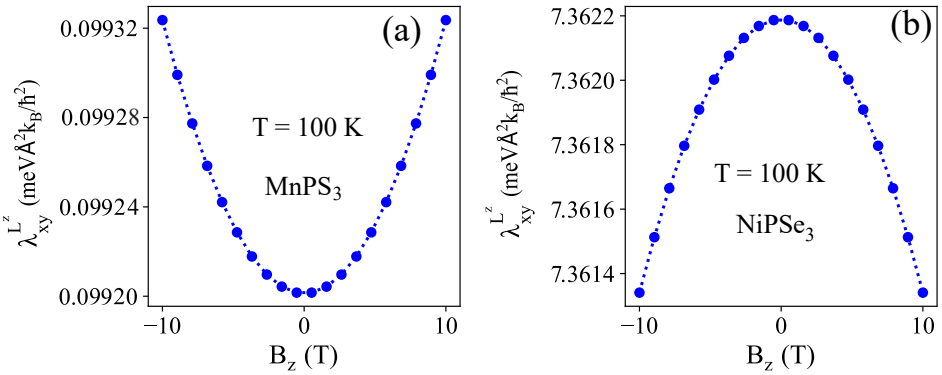

Fig. S5. The Orbital Nernst conductivity of $MnPS_3$ (a) and $NiPSe_3$ (b) as a function of externally applied magnetic field along z-direction B_z computed at fixed temperature $T = 100\ K$.

B. Responses of magnonic system to thermal gradient: Linear response theory. We are now deriving the expression describing the response of the magnon orbital angular moment current to a temperature gradient within the linear response theory. In this pursuit, we adopt the work of Matsumoto et al., in Ref. (12), Zyuzin et al., in Ref. (21), and Park et al., in Ref. (6) to deal with the magnon orbital angular moment current. Our analysis involves a 2D magnon system exposed to a temperature gradient, and the resulting orbital current can be represented as

$$\boldsymbol{j}^{L^\alpha}(\boldsymbol{r}) = \tilde{\Psi}^\dagger(\boldsymbol{r})\left[\frac{\hat{L}^\alpha \boldsymbol{\sigma}_3 \hat{\boldsymbol{v}} + \hat{\boldsymbol{v}} \boldsymbol{\sigma}_3 \hat{L}^\alpha}{4}\right]\tilde{\Psi}(\boldsymbol{r}) \tag{S226}$$

where $\tilde{\Psi}(\boldsymbol{r}) = \left(1 + \boldsymbol{r} \cdot \frac{\boldsymbol{\nabla}\chi}{2}\right)\Psi(\boldsymbol{r})$ so that

$$\boldsymbol{j}^{L^\alpha}(\boldsymbol{r}) = \Psi^\dagger(\boldsymbol{r})\left(1 + \boldsymbol{r} \cdot \frac{\boldsymbol{\nabla}\chi}{2}\right)\left[\frac{\hat{L}^\alpha \boldsymbol{\sigma}_3 \hat{\boldsymbol{v}} + \hat{\boldsymbol{v}} \boldsymbol{\sigma}_3 \hat{L}^\alpha}{4}\right]\left(1 + \boldsymbol{r} \cdot \frac{\boldsymbol{\nabla}\chi}{2}\right)\Psi(\boldsymbol{r}). \tag{S227}$$

To linear order in the temperature gradient the Orbital angular moment current is decomposed as

$$\boldsymbol{j}^{L^\alpha}(\boldsymbol{r}) = \boldsymbol{j}^{L^\alpha(0)}(\boldsymbol{r}) + \boldsymbol{j}^{L^\alpha(1)}(\boldsymbol{r}) \tag{S228}$$

where

$$\boldsymbol{j}^{L^\alpha(0)}(\boldsymbol{r}) = \Psi^\dagger(\boldsymbol{r})\frac{\hat{L}^\alpha \boldsymbol{\sigma}_3 \hat{\boldsymbol{v}} + \hat{\boldsymbol{v}} \boldsymbol{\sigma}_3 \hat{L}^\alpha}{4}\Psi(\boldsymbol{r}) \tag{S229}$$

and

$$\boldsymbol{j}^{L^\alpha(1)}(\boldsymbol{r}) = \frac{1}{2}\Psi^\dagger(\boldsymbol{r})\left[\left(\frac{\hat{L}^\alpha \boldsymbol{\sigma}_3 \hat{\boldsymbol{v}} + \hat{\boldsymbol{v}} \boldsymbol{\sigma}_3 \hat{L}^\alpha}{4}\right)\hat{\boldsymbol{r}} + \hat{\boldsymbol{r}}\left(\frac{\hat{L}^\alpha \boldsymbol{\sigma}_3 \hat{\boldsymbol{v}} + \hat{\boldsymbol{v}} \boldsymbol{\sigma}_3 \hat{L}^\alpha}{4}\right)\right]\Psi(\boldsymbol{r})\boldsymbol{\nabla}\chi. \tag{S230}$$

Defining $\boldsymbol{J}^{L^\alpha} = \int d\boldsymbol{r}\ \boldsymbol{j}^{L^\alpha}(\boldsymbol{r})$, one obtains

$$\left\langle \boldsymbol{J}^{L^\alpha} \right\rangle = \left\langle \boldsymbol{J}^{L^\alpha(0)} \right\rangle_{neq} + \left\langle \boldsymbol{J}^{L^\alpha(1)} \right\rangle_{eq}. \tag{S231}$$

Employing the Kubo formula (22–24) we evaluate the first term

$$\left\langle J_\mu^{L^\alpha(0)} \right\rangle_{neq} = -\lim_{\omega \to 0} \frac{\partial}{\partial \omega} \int_0^\beta d\tau e^{i\omega\tau} \left\langle T_\tau J_\mu^{L^\alpha(0)}(\tau)\, J_\nu^{(Q)}(0) \right\rangle \nabla_\nu \chi \equiv -S_{\mu\nu} \nabla_\nu \chi \tag{S232}$$

where

$$\boldsymbol{J}^{(Q)}=\frac{1}{4}\sum_{\boldsymbol{k}}\Psi_{\boldsymbol{k}}^{\dagger}\left[\hat{H}_{\boldsymbol{k}}\boldsymbol{\sigma}_3\hat{\boldsymbol{v}}_{\boldsymbol{k}}+\hat{\boldsymbol{v}}_{\boldsymbol{k}}\boldsymbol{\sigma}_3\hat{H}_{\boldsymbol{k}}\right]\Psi_{\boldsymbol{k}} \tag{S233}$$

and

$$\boldsymbol{J}^{L^{\alpha}(0)}=\frac{1}{4}\sum_{\boldsymbol{k}}\Psi_{\boldsymbol{k}}^{\dagger}\left[\hat{L}^{\alpha}\boldsymbol{\sigma}_3\hat{\boldsymbol{v}}_{\boldsymbol{k}}+\hat{\boldsymbol{v}}_{\boldsymbol{k}}\boldsymbol{\sigma}_3\hat{L}^{\alpha}\right]\Psi_{\boldsymbol{k}}. \tag{S234}$$

Introducing the field operator for the energy eigenstates

$$\Phi_{\boldsymbol{k}}=T_{\boldsymbol{k}}\Psi_{\boldsymbol{k}} \tag{S235}$$

one has

$$\begin{aligned}S_{\mu\nu}=\frac{1}{16}\lim_{\omega\to0}\frac{\partial}{\partial\omega}\int_0^{\beta}d\tau e^{i\omega\tau}\sum_{\boldsymbol{k},\boldsymbol{k}'}\Big\langle\Phi_{\boldsymbol{k}}^{\dagger}\left(\tau\right)T_{\boldsymbol{k}}^{\dagger}\left(\hat{L}^{\alpha}\boldsymbol{\sigma}_3\hat{v}_{\boldsymbol{k},\mu}+\hat{v}_{\boldsymbol{k},\mu}\boldsymbol{\sigma}_3\hat{L}^{\alpha}\right)T_{\boldsymbol{k}}\Phi_{\boldsymbol{k}}\left(\tau\right)\Phi_{\boldsymbol{k}'}^{\dagger}\left(0\right)\times\\ \times T_{\boldsymbol{k}'}^{\dagger}\left(\hat{H}_{\boldsymbol{k}'}\boldsymbol{\sigma}_3\hat{v}_{\boldsymbol{k}',\nu}+\hat{v}_{\boldsymbol{k}',\nu}\boldsymbol{\sigma}_3\hat{H}_{\boldsymbol{k}'}\right)T_{\boldsymbol{k}'}\Phi_{\boldsymbol{k}'}\left(0\right)\Big\rangle.\end{aligned} \tag{S236}$$

Using the identity

$$\begin{aligned}&\left\langle\Phi_{\boldsymbol{k},m}^{\dagger}\left(\tau\right)\Phi_{\boldsymbol{k},n}\left(\tau\right)\Phi_{\boldsymbol{k}',p}^{\dagger}\left(0\right)\Phi_{\boldsymbol{k}',q}\left(0\right)\right\rangle=\left\langle\Phi_{\boldsymbol{k},m}^{\dagger}\left(\tau\right)\Phi_{\boldsymbol{k},n}\left(\tau\right)\right\rangle\left\langle\Phi_{\boldsymbol{k}',p}^{\dagger}\left(0\right)\Phi_{\boldsymbol{k}',q}\left(0\right)\right\rangle\\&+\left\langle\Phi_{\boldsymbol{k},m}^{\dagger}\left(\tau\right)\Phi_{\boldsymbol{k}',p}^{\dagger}\left(0\right)\right\rangle\left\langle\Phi_{\boldsymbol{k},n}\left(\tau\right)\Phi_{\boldsymbol{k}',q}\left(0\right)\right\rangle+\left\langle\Phi_{\boldsymbol{k},m}^{\dagger}\left(\tau\right)\Phi_{\boldsymbol{k}',q}\left(0\right)\right\rangle\left\langle\Phi_{\boldsymbol{k},n}\left(\tau\right)\Phi_{\boldsymbol{k}',p}^{\dagger}\left(0\right)\right\rangle\end{aligned} \tag{S237}$$

the integral $\int_0^{\beta}e^{i\omega\tau}\left\langle\Phi_{\boldsymbol{k},m}^{\dagger}\left(\tau\right)\Phi_{\boldsymbol{k},n}\left(\tau\right)\right\rangle\left\langle\Phi_{\boldsymbol{k}',p}^{\dagger}\left(0\right)\Phi_{\boldsymbol{k}',q}\left(0\right)\right\rangle=0$ because $\omega=\frac{2n\pi}{\beta}$ and

$$\left\langle\Phi_{\boldsymbol{k},m}^{\dagger}\left(\tau\right)\Phi_{\boldsymbol{k}',p}^{\dagger}\left(0\right)\right\rangle=i\delta_{\boldsymbol{k},-\boldsymbol{k}'}\sigma_2^{mp}\rho\left[\left(\boldsymbol{\sigma}_3E_{\boldsymbol{k}}\right)_{mm}\right]e^{\left(\boldsymbol{\sigma}_3E_{\boldsymbol{k}}\right)_{mm}\tau} \tag{S238}$$

$$\left\langle\Phi_{\boldsymbol{k},n}\left(\tau\right)\Phi_{\boldsymbol{k}',q}\left(0\right)\right\rangle=-i\delta_{\boldsymbol{k},-\boldsymbol{k}'}\sigma_2^{nq}\rho\left[-\left(\boldsymbol{\sigma}_3E_{\boldsymbol{k}}\right)_{nn}\right]e^{-\left(\boldsymbol{\sigma}_3E_{\boldsymbol{k}}\right)_{nn}\tau} \tag{S239}$$

$$\left\langle\Phi_{\boldsymbol{k},m}^{\dagger}\left(\tau\right)\Phi_{\boldsymbol{k}',q}\left(0\right)\right\rangle=\delta_{\boldsymbol{k},\boldsymbol{k}'}\sigma_3^{mq}\rho\left[\left(\boldsymbol{\sigma}_3E_{\boldsymbol{k}}\right)_{mm}\right]e^{\left(\boldsymbol{\sigma}_3E_{\boldsymbol{k}}\right)_{mm}\tau} \tag{S240}$$

$$\left\langle\Phi_{\boldsymbol{k},n}\left(\tau\right)\Phi_{\boldsymbol{k}',p}^{\dagger}\left(0\right)\right\rangle=-\delta_{\boldsymbol{k},\boldsymbol{k}'}\sigma_3^{np}\rho\left[\left(-\boldsymbol{\sigma}_3E_{\boldsymbol{k}}\right)_{nn}\right]e^{-\left(\boldsymbol{\sigma}_3E_{\boldsymbol{k}}\right)_{nn}\tau} \tag{S241}$$

where $\rho(x)=\frac{1}{e^{\beta x}-1}$ is the Bose-Einstein distribution with $\beta=k_BT$. We define

$$\boldsymbol{\mathcal{V}}_{\boldsymbol{k}}^{L^{\alpha}}=T_{\boldsymbol{k}}^{\dagger}\left[\hat{L}^{\alpha}\boldsymbol{\sigma}_3\hat{\boldsymbol{v}}_{\boldsymbol{k}}+\hat{\boldsymbol{v}}_{\boldsymbol{k}}\boldsymbol{\sigma}_3\hat{L}^{\alpha}\right]T_{\boldsymbol{k}}, \tag{S242}$$

$$\boldsymbol{\mathcal{V}}_{\boldsymbol{k}}=T_{\boldsymbol{k}}^{\dagger}\hat{\boldsymbol{v}}_{\boldsymbol{k}}T_{\boldsymbol{k}}, \tag{S243}$$

which leads to

$$\begin{aligned}S_{\mu\nu}=\frac{1}{16}\lim_{\omega\to0}\frac{\partial}{\partial\omega}\int_0^{\beta}d\tau e^{i\omega\tau}\sum_{\boldsymbol{k},\boldsymbol{k}'}\left[\boldsymbol{\mathcal{V}}_{\boldsymbol{k},\mu}^{L^{\alpha}}\right]_{mn}\left[E_{\boldsymbol{k}'}\boldsymbol{\sigma}_3\boldsymbol{\mathcal{V}}_{\boldsymbol{k}',\nu}+\boldsymbol{\mathcal{V}}_{\boldsymbol{k}',\nu}\boldsymbol{\sigma}_3E_{\boldsymbol{k}'}\right]_{pq}\left[\sigma_2^{mp}\sigma_2^{nq}\delta_{\boldsymbol{k},-\boldsymbol{k}'}-\sigma_3^{mq}\sigma_3^{np}\delta_{\boldsymbol{k},\boldsymbol{k}'}\right]\\ \times\rho\left[\left(\boldsymbol{\sigma}_3E_{\boldsymbol{k}}\right)_{mm}\right]\rho\left[-\left(\boldsymbol{\sigma}_3E_{\boldsymbol{k}}\right)_{nn}\right]e^{\left[\left(\boldsymbol{\sigma}_3E_{\boldsymbol{k}}\right)_{mm}-\left(\boldsymbol{\sigma}_3E_{\boldsymbol{k}}\right)_{nn}\right]\tau}.\end{aligned} \tag{S244}$$

Using the integral

$$\lim_{\omega\to0}\frac{\partial}{\partial\omega}\int_0^{\beta}d\tau e^{\left[i\omega+\left(\boldsymbol{\sigma}_3E_{\boldsymbol{k}}\right)_{mm}-\left(\boldsymbol{\sigma}_3E_{\boldsymbol{k}}\right)_{nn}\right]\tau}=\lim_{\omega\to0}\frac{\partial}{\partial\omega}\frac{e^{\beta\left(\boldsymbol{\sigma}_3E_{\boldsymbol{k}}\right)_{mm}-\beta\left(\boldsymbol{\sigma}_3E_{\boldsymbol{k}}\right)_{nn}}-1}{i\omega+\left(\boldsymbol{\sigma}_3E_{\boldsymbol{k}}\right)_{mm}-\left(\boldsymbol{\sigma}_3E_{\boldsymbol{k}}\right)_{nn}}=-i\frac{e^{\beta\left(\boldsymbol{\sigma}_3E_{\boldsymbol{k}}\right)_{mm}-\beta\left(\boldsymbol{\sigma}_3E_{\boldsymbol{k}}\right)_{nn}}-1}{\left[\left(\boldsymbol{\sigma}_3E_{\boldsymbol{k}}\right)_{mm}-\left(\boldsymbol{\sigma}_3E_{\boldsymbol{k}}\right)_{nn}\right]^2} \tag{S245}$$

together with

$$\rho(x)-\rho(-y)=-\rho(x)\rho(-y)\left(e^{\beta x-\beta y}-1\right) \tag{S246}$$

one obtains

$$\begin{aligned}S_{\mu\nu}&=\frac{i}{16}\sum_{\boldsymbol{k},\boldsymbol{k}'}\left[\boldsymbol{\mathcal{V}}_{\boldsymbol{k},\mu}^{L^{\alpha}}\right]_{mn}\left[E_{\boldsymbol{k}'}\boldsymbol{\sigma}_3\boldsymbol{\mathcal{V}}_{\boldsymbol{k}',\nu}+\boldsymbol{\mathcal{V}}_{\boldsymbol{k}',\nu}\boldsymbol{\sigma}_3E_{\boldsymbol{k}'}\right]_{pq}\left[\sigma_2^{mp}\sigma_2^{nq}\delta_{\boldsymbol{k},-\boldsymbol{k}'}-\sigma_3^{mq}\sigma_3^{np}\delta_{\boldsymbol{k},\boldsymbol{k}'}\right]\times\\&\times\frac{\rho\left[\left(\boldsymbol{\sigma}_3E_{\boldsymbol{k}}\right)_{mm}\right]-\rho\left[\left(\boldsymbol{\sigma}_3E_{\boldsymbol{k}}\right)_{nn}\right]}{\left[\left(\boldsymbol{\sigma}_3E_{\boldsymbol{k}}\right)_{mm}-\left(\boldsymbol{\sigma}_3E_{\boldsymbol{k}}\right)_{nn}\right]^2}\end{aligned} \tag{S247}$$

$$=-\frac{i}{8}\sum_{\boldsymbol{k}}\left[\boldsymbol{\mathcal{V}}_{\boldsymbol{k},\mu}^{L^{\alpha}}\right]_{mn}\left[\boldsymbol{\sigma}_3\left(T_{\boldsymbol{k}}^{\dagger}\hat{v}_{\boldsymbol{k},\nu}T_{\boldsymbol{k}}\boldsymbol{\sigma}_3E_{\boldsymbol{k}}+E_{\boldsymbol{k}}\boldsymbol{\sigma}_3T_{\boldsymbol{k}}^{\dagger}\hat{v}_{\boldsymbol{k},\nu}T_{\boldsymbol{k}}\right)\boldsymbol{\sigma}_3\right]_{nm}\frac{\rho\left[\left(\boldsymbol{\sigma}_3E_{\boldsymbol{k}}\right)_{mm}\right]-\rho\left[\left(\boldsymbol{\sigma}_3E_{\boldsymbol{k}}\right)_{nn}\right]}{\left[\left(\boldsymbol{\sigma}_3E_{\boldsymbol{k}}\right)_{mm}-\left(\boldsymbol{\sigma}_3E_{\boldsymbol{k}}\right)_{nn}\right]^2} \tag{S248}$$

$$\begin{aligned}&=-\frac{i}{8}\sum_{\boldsymbol{k}}\langle n\left(\boldsymbol{k}\right)|\hat{L}^{\alpha}\boldsymbol{\sigma}_3\hat{v}_{\boldsymbol{k},\mu}+\hat{v}_{\boldsymbol{k},\mu}\boldsymbol{\sigma}_3\hat{L}^{\alpha}|m\left(\boldsymbol{k}\right)\rangle\langle m\left(\boldsymbol{k}\right)|\hat{v}_{\boldsymbol{k},\nu}|n\left(\boldsymbol{k}\right)\rangle\times\\&\times\frac{\left(E_{\boldsymbol{k}}^{nn}\sigma_3^{mm}+E_{\boldsymbol{k}}^{mm}\sigma_3^{nn}\right)\left\{\rho\left[\left(\boldsymbol{\sigma}_3E_{\boldsymbol{k}}\right)_{mm}\right]-\rho\left[\left(\boldsymbol{\sigma}_3E_{\boldsymbol{k}}\right)_{nn}\right]\right\}}{\left[\left(\boldsymbol{\sigma}_3E_{\boldsymbol{k}}\right)_{mm}-\left(\boldsymbol{\sigma}_3E_{\boldsymbol{k}}\right)_{nn}\right]^2}.\end{aligned} \tag{S249}$$

Consequently,

$$S_{\mu\nu} = -\frac{i}{8}\sum_{\boldsymbol{k}}\langle n\left(\boldsymbol{k}\right)|\hat{L}^{\alpha}\boldsymbol{\sigma}_3\hat{v}_{\boldsymbol{k},\mu} + \hat{v}_{\boldsymbol{k},\mu}\boldsymbol{\sigma}_3\hat{L}^{\alpha}|m\left(\boldsymbol{k}\right)\rangle\langle m\left(\boldsymbol{k}\right)|\hat{v}_{\boldsymbol{k},\nu}|n\left(\boldsymbol{k}\right)\rangle\times$$
$$\times\frac{\left(E^{nn}_{\boldsymbol{k}}\sigma_3^{mm} + E^{mm}_{\boldsymbol{k}}\sigma_3^{nn}\right)\left\{\rho\left[\left(\boldsymbol{\sigma}_3E_{\boldsymbol{k}}\right)_{mm}\right] - \rho\left[\left(\boldsymbol{\sigma}_3E_{\boldsymbol{k}}\right)_{nn}\right]\right\}}{\left[\left(\boldsymbol{\sigma}_3E_{\boldsymbol{k}}\right)_{mm} - \left(\boldsymbol{\sigma}_3E_{\boldsymbol{k}}\right)_{nn}\right]^2} \tag{S250}$$

In our next step we are going to evaluate

$$\left\langle J_{\mu}^{\hat{L}^{\alpha}(1)}\right\rangle_{eq} = -M_{\mu\nu}\nabla_{\nu}\chi \tag{S251}$$

by using the Smrcka and Streda method (12, 21, 25), where

$$M_{\mu\nu} = -\frac{1}{8}\sum_{\boldsymbol{k}}\int d\eta\rho\left(\eta\right)Tr\left\{\boldsymbol{\sigma}_3\left[\left(\hat{L}^{\alpha}\boldsymbol{\sigma}_3\hat{v}_{\mu,\boldsymbol{k}} + \hat{v}_{\mu,\boldsymbol{k}}\boldsymbol{\sigma}_3\hat{L}^{\alpha}\right)\hat{r}_{\nu} + \hat{r}_{\nu}\left(\hat{L}^{\alpha}\boldsymbol{\sigma}_3\hat{v}_{\mu,\boldsymbol{k}} + \hat{v}_{\mu,\boldsymbol{k}}\boldsymbol{\sigma}_3\hat{L}^{\alpha}\right)\right]\delta\left(\eta - \boldsymbol{\sigma}_3\hat{H}_{\boldsymbol{k}}\right)\right\}. \tag{S252}$$

We first define

$$\hat{\boldsymbol{w}}_{\boldsymbol{k}} = \hat{L}^{\alpha}\boldsymbol{\sigma}_3\hat{\boldsymbol{v}}_{\boldsymbol{k}}, \qquad \hat{\boldsymbol{u}}_{\boldsymbol{k}} = \hat{\boldsymbol{v}}_{\boldsymbol{k}}\boldsymbol{\sigma}_3\hat{L}^{\alpha}. \tag{S253}$$

For the sake of simplicity, we temporarily omit the notation dependent on the wave vector $\boldsymbol{k}$ and will reintroduce it at the conclusion of our discussion. We introduce

$$A_{\mu\nu} = \frac{i}{2}Tr\left[\boldsymbol{\sigma}_3\hat{w}_{\mu}\frac{dG^{+}}{d\eta}\boldsymbol{\sigma}_3\hat{v}_{\nu}\delta\left(\eta - \boldsymbol{\sigma}_3\hat{H}\right) - \boldsymbol{\sigma}_3\hat{w}_{\mu}\delta\left(\eta - \boldsymbol{\sigma}_3\hat{H}\right)\boldsymbol{\sigma}_3\hat{v}_{\nu}\frac{dG^{-}}{d\eta}\right] \tag{S254}$$

$$B_{\mu\nu} = \frac{i}{2}Tr\left[\boldsymbol{\sigma}_3\hat{w}_{\mu}G^{+}\boldsymbol{\sigma}_3\hat{v}_{\nu}\delta\left(\eta - \boldsymbol{\sigma}_3\hat{H}\right) - \boldsymbol{\sigma}_3\hat{w}_{\mu}\delta\left(\eta - \boldsymbol{\sigma}_3\hat{H}\right)\boldsymbol{\sigma}_3\hat{v}_{\nu}G^{-}\right] \tag{S255}$$

where

$$G^{\pm} = \frac{1}{\eta \pm i\epsilon - \sigma_3\hat{H}} \tag{S256}$$

is the Green's function that satisfies:

$$i\delta\left(\eta - \boldsymbol{\sigma}_3\hat{H}\right) = -\frac{1}{2\pi}\left(G^{+} - G^{-}\right), \qquad \frac{dG^{\pm}}{d\eta} = -\left(G^{\pm}\right)^2, \qquad i\frac{d}{d\eta}\delta\left(\eta - \boldsymbol{\sigma}_3\hat{H}\right) = \frac{1}{2\pi}\left[\left(G^{+}\right)^2 - \left(G^{-}\right)^2\right] \tag{S257}$$

so that one has

$$\frac{dB_{\mu\nu}}{d\eta} = \frac{i}{2}Tr\left[\boldsymbol{\sigma}_3\hat{w}_{\mu}\frac{dG^{+}}{d\eta}\boldsymbol{\sigma}_3\hat{v}_{\nu}\delta\left(\eta - \boldsymbol{\sigma}_3\hat{H}\right) + \boldsymbol{\sigma}_3\hat{w}_{\mu}G^{+}\boldsymbol{\sigma}_3\hat{v}_{\nu}\frac{d\delta\left(\eta - \boldsymbol{\sigma}_3\hat{H}\right)}{d\eta}\right. \tag{S258}$$

$$\left. - \boldsymbol{\sigma}_3\hat{w}_{\mu}\frac{d\delta\left(\eta - \boldsymbol{\sigma}_3\hat{H}\right)}{d\eta}\boldsymbol{\sigma}_3\hat{v}_{\nu}G^{-} - \boldsymbol{\sigma}_3\hat{w}_{\mu}\delta\left(\eta - \boldsymbol{\sigma}_3\hat{H}\right)\boldsymbol{\sigma}_3\hat{v}_{\nu}\frac{dG^{-}}{d\eta}\right]. \tag{S259}$$

Consequently,

$$A_{\mu\nu} - \frac{1}{2}\frac{dB_{\mu\nu}}{d\eta} = \frac{i}{4}Tr\left[\boldsymbol{\sigma}_3\hat{w}_{\mu}\frac{dG^{+}}{d\eta}\boldsymbol{\sigma}_3\hat{v}_{\nu}\delta\left(\eta - \boldsymbol{\sigma}_3\hat{H}\right) - \boldsymbol{\sigma}_3\hat{w}_{\mu}G^{+}\boldsymbol{\sigma}_3\hat{v}_{\nu}\frac{d\delta\left(\eta - \boldsymbol{\sigma}_3\hat{H}\right)}{d\eta}\right.$$
$$\left. + \boldsymbol{\sigma}_3\hat{w}_{\mu}\frac{d\delta\left(\eta - \boldsymbol{\sigma}_3\hat{H}\right)}{d\eta}\boldsymbol{\sigma}_3\hat{v}_{\nu}G^{-} - \boldsymbol{\sigma}_3\hat{w}_{\mu}\delta\left(\eta - \boldsymbol{\sigma}_3\hat{H}\right)\boldsymbol{\sigma}_3\hat{v}_{\nu}\frac{dG^{-}}{d\eta}\right] \tag{S260}$$

$$= \frac{1}{8\pi}Tr\left[\boldsymbol{\sigma}_3\hat{w}_{\mu}\left(G^{+}\right)^2\boldsymbol{\sigma}_3\hat{v}_{\nu}\left(G^{+} - G^{-}\right) - \boldsymbol{\sigma}_3\hat{w}_{\mu}G^{+}\boldsymbol{\sigma}_3\hat{v}_{\nu}\left[\left(G^{+}\right)^2 - \left(G^{-}\right)^2\right]\right.$$
$$\left. + \boldsymbol{\sigma}_3\hat{w}_{\mu}\left[\left(G^{+}\right)^2 - \left(G^{-}\right)^2\right]\boldsymbol{\sigma}_3\hat{v}_{\nu}G^{-} - \boldsymbol{\sigma}_3\hat{w}_{\mu}\left(G^{+} - G^{-}\right)\boldsymbol{\sigma}_3\hat{v}_{\nu}\left(G^{-}\right)^2\right] \tag{S261}$$

$$= \frac{1}{8\pi}Tr\left[\boldsymbol{\sigma}_3\hat{w}_{\mu}\left(G^{+}\right)^2\boldsymbol{\sigma}_3\hat{v}_{\nu}G^{+} + \boldsymbol{\sigma}_3\hat{w}_{\mu}G^{-}\boldsymbol{\sigma}_3\hat{v}_{\nu}\left(G^{-}\right)^2 - \boldsymbol{\sigma}_3\hat{w}_{\mu}G^{+}\boldsymbol{\sigma}_3\hat{v}_{\nu}\left(G^{+}\right)^2 - \boldsymbol{\sigma}_3\hat{w}_{\mu}\left(G^{-}\right)^2\boldsymbol{\sigma}_3\hat{v}_{\nu}G^{-}\right]. \tag{S262}$$

Note that

$$\hat{\boldsymbol{v}} = i\left[\hat{\boldsymbol{r}}, \boldsymbol{\sigma}_3\left(G^{\pm}\right)^{-1}\right], \qquad \hat{\boldsymbol{w}} = i\boldsymbol{\sigma}_3\hat{L}^{\alpha}\left[\hat{\boldsymbol{r}}, \boldsymbol{\sigma}_3\left(G^{\pm}\right)^{-1}\right], \qquad \hat{\boldsymbol{u}} = i\left[\hat{\boldsymbol{r}}, \boldsymbol{\sigma}_3\left(G^{\pm}\right)^{-1}\right]\boldsymbol{\sigma}_3\hat{L}^{\alpha}. \tag{S263}$$

Using those relations, we obtain

$$
\begin{aligned}
&A_{\mu\nu}-\frac{1}{2}\frac{dB_{\mu\nu}}{d\eta}\\
&=\frac{1}{8\pi}Tr\left[\boldsymbol{\sigma}_3\hat{w}_\mu\left(G^+\right)^2\boldsymbol{\sigma}_3\hat{v}_\nu G^+ +\boldsymbol{\sigma}_3\hat{w}_\mu G^-\boldsymbol{\sigma}_3\hat{v}_\nu\left(G^-\right)^2-\boldsymbol{\sigma}_3\hat{w}_\mu G^+\boldsymbol{\sigma}_3\hat{v}_\nu\left(G^+\right)^2-\boldsymbol{\sigma}_3\hat{w}_\mu\left(G^-\right)^2\boldsymbol{\sigma}_3\hat{v}_\nu G^-\right] \qquad \text{[S264]}\\
&=\frac{i}{8\pi}Tr\left\{\boldsymbol{\sigma}_3\hat{w}_\mu\left(G^+\right)^2\left[\left(G^+\right)^{-1}\hat{r}_\nu-\hat{r}_\nu\left(G^+\right)^{-1}\right]G^+ +\boldsymbol{\sigma}_3\hat{w}_\mu G^-\left[\left(G^-\right)^{-1}\hat{r}_\nu-\hat{r}_\nu\left(G^-\right)^{-1}\right]\left(G^-\right)^2\right.\\
&\left.-\boldsymbol{\sigma}_3\hat{w}_\mu G^+\left[\left(G^+\right)^{-1}\hat{r}_\nu-\hat{r}_\nu\left(G^+\right)^{-1}\right]\left(G^+\right)^2-\boldsymbol{\sigma}_3\hat{w}_\mu\left(G^-\right)^2\left[\left(G^-\right)^{-1}\hat{r}_\nu-\hat{r}_\nu\left(G^-\right)^{-1}\right]G^-\right\} \qquad \text{[S265]}
\end{aligned}
$$

where we have used $\boldsymbol{\sigma}_3\boldsymbol{\sigma}_3\equiv\mathcal{I}$, the identity matrix. Finally, we arrive at

$$
\begin{aligned}
&A_{\mu\nu}-\frac{1}{2}\frac{dB_{\mu\nu}}{d\eta}\\
&=\frac{i}{8\pi}Tr\left\{\boldsymbol{\sigma}_3\hat{w}_\mu\left[\left(G^+\right)^2-\left(G^-\right)^2\right]\hat{r}_\nu+\boldsymbol{\sigma}_3\hat{w}_\mu\hat{r}_\nu\left[\left(G^+\right)^2-\left(G^-\right)^2\right]+2\boldsymbol{\sigma}_3\hat{w}_\mu\left[G^-\hat{r}_\nu G^- -G^+\hat{r}_\nu G^+\right]\right\}. \qquad \text{[S266]}
\end{aligned}
$$

Considering the last term, one has

$$
\begin{aligned}
&2\boldsymbol{\sigma}_3\hat{w}_\mu\left[G^-\hat{r}_\nu G^- -G^+\hat{r}_\nu G^+\right]=2\boldsymbol{\sigma}_3 i\boldsymbol{\sigma}_3\hat{L}^\alpha\left[\hat{r}_\mu,\boldsymbol{\sigma}_3\left(G^\pm\right)^{-1}\right]\left[G^-\hat{r}_\nu G^- -G^+\hat{r}_\nu G^+\right] \qquad \text{[S267]}\\
&=2iC_{\hat{H},\hat{L}^\alpha}\hat{r}_\mu\delta\left(\eta-\boldsymbol{\sigma}_3\hat{H}\right)\hat{r}_\nu G^+ +2iC_{\hat{H},\hat{L}^\alpha}\hat{r}_\mu G^-\hat{r}_\nu\delta\left(\eta-\boldsymbol{\sigma}_3\hat{H}\right) \qquad \text{[S268]}
\end{aligned}
$$

where $C_{\hat{H},\hat{L}^\alpha}=\boldsymbol{\sigma}_3\left[\hat{H},\hat{L}^\alpha\boldsymbol{\sigma}_3\right]$. We note that for the models considered in this work both the exchange interaction and the Dzyaloshinskii-Moriya interaction preserve the rotational symmetry about the z-axis. Consequently, $C_{\hat{H},\hat{L}^z}=\boldsymbol{\sigma}_3\left[\hat{H},\hat{L}^z\boldsymbol{\sigma}_3\right]=0$. Generally, this particular term $C_{\hat{H},\hat{L}^\alpha}$ can also be anticipated to be relatively small compared to the other terms in Eq. (S266). For instance, in systems where magnon-phonon coupling is present, $C_{\hat{H},\hat{L}^\alpha}$ scales with the magnon-phonon coupling strength, which tends to be much smaller than the exchange interactions. Hence, it is reasonable to disregard this term in our analysis. Consequently, our final result can be summarized as

$$
A_{\mu\nu}-\frac{1}{2}\frac{dB_{\mu\nu}}{d\eta}=\frac{1}{4}Tr\left[\boldsymbol{\sigma}_3\hat{w}_\mu\frac{d}{d\eta}\delta\left(\eta-\boldsymbol{\sigma}_3\hat{H}\right)\hat{r}_\nu+\boldsymbol{\sigma}_3\hat{w}_\mu\hat{r}_\nu\frac{d}{d\eta}\delta\left(\eta-\boldsymbol{\sigma}_3\hat{H}\right)\right]. \qquad \text{[S269]}
$$

If we replace $\hat{\boldsymbol{w}}$ by $\hat{\boldsymbol{u}}$, we have

$$
\tilde{A}_{\mu\nu}-\frac{1}{2}\frac{d\tilde{B}_{\mu\nu}}{d\eta}=\frac{1}{4}Tr\left[\boldsymbol{\sigma}_3\hat{u}_\mu\frac{d}{d\eta}\delta\left(\eta-\boldsymbol{\sigma}_3\hat{H}\right)\hat{r}_\nu+\boldsymbol{\sigma}_3\hat{u}_\mu\hat{r}_\nu\frac{d}{d\eta}\delta\left(\eta-\boldsymbol{\sigma}_3\hat{H}\right)\right]. \qquad \text{[S270]}
$$

Note that for a bounded spectrum we have $\delta\left[\pm\infty-\left(\boldsymbol{\sigma}_3E\right)_{nn}\right]=0\ \forall\ n$ leading to

$$
\int_{-\infty}^{+\infty}d\eta\left[A_{\mu\nu}\left(\eta\right)-\frac{1}{2}\frac{dB_{\mu\nu}\left(\eta\right)}{d\eta}\right]=0,\qquad\int_{-\infty}^{+\infty}d\eta\left[\tilde{A}_{\mu\nu}\left(\eta\right)-\frac{1}{2}\frac{d\tilde{B}_{\mu\nu}\left(\eta\right)}{d\eta}\right]=0. \qquad \text{[S271]}
$$

Consequently,

$$
M_{\mu\nu}=\frac{1}{2}\sum_{\boldsymbol{k}}\int_{-\infty}^{+\infty}d\eta\rho\left(\eta\right)\int_{-\infty}^{\eta}d\tilde{\eta}\left[A_{\mu\nu}\left(\tilde{\eta}\right)-\frac{1}{2}\frac{dB_{\mu\nu}\left(\tilde{\eta}\right)}{d\tilde{\eta}}+\tilde{A}_{\mu\nu}\left(\tilde{\eta}\right)-\frac{1}{2}\frac{d\tilde{B}_{\mu\nu}\left(\tilde{\eta}\right)}{d\tilde{\eta}}\right]. \qquad \text{[S272]}
$$

Using

$$
\begin{aligned}
A_{\mu\nu}\left(\tilde{\eta}\right)-\frac{1}{2}\frac{dB_{\mu\nu}\left(\tilde{\eta}\right)}{d\eta}=\frac{i}{4}Tr\left[\boldsymbol{\sigma}_3\hat{w}_\mu\frac{dG^+}{d\tilde{\eta}}\boldsymbol{\sigma}_3\hat{v}_\nu\delta\left(\tilde{\eta}-\boldsymbol{\sigma}_3\hat{H}\right)-\boldsymbol{\sigma}_3\hat{w}_\mu G^+\boldsymbol{\sigma}_3\hat{v}_\nu\frac{d\delta\left(\tilde{\eta}-\boldsymbol{\sigma}_3\hat{H}\right)}{d\tilde{\eta}}\right.\\
\left.+\boldsymbol{\sigma}_3\hat{w}_\mu\frac{d\delta\left(\tilde{\eta}-\boldsymbol{\sigma}_3\hat{H}\right)}{d\tilde{\eta}}\boldsymbol{\sigma}_3\hat{v}_\nu G^- -\boldsymbol{\sigma}_3\hat{w}_\mu\delta\left(\tilde{\eta}-\boldsymbol{\sigma}_3\hat{H}\right)\boldsymbol{\sigma}_3\hat{v}_\nu\frac{dG^-}{d\tilde{\eta}}\right] \qquad \text{[S273]}
\end{aligned}
$$

and

$$
\begin{aligned}
\tilde{A}_{\mu\nu}\left(\tilde{\eta}\right)-\frac{1}{2}\frac{d\tilde{B}_{\mu\nu}\left(\tilde{\eta}\right)}{d\tilde{\eta}}=\frac{i}{4}Tr\left[\boldsymbol{\sigma}_3\hat{u}_\mu\frac{dG^+}{d\tilde{\eta}}\boldsymbol{\sigma}_3\hat{v}_\nu\delta\left(\tilde{\eta}-\boldsymbol{\sigma}_3\hat{H}\right)-\boldsymbol{\sigma}_3\hat{u}_\mu G^+\boldsymbol{\sigma}_3\hat{v}_\nu\frac{d\delta\left(\tilde{\eta}-\boldsymbol{\sigma}_3\hat{H}\right)}{d\tilde{\eta}}\right.\\
\left.+\boldsymbol{\sigma}_3\hat{u}_\mu\frac{d\delta\left(\tilde{\eta}-\boldsymbol{\sigma}_3\hat{H}\right)}{d\tilde{\eta}}\boldsymbol{\sigma}_3\hat{v}_\nu G^- -\boldsymbol{\sigma}_3\hat{u}_\mu\delta\left(\tilde{\eta}-\boldsymbol{\sigma}_3\hat{H}\right)\boldsymbol{\sigma}_3\hat{v}_\nu\frac{dG^-}{d\tilde{\eta}}\right] \qquad \text{[S274]}
\end{aligned}
$$

along with relations Eq. (S257) we obtain

$$M_{\mu\nu} = \frac{i}{4}\sum_{\boldsymbol{k}} \sigma_3^{nn}\sigma_3^{mm} \frac{\langle n(\boldsymbol{k})|\hat{w}_{\boldsymbol{k},\mu}+\hat{u}_{\boldsymbol{k},\mu}|m(\boldsymbol{k})\rangle\langle m(\boldsymbol{k})|\hat{v}_\nu|n(\boldsymbol{k})\rangle}{\left[(\boldsymbol{\sigma}_3 E)_{nn}-(\boldsymbol{\sigma}_3 E)_{mm}\right]^2}\int_{(\boldsymbol{\sigma}_3 E)_{nn}}^{(\boldsymbol{\sigma}_3 E)_{mm}} d\eta\rho(\eta)$$
$$+\frac{i}{8}\sum_{\boldsymbol{k}}\Bigg[\langle n(\boldsymbol{k})|\hat{w}_{\boldsymbol{k},\mu}+\hat{u}_{\boldsymbol{k},\mu}|m(\boldsymbol{k})\rangle\langle m(\boldsymbol{k})|\hat{v}_\nu|n(\boldsymbol{k})\rangle\times$$
$$\times\frac{(\sigma_3^{mm}E_{nn}-\sigma_3^{nn}E_{mm})\left\{\rho\left[(\boldsymbol{\sigma}_3 E)_{mm}\right]+\rho\left[(\boldsymbol{\sigma}_3 E)_{nn}\right]\right\}}{\left[(\boldsymbol{\sigma}_3 E)_{nn}-(\boldsymbol{\sigma}_3 E)_{mm}\right]^2}\Bigg]. \quad [S275]$$

Therefore, we have

$$S_{\mu\nu}+M_{\mu\nu} = \frac{i}{4}\sum_{\boldsymbol{k}} \sigma_3^{nn}\sigma_3^{mm} \frac{\langle n(\boldsymbol{k})|\hat{w}_{\boldsymbol{k},\mu}+\hat{u}_{\boldsymbol{k},\mu}|m(\boldsymbol{k})\rangle\langle m(\boldsymbol{k})|\hat{v}_\nu|n(\boldsymbol{k})\rangle}{\left[(\boldsymbol{\sigma}_3 E)_{nn}-(\boldsymbol{\sigma}_3 E)_{mm}\right]^2}\int_{(\boldsymbol{\sigma}_3 E)_{nn}}^{(\boldsymbol{\sigma}_3 E)_{mm}} d\eta\rho(\eta)$$
$$+\frac{i}{4}\sum_{\boldsymbol{k}}\left[\langle n(\boldsymbol{k})|\hat{w}_{\boldsymbol{k},\mu}+\hat{u}_{\boldsymbol{k},\mu}|m(\boldsymbol{k})\rangle\langle m(\boldsymbol{k})|\hat{v}_\nu|n(\boldsymbol{k})\rangle\frac{\sigma_3^{mm}E_{nn}\rho\left[(\boldsymbol{\sigma}_3 E)_{nn}\right]-\sigma_3^{nn}E_{mm}\rho\left[(\boldsymbol{\sigma}_3 E)_{mm}\right]}{\left[(\boldsymbol{\sigma}_3 E)_{mm}-(\boldsymbol{\sigma}_3 E)_{nn}\right]^2}\right] \quad [S276]$$
$$=\frac{i}{4}\sum_{\boldsymbol{k}} \sigma_3^{nn}\sigma_3^{mm} \frac{\langle n(\boldsymbol{k})|\hat{w}_{\boldsymbol{k},\mu}+\hat{u}_{\boldsymbol{k},\mu}|m(\boldsymbol{k})\rangle\langle m(\boldsymbol{k})|\hat{v}_\nu|n(\boldsymbol{k})\rangle}{\left[(\boldsymbol{\sigma}_3 E)_{nn}-(\boldsymbol{\sigma}_3 E)_{mm}\right]^2}\int_{(\boldsymbol{\sigma}_3 E)_{nn}}^{(\boldsymbol{\sigma}_3 E)_{mm}} d\eta\rho(\eta)$$
$$+\frac{i}{4}\sum_{\boldsymbol{k}}\left[\sigma_3^{nn}\sigma_3^{mm}\langle n(\boldsymbol{k})|\hat{w}_{\boldsymbol{k},\mu}+\hat{u}_{\boldsymbol{k},\mu}|m(\boldsymbol{k})\rangle\langle m(\boldsymbol{k})|\hat{v}_\nu|n(\boldsymbol{k})\rangle\frac{\sigma_3^{nn}E_{nn}\rho\left[(\boldsymbol{\sigma}_3 E)_{nn}\right]-\sigma_3^{mm}E_{mm}\rho\left[(\boldsymbol{\sigma}_3 E)_{mm}\right]}{\left[(\boldsymbol{\sigma}_3 E)_{mm}-(\boldsymbol{\sigma}_3 E)_{nn}\right]^2}\right] \quad [S277]$$
$$=\frac{i}{4}\sum_{\boldsymbol{k}} \sigma_3^{nn}\sigma_3^{mm} \frac{\langle n(\boldsymbol{k})|\hat{w}_{\boldsymbol{k},\mu}+\hat{u}_{\boldsymbol{k},\mu}|m(\boldsymbol{k})\rangle\langle m(\boldsymbol{k})|\hat{v}_\nu|n(\boldsymbol{k})\rangle}{\left[(\boldsymbol{\sigma}_3 E)_{nn}-(\boldsymbol{\sigma}_3 E)_{mm}\right]^2}\int_{(\boldsymbol{\sigma}_3 E)_{nn}}^{(\boldsymbol{\sigma}_3 E)_{mm}} d\eta\rho(\eta)$$
$$-\frac{i}{4}\sum_{\boldsymbol{k}}\left[\sigma_3^{nn}\sigma_3^{mm}\frac{\langle n(\boldsymbol{k})|\hat{w}_{\boldsymbol{k},\mu}+\hat{u}_{\boldsymbol{k},\mu}|m(\boldsymbol{k})\rangle\langle m(\boldsymbol{k})|\hat{v}_\nu|n(\boldsymbol{k})\rangle}{\left[(\boldsymbol{\sigma}_3 E)_{mm}-(\boldsymbol{\sigma}_3 E)_{nn}\right]^2}\int_{(\boldsymbol{\sigma}_3 E)_{nn}}^{(\boldsymbol{\sigma}_3 E)_{mm}} d\left[\eta\rho(\eta)\right]\right] \quad [S278]$$
$$=-\frac{i}{4}\sum_{\boldsymbol{k}}\left[\sigma_3^{nn}\sigma_3^{mm}\frac{\langle n(\boldsymbol{k})|\hat{w}_{\boldsymbol{k},\mu}+\hat{u}_{\boldsymbol{k},\mu}|m(\boldsymbol{k})\rangle\langle m(\boldsymbol{k})|\hat{v}_\nu|n(\boldsymbol{k})\rangle}{\left[(\boldsymbol{\sigma}_3 E)_{mm}-(\boldsymbol{\sigma}_3 E)_{nn}\right]^2}\int_{(\boldsymbol{\sigma}_3 E)_{nn}}^{(\boldsymbol{\sigma}_3 E)_{mm}} \eta d\left[\rho(\eta)\right]\right] \quad [S279]$$
$$=\frac{i}{4}\sum_{\boldsymbol{k}}\left[\sigma_3^{nn}\sigma_3^{mm}\frac{\langle n(\boldsymbol{k})|\hat{w}_{\boldsymbol{k},\mu}+\hat{u}_{\boldsymbol{k},\mu}|m(\boldsymbol{k})\rangle\langle m(\boldsymbol{k})|\hat{v}_\nu|n(\boldsymbol{k})\rangle}{\left[(\boldsymbol{\sigma}_3 E)_{mm}-(\boldsymbol{\sigma}_3 E)_{nn}\right]^2}\int_{(\boldsymbol{\sigma}_3 E)_{mm}}^{(\boldsymbol{\sigma}_3 E)_{nn}} \eta d\left[\rho(\eta)\right]\right] \quad [S280]$$

where we have used $d[\eta\rho(\eta)] = \eta d[\rho(\eta)] + d\eta\rho(\eta)$. Finally, by restoring the sum over the repeated Roman indices and the Planck constant $\hbar$ we arrive at the following expression

$$S_{\mu\nu}+M_{\mu\nu} \quad [S281]$$
$$=\frac{i\hbar}{4}\sum_{\boldsymbol{k}}\sum_{m\neq n}\left[\sigma_3^{nn}\sigma_3^{mm}\frac{\left\langle n(\boldsymbol{k})\left|\hat{L}^\alpha\boldsymbol{\sigma}_3\hat{v}_{\boldsymbol{k},\mu}+\hat{v}_{\boldsymbol{k},\mu}\boldsymbol{\sigma}_3\hat{L}^\alpha\right|m(\boldsymbol{k})\right\rangle\langle m(\boldsymbol{k})|\hat{v}_\nu|n(\boldsymbol{k})\rangle}{\left[(\boldsymbol{\sigma}_3 E_{\boldsymbol{k}})_{mm}-(\boldsymbol{\sigma}_3 E_{\boldsymbol{k}})_{nn}\right]^2}\int_{(\boldsymbol{\sigma}_3 E_{\boldsymbol{k}})_{mm}}^{(\boldsymbol{\sigma}_3 E_{\boldsymbol{k}})_{nn}}\eta d\left[\rho(\eta)\right]\right]. \quad [S282]$$

Inserting the $\eta = k_B T\zeta$ and the Orbital angular moment current operator $\hat{j}_\mu^{L^\alpha} = \frac{1}{4}\left(\hat{L}^\alpha\boldsymbol{\sigma}_3\hat{v}_{\boldsymbol{k},\mu}+\hat{v}_{\boldsymbol{k},\mu}\boldsymbol{\sigma}_3\hat{L}^\alpha\right)$, we obtain the Orbital Nernst conductivity $\lambda_{\mu\nu}^{L^\alpha} = \frac{S_{\mu\nu}+M_{\mu\nu}}{VT}$:

$$\lambda_{\mu\nu}^{L^\alpha} = \frac{k_B}{\hbar V}\sum_{\boldsymbol{k}}\sum_{m\neq n}\left[i\hbar^2\sigma_3^{nn}\sigma_3^{mm}\frac{\left\langle n(\boldsymbol{k})\left|\hat{j}_\mu^{L^\alpha}\right|m(\boldsymbol{k})\right\rangle\langle m(\boldsymbol{k})|\hat{v}_\nu|n(\boldsymbol{k})\rangle}{\left[(\boldsymbol{\sigma}_3 E_{\boldsymbol{k}})_{mm}-(\boldsymbol{\sigma}_3 E_{\boldsymbol{k}})_{nn}\right]^2}\int_{(\boldsymbol{\sigma}_3 E)_{mm}}^{(\boldsymbol{\sigma}_3 E)_{nn}}\zeta d\left[\rho(\zeta)\right]\right] \quad [S283]$$
$$=\frac{k_B}{\hbar V}\sum_{\boldsymbol{k}}\sum_{m\neq n} i\hbar^2\sigma_3^{nn}\sigma_3^{mm}\frac{\left\langle n(\boldsymbol{k})\left|\hat{j}_\mu^{L^\alpha}\right|m(\boldsymbol{k})\right\rangle\langle m(\boldsymbol{k})|\hat{v}_\nu|n(\boldsymbol{k})\rangle}{\left[(\boldsymbol{\sigma}_3 E_{\boldsymbol{k}})_{mm}-(\boldsymbol{\sigma}_3 E_{\boldsymbol{k}})_{nn}\right]^2}\left[F(\rho_n)-F(\rho_m)\right] \quad [S284]$$
$$=-\frac{k_B}{\hbar V}\sum_{\boldsymbol{k}}\sum_{m\neq n} 2\hbar^2\sigma_3^{nn}\sigma_3^{mm}Im\left[\frac{\left\langle n(\boldsymbol{k})\left|\hat{j}_\mu^{L^\alpha}\right|m(\boldsymbol{k})\right\rangle\langle m(\boldsymbol{k})|\hat{v}_\nu|n(\boldsymbol{k})\rangle}{\left[(\boldsymbol{\sigma}_3 E_{\boldsymbol{k}})_{mm}-(\boldsymbol{\sigma}_3 E_{\boldsymbol{k}})_{nn}\right]^2}\right]F(\rho_n), \quad [S285]$$

which leads to

$$\lambda_{\mu\nu}^{L^\alpha} = \frac{k_B}{\hbar V}\sum_{\boldsymbol{k}}\sum_n \Omega_{\mu\nu}^{L^\alpha,n}(\boldsymbol{k})F(\rho_n) \equiv \frac{2k_B}{\hbar V}\sum_{\boldsymbol{k}}\sum_{n=1}^{N}\Omega_{\mu\nu}^{L^\alpha,n}(\boldsymbol{k})F(\rho_n) \quad [S286]$$

where $\Omega_{\mu\nu}^{L^\alpha,n}(\boldsymbol{k}) = \sum_{m\neq n}\Omega_{\mu\nu}^{L^\alpha,nm}(\boldsymbol{k})$ is the Orbital Berry curvature of the nth band,

$$\Omega_{\mu\nu}^{L^\alpha,nm}(\boldsymbol{k}) = -2\hbar^2\sigma_3^{nn}\sigma_3^{mm}Im\left[\frac{\left\langle n(\boldsymbol{k})\left|\hat{j}_\mu^{L^\alpha}\right|m(\boldsymbol{k})\right\rangle\left\langle m(\boldsymbol{k})\left|\hat{v}_\nu\right|n(\boldsymbol{k})\right\rangle}{\left[(\boldsymbol{\sigma}_3E_{\boldsymbol{k}})_{mm}-(\boldsymbol{\sigma}_3E_{\boldsymbol{k}})_{nn}\right]^2}\right] \tag{S287}$$

is the projected Orbital Berry curvature of the nth band on the mth band, and

$$F(\rho_n) = (1+\rho_n)\,ln(1+\rho_n) - \rho_n ln(\rho_n), \tag{S288}$$

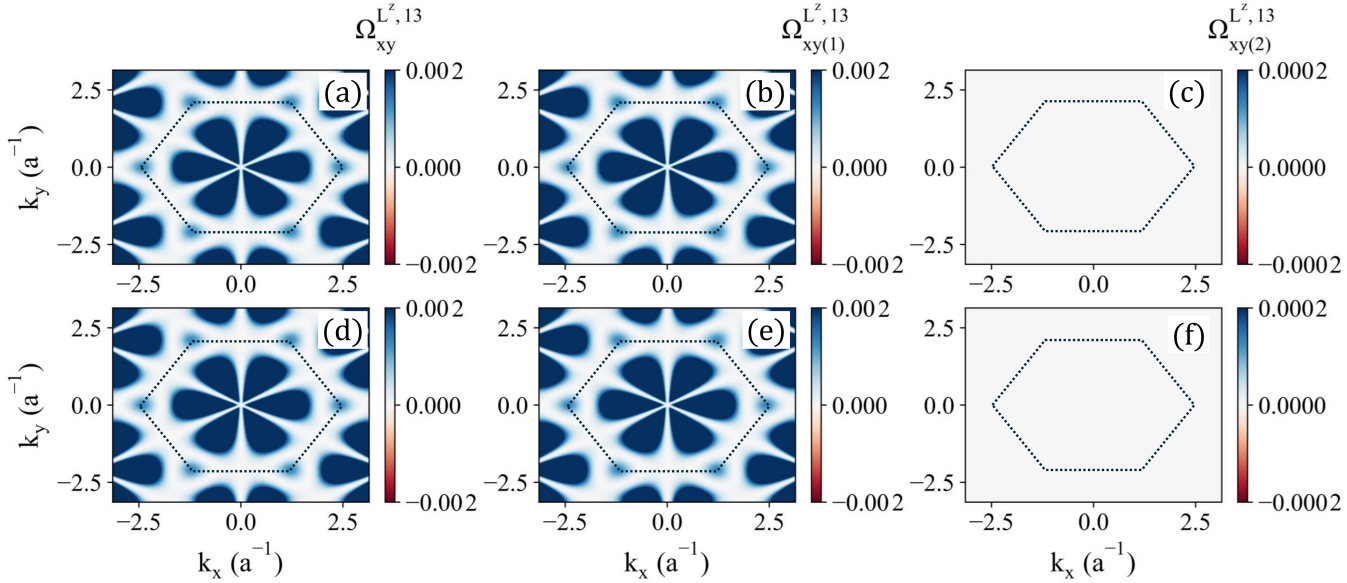

Fig. S6. The projected Orbital Berry curvatures from 1st to 3rd band $\Omega_{xy}^{L^z,13}(\boldsymbol{k})$ (a,d), $\Omega_{xy(1)}^{L^z,13}(\boldsymbol{k})$ (b,e) and $\Omega_{xy(2)}^{L^z,13}(\boldsymbol{k})$ (c,f) for $MnPS_3$ as a function of in-plane wave vector (k_x, k_y) without (a-c) and with (d-f) the DMI. These calculations were performed with the externally applied magnetic field $B_z = 1\,T$.

Overall, the Orbital transverse current of quasiparticle transport underlying the Orbital Nernst effect is computed as:

$$j_\mu^{L^\alpha} = -\lambda_{\mu\nu}^{L^\alpha}\partial_\nu T \tag{S289}$$

In Fig. S5, we present the computed orbital Nernst conductivity (ONC) of $MnPS_3$ [Fig. S5(a)] and NiPSe3 [Fig. S5(b)] as functions of the external magnetic field B_z, computed at a constant temperature of 100 K. We observe that the ONC behaves as an even function of B_z for both Néel and Zigzag orders. Importantly, the ONC remains finite even without an applied magnetic field, allowing for the probing of this effect in the absence of an external field. Moreover, the ONC for both Néel and Zigzag orders exhibits only a slight dependence on the out-of-plane magnetic field B_z. This minimal impact results from the magnetic field causing a splitting in the magnon bands corresponding to opposite spins, without inducing any coupling between these distinct bands. Consequently, the weak response of the ONC to the magnetic field B_z arises solely from changes in the magnon population ρ_n and hence the function $F(\rho_n)$ in Eq. (S286), which are due to the shift in the magnon energy band caused by the Zeeman interaction between local spins and external applied magnetic field akin to the behavior of electric polarization under the applied magnetic field as discussed in the main text.

C. Orbital Berry curvature. It is worth emphasizing that our linear response theory, as presented here, and our utilization of the Orbital angular moment representation within the Bloch states enable us to treat the intra-band and inter-band orbital angular moment contributions to the orbital Nernst effect equally. In this section, we will distinguish between these two contributions and derive the expression for the topological thermal magnon contribution to the ONE, as utilized in the main text. We begin with the projected Orbital Berry curvature given by:

$$\Omega_{\mu\nu}^{L^\alpha,nm}(\boldsymbol{k}) = -\frac{1}{2}\hbar^2\sigma_3^{nn}\sigma_3^{mm}Im\left[\frac{\left\langle n(\boldsymbol{k})\left|\hat{L}^\alpha\boldsymbol{\sigma}_3\hat{v}_\mu+\hat{v}_\mu\boldsymbol{\sigma}_3\hat{L}^\alpha\right|m(\boldsymbol{k})\right\rangle\left\langle m(\boldsymbol{k})\left|\hat{v}_\nu\right|n(\boldsymbol{k})\right\rangle}{\left[(\boldsymbol{\sigma}_3E_{\boldsymbol{k}})_{mm}-(\boldsymbol{\sigma}_3E_{\boldsymbol{k}})_{nn}\right]^2}\right]. \tag{S290}$$

Using the completeness relation

$$\sum_l \sigma_3^{ll}\left|l(\boldsymbol{k})\right\rangle\left\langle l(\boldsymbol{k})\right|\boldsymbol{\sigma}_3 = \mathcal{I} \tag{S291}$$

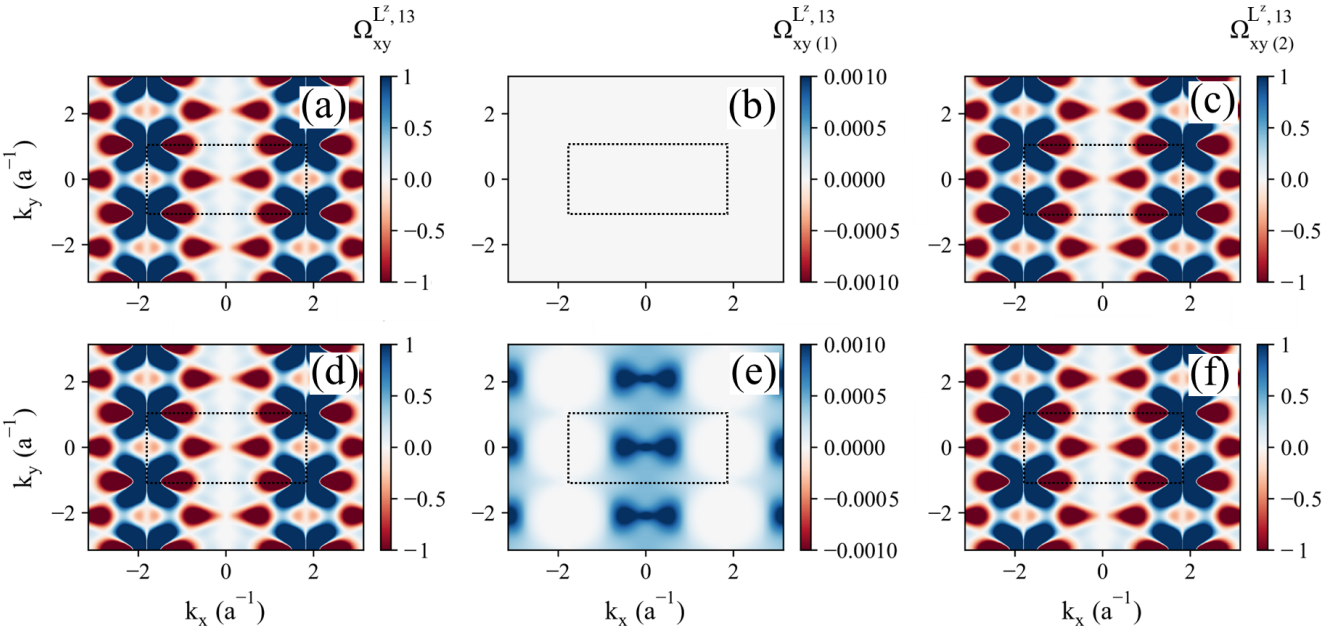

Fig. S7. The projected Orbital Berry curvatures from 1st to 3rd band $\Omega^{L^z,13}_{xy}(\boldsymbol{k})$ (a,d), $\Omega^{L^z,13}_{xy(1)}(\boldsymbol{k})$ (b,e) and $\Omega^{L^z,13}_{xy(2)}(\boldsymbol{k})$ (c,f) for $NiPSe_3$ as a function of in-plane wave vector (k_x, k_y) without (a-c) and with (d-f) the DMI. These calculations were performed with the externally applied magnetic field $B_z = 1\,T$.

we have

$$\langle n(\boldsymbol{k})|\left(\hat{L}^{\alpha}\boldsymbol{\sigma}_3\hat{v}_{\mu}+\hat{v}_{\mu}\boldsymbol{\sigma}_3\hat{L}^{\alpha}\right)|m(\boldsymbol{k})\rangle \tag{S292}$$

$$=\langle n(\boldsymbol{k})|\left(\hat{L}^{\alpha}\sum_{l}\sigma_3^{ll}\,|l\,(\boldsymbol{k})\rangle\,\langle l\,(\boldsymbol{k})|\,\boldsymbol{\sigma}_3\boldsymbol{\sigma}_3\hat{v}_{\mu}+\hat{v}_{\mu}\sum_{q}\sigma_3^{qq}\,|q\,(\boldsymbol{k})\rangle\,\langle q\,(\boldsymbol{k})|\,\boldsymbol{\sigma}_3\boldsymbol{\sigma}_3\hat{L}^{\alpha}\right)|m(\boldsymbol{k})\rangle \tag{S293}$$

$$=\langle n(\boldsymbol{k})|\left(\hat{L}^{\alpha}\sum_{l}\sigma_3^{ll}\,|l\,(\boldsymbol{k})\rangle\,\langle l\,(\boldsymbol{k})|\,\hat{v}_{\mu}+\hat{v}_{\mu}\sum_{q}\sigma_3^{qq}\,|q\,(\boldsymbol{k})\rangle\,\langle q\,(\boldsymbol{k})|\,\hat{L}^{\alpha}\right)|m(\boldsymbol{k})\rangle \tag{S294}$$

$$=\sum_{l}\sigma_3^{ll}\langle n(\boldsymbol{k})|\hat{L}^{\alpha}\,|l\,(\boldsymbol{k})\rangle\,\langle l\,(\boldsymbol{k})|\,\hat{v}_{\mu}|m(\boldsymbol{k})\rangle+\sum_{q}\sigma_3^{qq}\langle n(\boldsymbol{k})|\hat{v}_{\mu}\,|q\,(\boldsymbol{k})\rangle\,\langle q\,(\boldsymbol{k})|\,\hat{L}^{\alpha}|m(\boldsymbol{k})\rangle \tag{S295}$$

$$=[\sigma_3^{nn}L^{\alpha}_{nn}\,(\boldsymbol{k})+\sigma_3^{mm}L^{\alpha}_{mm}\,(\boldsymbol{k})]\,\langle n(\boldsymbol{k})|\hat{v}_{\mu}\,|m\,(\boldsymbol{k})\rangle+\sum_{l\neq n}\sigma_3^{ll}\langle n(\boldsymbol{k})|\hat{L}^{\alpha}\,|l\,(\boldsymbol{k})\rangle\,\langle l\,(\boldsymbol{k})|\,\hat{v}_{\mu}|m(\boldsymbol{k})\rangle \tag{S296}$$

$$+\sum_{q\neq m}\sigma_3^{qq}\langle n(\boldsymbol{k})|\hat{v}_{\mu}\,|q\,(\boldsymbol{k})\rangle\,\langle q\,(\boldsymbol{k})|\,\hat{L}^{\alpha}|m(\boldsymbol{k})\rangle, \tag{S297}$$

which leads to

$$\Omega^{L^{\alpha},nm}_{\mu\nu}\,(\boldsymbol{k})=-\frac{1}{2}\hbar^2\sigma_3^{nn}\sigma_3^{mm}Im\left\{\sum_{l}\frac{\left[\sigma_3^{ll}\langle n(\boldsymbol{k})|\hat{L}^{\alpha}\,|l\,(\boldsymbol{k})\rangle\,\langle l\,(\boldsymbol{k})|\,\hat{v}_{\mu}|m(\boldsymbol{k})\rangle\right]\,\langle m(\boldsymbol{k})|\hat{v}_{\nu}|n(\boldsymbol{k})\rangle}{\left[\sigma_3^{nn}\,(E_{\boldsymbol{k}})_{nn}-\sigma_3^{mm}\,(E_{\boldsymbol{k}})_{mm}\right]^2}\right\} \tag{S298}$$

$$-\frac{1}{2}\hbar^2\sigma_3^{nn}\sigma_3^{mm}Im\left\{\sum_{q}\frac{\left[\sigma_3^{qq}\langle n(\boldsymbol{k})|\hat{v}_{\mu}\,|q\,(\boldsymbol{k})\rangle\,\langle q\,(\boldsymbol{k})|\,\hat{L}^{\alpha}|m(\boldsymbol{k})\rangle\right]\,\langle m(\boldsymbol{k})|\hat{v}_{\nu}|n(\boldsymbol{k})\rangle}{\left[\sigma_3^{nn}\,(E_{\boldsymbol{k}})_{nn}-\sigma_3^{mm}\,(E_{\boldsymbol{k}})_{mm}\right]^2}\right\} \tag{S299}$$

$$=-\frac{1}{2}\hbar^2\sigma_3^{nn}\sigma_3^{mm}\left[\sigma_3^{nn}L^{\alpha}_{nn}\,(\boldsymbol{k})+\sigma_3^{mm}L^{\alpha}_{mm}\,(\boldsymbol{k})\right]Im\left\{\frac{\langle n\,(\boldsymbol{k})|\,\hat{v}_{\mu}|m(\boldsymbol{k})\langle m(\boldsymbol{k})|\hat{v}_{\nu}|n(\boldsymbol{k})\rangle}{\left[\sigma_3^{nn}\,(E_{\boldsymbol{k}})_{nn}-\sigma_3^{mm}\,(E_{\boldsymbol{k}})_{mm}\right]^2}\right\} \tag{S300}$$

$$-\frac{1}{2}\hbar^2\sigma_3^{nn}\sigma_3^{mm}Im\left\{\sum_{l\neq n}\frac{\left[\sigma_3^{ll}\langle n(\boldsymbol{k})|\hat{L}^{\alpha}\,|l\,(\boldsymbol{k})\rangle\,\langle l\,(\boldsymbol{k})|\,\hat{v}_{\mu}|m(\boldsymbol{k})\rangle\right]\,\langle m(\boldsymbol{k})|\hat{v}_{\nu}|n(\boldsymbol{k})\rangle}{\left[\sigma_3^{nn}\,(E_{\boldsymbol{k}})_{nn}-\sigma_3^{mm}\,(E_{\boldsymbol{k}})_{mm}\right]^2}\right\} \tag{S301}$$

$$-\frac{1}{2}\hbar^2\sigma_3^{nn}\sigma_3^{mm}Im\left\{\sum_{q\neq m}\frac{\left[\sigma_3^{qq}\langle n(\boldsymbol{k})|\hat{v}_{\mu}\,|q\,(\boldsymbol{k})\rangle\,\langle q\,(\boldsymbol{k})|\,\hat{L}^{\alpha}|m(\boldsymbol{k})\rangle\right]\,\langle m(\boldsymbol{k})|\hat{v}_{\nu}|n(\boldsymbol{k})\rangle}{\left[\sigma_3^{nn}\,(E_{\boldsymbol{k}})_{nn}-\sigma_3^{mm}\,(E_{\boldsymbol{k}})_{mm}\right]^2}\right\} \tag{S302}$$

$$=\Omega^{L^{\alpha},nm}_{\mu\nu(1)}\,(\boldsymbol{k})+\Omega^{L^{\alpha},nm}_{\mu\nu(2)}\,(\boldsymbol{k}) \tag{S303}$$

where

$$\Omega_{\mu\nu(1)}^{L^{\alpha},nm}\left(\boldsymbol{k}\right)=-\frac{1}{2}\hbar^{2}\sigma_{3}^{nn}\sigma_{3}^{mm}\left[\sigma_{3}^{nn}L_{nn}^{\alpha}\left(\boldsymbol{k}\right)+\sigma_{3}^{mm}L_{mm}^{\alpha}\left(\boldsymbol{k}\right)\right]Im\left\{\frac{\langle n\left(\boldsymbol{k}\right)|\,\hat{v}_{\mu}|m(\boldsymbol{k})\langle m(\boldsymbol{k})|\hat{v}_{\nu}|n(\boldsymbol{k})\rangle}{\left[\sigma_{3}^{nn}\left(E_{\boldsymbol{k}}\right)_{nn}-\sigma_{3}^{mm}\left(E_{\boldsymbol{k}}\right)_{mm}\right]^{2}}\right\} \tag{S304}$$

and

$$\Omega_{\mu\nu(2)}^{L^{\alpha},nm}\left(\boldsymbol{k}\right)=-\frac{1}{2}\hbar^{2}\sigma_{3}^{nn}\sigma_{3}^{mm}Im\left\{\sum_{l\neq n}\frac{\left[\sigma_{3}^{ll}\langle n(\boldsymbol{k})|\hat{L}^{\alpha}\,|l\left(\boldsymbol{k}\right)\rangle\,\langle l\left(\boldsymbol{k}\right)|\,\hat{v}_{\mu}|m(\boldsymbol{k})\rangle\right]\,\langle m(\boldsymbol{k})|\hat{v}_{\nu}|n(\boldsymbol{k})\rangle}{\left[\sigma_{3}^{nn}\left(E_{\boldsymbol{k}}\right)_{nn}-\sigma_{3}^{mm}\left(E_{\boldsymbol{k}}\right)_{mm}\right]^{2}}\right\} \tag{S305}$$

$$-\frac{1}{2}\hbar^{2}\sigma_{3}^{nn}\sigma_{3}^{mm}Im\left\{\sum_{q\neq m}\frac{\left[\sigma_{3}^{qq}\langle n(\boldsymbol{k})|\hat{v}_{\mu}\,|q\left(\boldsymbol{k}\right)\rangle\,\langle q\left(\boldsymbol{k}\right)|\,\hat{L}^{\alpha}|m(\boldsymbol{k})\rangle\right]\,\langle m(\boldsymbol{k})|\hat{v}_{\nu}|n(\boldsymbol{k})\rangle}{\left[\sigma_{3}^{nn}\left(E_{\boldsymbol{k}}\right)_{nn}-\sigma_{3}^{mm}\left(E_{\boldsymbol{k}}\right)_{mm}\right]^{2}}\right\}. \tag{S306}$$

Notice that

$$-2\hbar^{2}\sigma_{3}^{nn}\sigma_{3}^{mm}Im\left\{\frac{\langle n\left(\boldsymbol{k}\right)|\,\hat{v}_{\mu}|m(\boldsymbol{k})\langle m(\boldsymbol{k})|\hat{v}_{\nu}|n(\boldsymbol{k})\rangle}{\left[\sigma_{3}^{nn}\left(E_{\boldsymbol{k}}\right)_{nn}-\sigma_{3}^{mm}\left(E_{\boldsymbol{k}}\right)_{mm}\right]^{2}}\right\}\equiv\Omega_{\mu\nu}^{nm}\left(\boldsymbol{k}\right) \tag{S307}$$

is the projected Berry curvature of the nth band on the mth band as defined in Equation (6) in the main text. We can then rewrite the first term as

$$\Omega_{\mu\nu(1)}^{L^{\alpha},nm}\left(\boldsymbol{k}\right)=\frac{1}{4}\left[\sigma_{3}^{nn}L_{nn}^{\alpha}\left(\boldsymbol{k}\right)+\sigma_{3}^{mm}L_{mm}^{\alpha}\left(\boldsymbol{k}\right)\right]\Omega_{\mu\nu}^{nm}\left(\boldsymbol{k}\right), \tag{S308}$$

which leads to

$$\Omega_{\mu\nu(1)}^{L^{\alpha},n}\left(\boldsymbol{k}\right)=\sum_{m\neq n}\Omega_{\mu\nu(1)}^{L^{\alpha},nm}\left(\boldsymbol{k}\right)=\sum_{m\neq n}\frac{1}{4}\left[\sigma_{3}^{nn}L_{nn}^{\alpha}\left(\boldsymbol{k}\right)+\sigma_{3}^{mm}L_{mm}^{\alpha}\left(\boldsymbol{k}\right)\right]\Omega_{\mu\nu}^{nm}\left(\boldsymbol{k}\right). \tag{S309}$$

Consequently, the magnon orbital Nernst conductivity arising from the $\Omega_{\mu\nu(1)}^{L^{\alpha},n}\left(\boldsymbol{k}\right)$ is

$$\lambda_{\mu\nu(1)}^{L^{\alpha}}=\frac{2k_{B}}{\hbar V}\sum_{k}\sum_{n=1}^{N}\Omega_{\mu\nu(1)}^{L^{\alpha},n}\left(\boldsymbol{k}\right)F(\rho_{n})=\frac{k_{B}}{2\hbar V}\sum_{k}\sum_{n=1}^{N}\sum_{m\neq n}\left[\sigma_{3}^{nn}L_{nn}^{\alpha}\left(\boldsymbol{k}\right)+\sigma_{3}^{mm}L_{mm}^{\alpha}\left(\boldsymbol{k}\right)\right]\Omega_{\mu\nu}^{nm}\left(\boldsymbol{k}\right)F(\rho_{n}). \tag{S310}$$

Notably, the expression of $\Omega_{\mu\nu(1)}^{L^{\alpha},n}\left(\boldsymbol{k}\right)$ represents the product of intra-band magnon orbital angular moment and Berry curvature. Consequently, Eq. (S310) underscores the role of topological thermal magnon bands in inducing the Orbital Nernst effect, specifically via the intra-band magnon OAM. On the other hand, the second term $\Omega_{\mu\nu(2)}^{L^{\alpha},nm}\left(\boldsymbol{k}\right)$ captures the magnon Orbital Nernst effect arising from inter-band magnon orbital angular moment.

We observe that both $\Omega_{\mu\nu(1)}^{L^{\alpha},nm}\left(\boldsymbol{k}\right)$ and $\Omega_{\mu\nu(2)}^{L^{\alpha},nm}\left(\boldsymbol{k}\right)$ depend on the inter-band current density and the energy spacing between two subbands. Because there is no coupling between the two magnons with opposite spin in the systems we consider here, the inter-band current between two-subbands with opposite spin vanishes. Consequently, only the projected orbital Berry curvatures between bands of the same spin remains finite, originating in non-zero interband transitions that adhere to the spin selection rules. Thus, the magnon orbital Nernst conductivities are predominantly influenced by the interband transitions between two magnon subbands with the same spin. This accounts for the weak dependence of the magnon ONCs on the externally applied magnetic field B_z for both $MnPS_3$ and $NiPSe_3$, as shown in Fig. S5: the changing magnetic field does not affect the magnon wavefunction or change the energy spacing between two subbands of the same spin.

In Figs. S6 and S7 we plot the projected Orbital Berry curvatures of the 1st magnon subband onto the 3rd magnon subband with the same spin up: $\Omega_{xy}^{L^{z},13}\left(\boldsymbol{k}\right)$ (a,d), $\Omega_{xy(1)}^{L^{z},13}\left(\boldsymbol{k}\right)$ (b,e) and $\Omega_{xy(2)}^{L^{z},13}\left(\boldsymbol{k}\right)$ (c,f) for, respectively, $MnPS_3$ (Fig. S6) and $NiPSe_3$ (Fig. S7) as a function of the in-plane wave vector (k_x, k_y) without (a-c) and with (d-f) the DMI. As shown in Fig. S6, the Orbital Berry curvature of $MnPS_3$ is primarily determined by the topological properties of the magnon bands through the first term $\Omega_{xy(1)}^{L^{z},13}\left(\boldsymbol{k}\right)$ because the second term $\Omega_{xy(2)}^{L^{z},13}\left(\boldsymbol{k}\right)$ vanishes regardless of the presence of DMI. As discussed in the main text, due to the symmetry of the Néel order, this first term $\Omega_{xy(1)}^{L^{z},13}\left(\boldsymbol{k}\right)$ remains finite even without DMI because both Berry curvature and the intra-band orbital angular moment of the Néel phase are finite regardless of the DMI. Additionally, because the wavefunction is unaffected by DMI, the projected orbital Berry curvature $\Omega_{xy(1)}^{L^{z},13}\left(\boldsymbol{k}\right)$ and hence $\Omega_{xy}^{L^{z},13}\left(\boldsymbol{k}\right)$ remains unchanged for $MnPS_3$ when DMI is turned off. Consequently, the orbital Nernst conductivity of $MnPS_3$ exhibits an extremely weak dependence on DMI, as shown in Fig. S8(a). The relative difference between the black and pink curves shown in the inset of Fig. S8(a) arises solely from changes in the function $F\left(\rho_n\right)$ in Eq. (S310) due to the shift in magnon dispersion under the DMI. Since the DMI in $MnPS_3$ is very weak (see Table S1), the resulting difference is negligibly small. This is evident in the inset of Fig. S8(a) where the relative difference between the black and pink curves is on the order of 10^{-7}.

In contrast, for $NiPSe_3$ in the absence of the DMI the projected Orbital Berry curvatures $\Omega_{xy(1)}^{L^{z},13}\left(\boldsymbol{k}\right)$ vanish simply because of the vanishing intra-band OAM of the magnon in the 2D honeycomb AFM with Zigzag order, as discussed previously. Therefore the projected Berry curvatures $\Omega_{xy}^{L^{z},13}\left(\boldsymbol{k}\right)$ are primarily determined by the $\Omega_{xy(2)}^{L^{z},13}\left(\boldsymbol{k}\right)$. When the DMI is present, the $\Omega_{xy(1)}^{L^{z},13}\left(\boldsymbol{k}\right)$

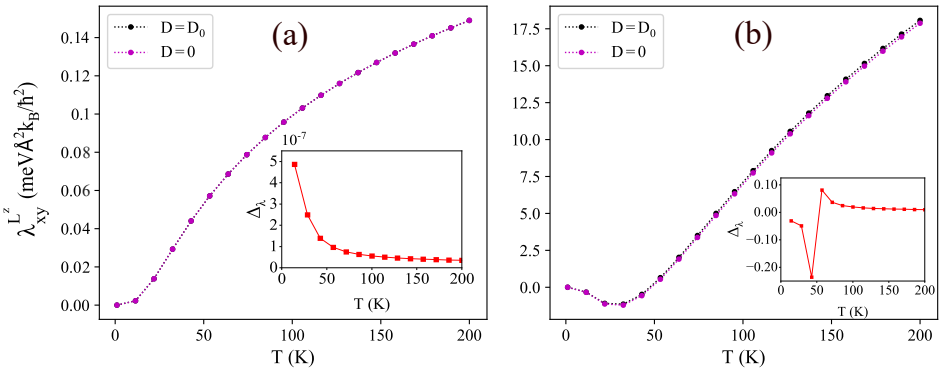

Fig. S8. The orbital Nernst conductivity of $MnPS_3$ (a) and $NiPSe_3$ (b) as a function of temperature at fixed applied magnetic field $B_z = 1\ T$. The black and pink colors indicate the results calculated with and without DMI, respectively. The insets show the relative difference between the black and pink data points, defined as $\Delta_\lambda = \frac{\lambda^{L_z}_{xy}(D=D_0) - \lambda^{L_z}_{xy}(D=0)}{\lambda^{L_z}_{xy}(D=D_0)}$ plotted as a function of temperature. The results indicate a negligible difference for $MnPS_3$, while in $NiPSe_3$, the ONC exhibits a weak dependence on DMI.

becomes finite while the $\Omega^{L^z,13}_{xy(2)}(\boldsymbol{k})$ remains unchanged. However, the magnitude of $\Omega^{L^z,13}_{xy(1)}(\boldsymbol{k})$ is approximately three orders smaller than that of $\Omega^{L^z,13}_{xy(2)}(\boldsymbol{k})$, highlighting that the inter-band magnon OAM is the primary contributor to the magnon Orbital Nernst effect. This observation also clarifies why the magnon orbital Nernst conductivity shows a weak dependence on DMI, which is due to the combined effects of changes in the function $F(\rho_n)$ caused by the shift in magnon dispersion and the finiteness of $\Omega^{L^z,13}_{xy(1)}(\boldsymbol{k})$ under the DMI, as shown in Fig. S8(b).

We conclude this section by illustrating the dependence of the orbital Nernst conductivity of both $MnPS_3$ and $NiPSe_3$ on DMI strength, parameterized by the ratio D/D_0 in Fig. S9.

S5. Symmetry and magnon spin current

We now analyze symmetry constraints on the magnon spin current in the 2D collinear honeycomb AFMs considered in this work. Specifically, we consider the $\mathcal{C}_S\mathcal{M}_x\mathcal{T}_a$ symmetry operation discussed in the main text. The total transverse spin current carried by a magnon along the y-direction under the applied temperature gradient along the x-direction is given by

$$j_y^{S^z} = j_y^{S^z\uparrow} - j_y^{S^z\downarrow} = -\lambda^{S^z}_{xy}\partial_x T \tag{S311}$$

where $\lambda^{S^z}_{xy}$ is the magon spin conductivity.

Under the $\mathcal{C}_S\mathcal{M}_x\mathcal{T}_a$ symmetry operation, the temperature gradient changes only its sign:

$$[\mathcal{C}_S\mathcal{M}_x\mathcal{T}_a]\,\partial_x T = -\partial_x T \tag{S312}$$

while the magnon spin up and down current remain unchanged:

$$[\mathcal{C}_S\mathcal{M}_x\mathcal{T}_a]\, j_y^{S^z\uparrow} \to j_y^{S^z\uparrow} \tag{S313}$$

$$[\mathcal{C}_S\mathcal{M}_x\mathcal{T}_a]\, j_y^{S^z\downarrow} \to j_y^{S^z\downarrow} \tag{S314}$$

which leads to

$$[\mathcal{C}_S\mathcal{M}_x\mathcal{T}_a]\, j_y^{S^z} = [\mathcal{C}_S\mathcal{M}_x\mathcal{T}_a]\, j_y^{S^z\uparrow} - [\mathcal{C}_S\mathcal{M}_x\mathcal{T}_a]\, j_y^{S^z\downarrow} = j_y^{S^z\uparrow} - j_y^{S^z\downarrow} = j_y^{S^z}. \tag{S315}$$

Because the 2D honecomb AFMs with Néel and Zigzag order both preserve $\mathcal{C}_S\mathcal{M}_x\mathcal{T}_a$ symmetry in the absence of DMI, the magnon spin conductivity is unchanged under this operation. Combining Eq. (S311), Eq. (S312) and Eq. (S315), one obtains

$$-\lambda^{S^z}_{xy}\partial_x T = \lambda^{S^z}_{xy}\partial_x T. \tag{S316}$$

Consequently, the magnon spin conductivity must vanish, i.e. $\lambda^{S^z}_{xy} = 0$, under the $\mathcal{C}_S\mathcal{M}_x\mathcal{T}_a$ symmetry constraint because $\partial_x T$ is finite. In other words, there is no transverse spin polarized current carried by magnons in the 2D honeycomb AFMs considered in this work in the absence of DMI regardless of the externally applied magnetic field.

We note that the orbital current remains finite regardless of DMI as discussed in the main text. This suggests that the orbital Nernst effect of magnons is a more universal phenomenon than the magnon spin Nernst effect. Furthermore, a finite transverse spin current carried by magnons under a temperature gradient in the 2D honeycomb antiferromagnets considered here must be identical to the spin current resulting from the spin Nernst effect. This finite spin current arises due to the broken $\mathcal{C}_S\mathcal{M}_x\mathcal{T}_a$ symmetry discussed above, caused by interactions such as the Dzyaloshinskii-Moriya interaction or magnon-phonon coupling that resemble spin-orbit coupling (SOC) in that they couple the spin and orbital angular moment of magnons. In this context, the magnon spin current resulting from the SNE may be viewed as a conversion of orbital current into spin current.

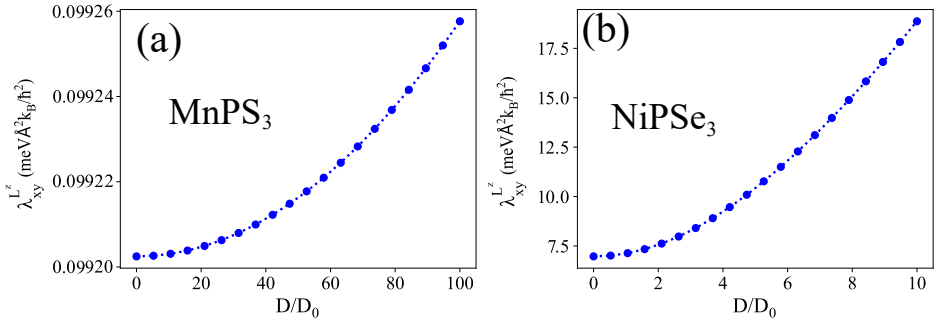

Fig. S9. The ONC of $MnPS_3$ (Figure a) and $NiPSe_3$ (Figure b) varies as a function of the Dzyaloshinskii-Moriya interaction strength, parameterized by the ratio D/D_0. Here D_0 represents the baseline DMI strength for each material. These calculations were conducted under a constant applied magnetic field of $B_z = 1\ T$ and temperature of 100 K.

S6. Spin, Orbital and local charge polarization accumulations induced by the magnon Nernst effects

The magnon Nernst effects lead to the accumulation of orbital, spin moments and local charge polarization at the boundaries of finite systems. In this section, we present the formalism for calculating these accumulations at the system's edges, resulting from the magnon Nernst effects, without delving into detailed computations for specific systems, as that is beyond the scope of this work. To achieve this, we assume the system is periodic along the direction of the temperature gradient but finite in the perpendicular direction to ∇T. The accumulation of magnon spin and orbital moments under an applied temperature gradient can be attributed to two distinct contributions: intrinsic and extrinsic.

A. Intrinsic Contribution: Kubo Formula. First, we focus on the intrinsic contributions to the spin and orbital density which reads

$$\langle \delta \mathcal{M}^{\alpha}(\boldsymbol{r}) \rangle^{in} = \langle \mathcal{M}^{\alpha}(\boldsymbol{r}) \rangle^{in}_{neq} - \langle \mathcal{M}^{\alpha}(\boldsymbol{r}) \rangle^{in}_{eq} \tag{S317}$$

Using the Kubo formula, we derive these intrinsic contributions to the spin and orbital densities as follows:

$$\langle \delta \mathcal{M}^{\alpha}(\boldsymbol{r}) \rangle^{in} = -\lim_{\omega \to 0} \frac{\partial}{\partial \omega} \int_0^{\beta} d\tau e^{i\omega\tau} \left\langle T_{\tau} \mathcal{M}^{\alpha}(\boldsymbol{r}, \tau) J^{Q}_{\nu}(0) \right\rangle \nabla_{\nu} \chi \tag{S318}$$

where $\mathcal{M}^{\alpha}(\boldsymbol{r}) \equiv S^{\alpha}(\boldsymbol{r}), L^{\alpha}(\boldsymbol{r}), p^{\alpha}(\boldsymbol{r})$ which are the α-component of spin, orbital angular moment and local charge polarization of magnon wavepacket at position $\boldsymbol{r}$ respectively. For the finite size, $\boldsymbol{r}$ will become the index r for the unit cells along this dimension which is denoted by y-direction in our consideration. By using the Fourier transformation, one obtains:

$$\mathcal{M}^{\alpha}(\boldsymbol{r}) = \frac{1}{2} \sum_{\boldsymbol{k}} \Psi^{\dagger}_{\boldsymbol{k}} M^{\alpha}_{r} \Psi_{\boldsymbol{k}} \tag{S319}$$

$$\boldsymbol{J}^{Q} = \frac{1}{4} \int d\boldsymbol{r} \Psi^{\dagger}_{\boldsymbol{k}} \left(\hat{H}_{\boldsymbol{k}} \boldsymbol{\sigma}_3 \hat{v}_{\boldsymbol{k}} + \hat{v}_{\boldsymbol{k}} \boldsymbol{\sigma}_3 \hat{H}_{\boldsymbol{k}} \right) \Psi_{\boldsymbol{k}} \tag{S320}$$

where M^{α}_{r} represents the α component of spin $\left(\hat{\boldsymbol{S}}\right)$, orbital moment $\left[\hat{\boldsymbol{L}} = \frac{1}{4}\left(\hat{\boldsymbol{r}} \times \hat{\boldsymbol{v}} - \hat{\boldsymbol{v}} \times \hat{\boldsymbol{r}}\right)\right]$ and local charge polarization density $\left[\hat{\boldsymbol{p}} = \frac{g\mu_B}{2V_0 c^2}\left(\hat{\boldsymbol{v}} \times \hat{\boldsymbol{S}} - \hat{\boldsymbol{S}} \times \hat{\boldsymbol{v}}\right)\right]$ operator of the rth strip.

In the same manner as the orbital moment current, after evaluating the Kubo terms, one obtains:

$$\langle \delta \mathcal{M}^{\alpha}(\boldsymbol{r}) \rangle^{in} = \kappa^{in}_{\nu}(r) \nabla_{\nu} T \tag{S321}$$

where

$$\kappa^{in}_{\nu}(r) = -\frac{i}{2T} \sum_{\boldsymbol{k}, m \neq n} \langle n(\boldsymbol{k}) | M^{\alpha}_{r} | m(\boldsymbol{k}) \rangle \langle m(\boldsymbol{k}) | \hat{v}_{\boldsymbol{k},\nu} | n(\boldsymbol{k}) \rangle \times \\ \times \frac{\left(E^{nn}_{\boldsymbol{k}} \sigma^{mm}_3 + E^{mm}_{\boldsymbol{k}} \sigma^{nn}_3\right) \left\{ \rho\left[\left(\boldsymbol{\sigma}_3 E_{\boldsymbol{k}}\right)_{mm}\right] - \rho\left[\left(\boldsymbol{\sigma}_3 E_{\boldsymbol{k}}\right)_{nn}\right] \right\}}{\left[\left(\boldsymbol{\sigma}_3 E_{\boldsymbol{k}}\right)_{mm} - \left(\boldsymbol{\sigma}_3 E_{\boldsymbol{k}}\right)_{nn}\right]^2} \tag{S322}$$

where the superscript 'in' denotes the intrinsic contribution.

B. Extrinsic contribution: Boltzmann equation. We will now assess the extrinsic contribution to the spin, orbital moment and and local charge polarization density using the Boltzmann equation. Under the relaxation time approximation, denoted by τ_0 the Boltzmann equation is expressed as follows:

$$\frac{\rho_{neq}-\rho_{eq}}{\tau_0}=-v_\nu\nabla_\nu T\frac{\partial\rho_{eq}}{\partial T}=-v_\nu\nabla_\nu T\frac{E}{k_BT^2}\frac{e^{E/k_BT}}{\left(e^{E/k_BT}-1\right)^2} \tag{S323}$$

where $\rho_{eq}=\left(e^{E/k_BT}-1\right)^{-1}$.

The spin and orbital moment density is given by

$$\left\langle\delta\mathcal{M}^\alpha\left(\boldsymbol{r}\right)\right\rangle^{ex}=\frac{1}{V}\mathcal{M}^\alpha\left(\boldsymbol{r}\right)\left(\rho_{neq}-\rho_{eq}\right)=-\frac{1}{V}\mathcal{M}^\alpha\left(\boldsymbol{r}\right)v_\nu\frac{\tau_0E}{k_BT^2}\frac{e^{E/k_BT}}{\left(e^{E/k_BT}-1\right)^2}\nabla_\nu T \tag{S324}$$

$$=\kappa_\nu^{ex}\left(r\right)\nabla_\nu T \tag{S325}$$

where V is the volume of the system.

By using the Fourier transformation, one obtains:

$$\kappa_\nu^{ex}\left(r\right)=-\frac{\tau_0}{2Vk_BT^2}\sum_{\boldsymbol{k}}\sum_{n=1}^{2N}\langle n\left(\boldsymbol{k}\right)|M_r^\alpha|n\left(\boldsymbol{k}\right)\rangle\langle n\left(\boldsymbol{k}\right)|\hat{v}_{\boldsymbol{k},\nu}|n\left(\boldsymbol{k}\right)\rangle\frac{\left(\boldsymbol{\sigma}_3E_{\boldsymbol{k}}\right)_{nn}e^{\left(\boldsymbol{\sigma}_3E_{\boldsymbol{k}}\right)_{nn}/k_BT}}{\left(e^{\left(\boldsymbol{\sigma}_3E_{\boldsymbol{k}}\right)_{nn}/k_BT}-1\right)^2} \tag{S326}$$

Eq. (S322) and Eq. (S326) establish a basic framework for calculating the accumulation of angular moment (both spin and orbital) of magnons and and local charge polarization induced by magnons at the boundary of a finite system, incorporating intrinsic and extrinsic contributions. An investigation of a finite system, however is beyond the scope of the present paper, and we leave it for future exploration.

S7. Magnon-magnon interaction effects

The topological properties of the magnon bands hosted by 2D honeycomb AFMs, for example Berry curvature and Chern number, are introduced in close analogy with electronic bands in the celebrated Haldane model (26). In both cases, one considers noninteracting (i.e., infinitely long-lived) quasiparticles as described by the magnon Hamiltonian or Haldane Hamiltonian containing only terms that are quadratic in bosonic or fermionic operators, respectively. Such a quadratic Hamiltonian for magnons is generated by a linearized [i.e., truncated (2)] HP transformation. We employ the same tranformation [Eq. (S2) and Eq. (S3)] with the belief that its success in describing ferromagnets at low temperatures will translate to honeycomb AFMs—that is, conclusions made about the topology of noninteracting magnons produced by the linearized HP transformation can carry over to the full spin Hamiltonian [Eq. (S1)].

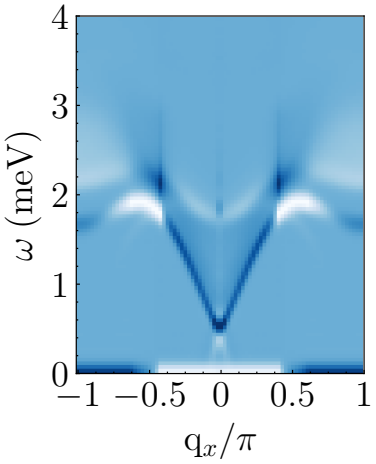

Fig. S10. Spin structure factor for a brick ladder, corresponding to a single row of hexagons of the honeycomb lattice, which hosts quantum spins $S=1/2$ interacting via nearest-neighbor antiferromagnetic exchange interaction and next-nearest-neighbor DMI with $\mathbf{D}_{ij}$ vector in Eq. (S1) that is *not* parallel to the staggered magnetization.

In this section we consider the possible consequences of magnon-magnon interactions. We stress that in the work reported in the main manuscript and previous sections of the supplement we consider only DMI oriented strictly out-of-plane, which means that it cannot introduce maganon-magnon interactions. Thus in this section we are considering a more general case in which the DMI has an in-plane component in the full spin Hamiltonian that can lead to important magnon-magnon interaction effects, even at zero temperature. The importance of such effects was revealed by recent perturbative analyses (27, 28) of the resulting

nonquadratic terms in the bosonic Hamiltonian (e.g. those containing three bosonic operators). For example, such an effect can lead to (28): spontaneous decay (29) of edge magnon modes; their hybridization with bulk magnons, thereby delocalizing them away from the edge; and even hybridization of magnons at opposite edges, as mediated by bulk magnons. The three magnon interactions can also lift spurious symmetries (30) present in the quadratic Hamiltonian, thereby making possible a nonzero transport response (31) to applied thermal gradient that is absent when one considers only noninteracting magnons.

To illustrate the potential importance of magnon-magnon interactions, assume that the $\mathbf{D}_{\text{ij}}$ vector has a component in the x-direction, which means that the corresponding DMI contains a term

$$\sum_{\langle\langle i,j\rangle\rangle} \frac{D^x_{ij}}{2}(\hat{S}^+_i + \hat{S}^-_i)\hat{S}^z_j - \hat{S}^z_i(\hat{S}^+_j + \hat{S}^-_j). \tag{S327}$$

The presence of this term in the full spin Hamiltonian [Eq. (S1)] generates terms containing three bosonic operators when the square root of the HP transformation is expanded (2) beyond the lowest order used in Eq. (S2) and Eq. (S3). To understand the importance of these effects, here we employ *nonperturbative* calculations for the full spin Hamiltonian using a time-dependent density matrix renormalization group algorithm for the spin structure factor (32), which we implement via time-dependent variational principle (33, 34) calculations within the `ITensor` (35) package. For purposes of illustrating the effects of magnon-magnon interactions, we use a honeycomb lattice composed of only one row of hexagons hosting an antiferromagnetic nearest-neighbor exchange and next-nearest neighbor DMI. The spin structure factor for this system, which is plotted in Fig. S10, reveals that the degeneracy of the bands of the quadratic Hamiltonian obtained from the linearized HP transformation is lifted when the $\mathbf{D}_{\text{ij}}$ vector has a component in the x-direction. In other words, the presence of maganon-magnon interactions breaks the degeneracy of the bands. We stress, however, that our analysis in the main text and other sections of the SI remains valid as long as the DMI vector remains parallel to the staggered magnetization $\mathbf{M}_{\text{stag}} = \mathbf{M}_A - \mathbf{M}_B$.

References

1. T Holstein, H Primakoff, Field dependence of the intrinsic domain magnetization of a ferromagnet. *Phys. Rev.* **58**, 1098–1113 (1940).
2. U Bajpai, A Suresh, BK Nikolić, Quantum many-body states and Green's functions of nonequilibrium electron-magnon systems: Localized spin operators versus their mapping to Holstein-Primakoff bosons. *Phys. Rev. B* **104**, 184425 (2021).
3. N Bazazzadeh, et al., Magnetoelastic coupling enabled tunability of magnon spin current generation in two-dimensional antiferromagnets. *Phys. Rev. B* **104**, L180402 (2021).
4. N Bazazzadeh, et al., Symmetry enhanced spin-nernst effect in honeycomb antiferromagnetic transition metal trichalcogenide monolayers. *Phys. Rev. B* **103**, 014425 (2021).
5. J Colpa, Diagonalization of the quadratic boson hamiltonian. *Phys. A: Stat. Mech. its Appl.* **93**, 327–353 (1978).
6. S Park, N Nagaosa, BJ Yang, Thermal Hall effect, spin nernst effect, and spin density induced by a thermal gradient in collinear ferrimagnets from magnon–phonon interaction. *Nano letters* **20**, 2741–2746 (2020).
7. R Cheng, S Okamoto, D Xiao, Spin Nernst effect of magnons in collinear antiferromagnets. *Phys. Rev. Lett.* **117**, 217202 (2016).
8. K Matan, et al., Spin waves in the frustrated kagomé lattice antiferromagnet $\text{kfe}_3(\text{OH})_6(\text{so}_4)_2$. *Phys. Rev. Lett.* **96**, 247201 (2006).
9. P Laurell, GA Fiete, Magnon thermal hall effect in kagome antiferromagnets with dzyaloshinskii-moriya interactions. *Phys. Rev. B* **98**, 094419 (2018).
10. Y Lu, X Guo, V Koval, C Jia, Topological thermal hall effect driven by spin-chirality fluctuations in frustrated antiferromagnets. *Phys. Rev. B* **99**, 054409 (2019).
11. B Li, S Sandhoefner, AA Kovalev, Intrinsic spin Nernst effect of magnons in a noncollinear antiferromagnet. *Phys. Rev. Res.* **2**, 013079 (2020).
12. R Matsumoto, R Shindou, S Murakami, Thermal Hall effect of magnons in magnets with dipolar interaction. *Phys. Rev. B* **89**, 054420 (2014).
13. DQ To, et al., Giant spin nernst effect in a two-dimensional antiferromagnet due to magnetoelastic coupling induced gaps and interband transitions between magnonlike bands. *Phys. Rev. B* **108**, 085435 (2023).
14. A Mook, B Göbel, J Henk, I Mertig, Taking an electron-magnon duality shortcut from electron to magnon transport. *Phys. Rev. B* **97**, 140401 (2018).
15. RR Neumann, J Henk, I Mertig, A Mook, Electrical activity of topological chiral edge magnons. *Phys. Rev. B* **109**, L180412 (2024).
16. T Thonhauser, D Ceresoli, D Vanderbilt, R Resta, Orbital magnetization in periodic insulators. *Phys. Rev. Lett.* **95**, 137205 (2005).
17. D Xiao, J Shi, Q Niu, Berry phase correction to electron density of states in solids. *Phys. Rev. Lett.* **95**, 137204 (2005).
18. J Shi, G Vignale, D Xiao, Q Niu, Quantum theory of orbital magnetization and its generalization to interacting systems. *Phys. Rev. Lett.* **99**, 197202 (2007).
19. J Luo, et al., Evidence for topological magnon–phonon hybridization in a 2d antiferromagnet down to the monolayer limit. *Nano letters* **23**, 2023–2030 (2023).
20. D Go, HW Lee, Orbital torque: Torque generation by orbital current injection. *Phys. Rev. Res.* **2**, 013177 (2020).

21. VA Zyuzin, AA Kovalev, Magnon spin Nernst effect in antiferromagnets. *Phys. Rev. Lett.* **117**, 217203 (2016).
22. R Kubo, Statistical-mechanical theory of irreversible processes. i. general theory and simple applications to magnetic and conduction problems. *J. physical society Jpn.* **12**, 570–586 (1957).
23. R Kubo, M Yokota, S Nakajima, Statistical-mechanical theory of irreversible processes. ii. response to thermal disturbance. *J. Phys. Soc. Jpn.* **12**, 1203–1211 (1957).
24. GD Mahan, *Many-particle physics.* (Springer Science & Business Media), (2013).
25. L Smrcka, P Streda, Transport coefficients in strong magnetic fields. *J. Phys. C: Solid State Phys.* **10**, 2153 (1977).
26. FDM Haldane, Model for a quantum hall effect without landau levels: Condensed-matter realization of the "parity anomaly". *Phys. Rev. Lett.* **61**, 2015–2018 (1988).
27. AL Chernyshev, PA Maksimov, Damped topological magnons in the kagome-lattice ferromagnets. *Phys. Rev. Lett.* **117**, 187203 (2016).
28. J Habel, A Mook, J Willsher, J Knolle, Breakdown of chiral edge modes in topological magnon insulators. *Phys. Rev. B* **109**, 024441 (2024).
29. ME Zhitomirsky, AL Chernyshev, Colloquium: Spontaneous magnon decays. *Rev. Mod. Phys.* **85**, 219–242 (2013).
30. M Gohlke, A Corticelli, R Moessner, PA McClarty, A Mook, Spurious symmetry enhancement in linear spin wave theory and interaction-induced topology in magnons. *Phys. Rev. Lett.* **131**, 186702 (2023).
31. R Hoyer, R Jaeschke-Ubiergo, KH Ahn, L Šmejkal, A Mook, Spontaneous crystal thermal hall effect in insulating altermagnets (2024).
32. SR White, AE Feiguin, Real-time evolution using the density matrix renormalization group. *Phys. Rev. Lett.* **93**, 076401 (2004).
33. J Haegeman, C Lubich, I Oseledets, B Vandereycken, F Verstraete, Unifying time evolution and optimization with matrix product states. *Phys. Rev. B* **94**, 165116 (2016).
34. T Chanda, P Sierant, J Zakrzewski, Time dynamics with matrix product states: Many-body localization transition of large systems revisited. *Phys. Rev. B* **101**, 035148 (2020).
35. M Fishman, SR White, EM Stoudenmire, The ITensor software library for tensor network calculations. *SciPost Phys. Codebases* p. 4 (2022).